

University of Dundee

## USP7 small-molecule inhibitors interfere with ubiquitin binding

Kategaya, Lorna; Di Lello, Paola; Rougé, Lionel; Pastor, Richard; Clark, Kevin R.;  
Drummond, Jason

*Published in:*  
Nature

*DOI:*  
[10.1038/nature24006](https://doi.org/10.1038/nature24006)

*Publication date:*  
2017

*Document Version*  
Peer reviewed version

[Link to publication in Discovery Research Portal](#)

### *Citation for published version (APA):*

Kategaya, L., Di Lello, P., Rougé, L., Pastor, R., Clark, K. R., Drummond, J., Kleinheinz, T., Lin, E., Upton, J-P., Prakash, S., Heideker, J., McClelland, M., Ritorto, M. S., Alessi, D. R., Trost, M., Bainbridge, T. W., Kwok, M. C. M., Ma, T. P., Stiffler, Z., ... Wertz, I. E. (2017). USP7 small-molecule inhibitors interfere with ubiquitin binding. *Nature*, 550, 534-538. <https://doi.org/10.1038/nature24006>

### **General rights**

Copyright and moral rights for the publications made accessible in Discovery Research Portal are retained by the authors and/or other copyright owners and it is a condition of accessing publications that users recognise and abide by the legal requirements associated with these rights.

- Users may download and print one copy of any publication from Discovery Research Portal for the purpose of private study or research.
- You may not further distribute the material or use it for any profit-making activity or commercial gain.
- You may freely distribute the URL identifying the publication in the public portal.

### **Take down policy**

If you believe that this document breaches copyright please contact us providing details, and we will remove access to the work immediately and investigate your claim.

## 1 **USP7 Small Molecule Inhibitors Interfere with Ubiquitin Binding**

2  
3 Lorna Kategaya<sup>1,2†</sup>, Paola Di Lello<sup>3†</sup>, Lionel Rougé<sup>3</sup>, Richard Pastor<sup>4</sup>, Kevin R. Clark<sup>5</sup>,  
4 Jason Drummond<sup>5</sup>, Tracy Kleinheinz<sup>5</sup>, Eva Lin<sup>1</sup>, John-Paul Upton<sup>1,2</sup>, Sumit Prakash<sup>1,2</sup>,  
5 Johanna Heideker<sup>1,2</sup>, Mark McClelland<sup>1,2</sup>, Maria Stella Ritorto<sup>6</sup>, Travis W. Bainbridge<sup>7</sup>,  
6 Taylur P. Ma<sup>8</sup>, Michael C.M. Kwok<sup>7</sup>, Zachary Stiffler<sup>9</sup>, Bradley Brasher<sup>9</sup>, Dario R. Alessi<sup>6</sup>,  
7 Matthias Trost<sup>6</sup>, Adam R. Renslo<sup>10</sup>, Michelle R. Arkin<sup>10</sup>, Frederick Cohen<sup>4</sup>, Kebing Yu<sup>8</sup>,  
8 Frank Peale<sup>11</sup>, Florian Gnad<sup>12</sup>, Matthew T. Chang<sup>12</sup>, Christiaan Klijn<sup>12</sup>, Elizabeth  
9 Blackwood<sup>13</sup>, Scott E. Martin<sup>1</sup>, William F. Forrest<sup>12</sup>, James A. Ernst<sup>7</sup>, Chudi Ndubaku<sup>4</sup>,  
10 Xiaojing Wang<sup>4</sup>, Maureen H. Beresini<sup>5</sup>, Vickie Tsui<sup>4</sup>, Carsten Schwerdtfeger<sup>9</sup>, Robert A.  
11 Blake<sup>5</sup>, Jeremy Murray<sup>3</sup>, Till Maurer<sup>3\*</sup> and Ingrid E. Wertz<sup>1,2\*</sup>

12 Departments of <sup>1</sup>Discovery Oncology, <sup>2</sup>Early Discovery Biochemistry, <sup>3</sup>Structural Biology,  
13 <sup>4</sup>Discovery Chemistry, <sup>5</sup>Biochemical and Cellular Pharmacology, <sup>7</sup>Protein Chemistry,  
14 <sup>8</sup>Microchemistry, Proteomics, and Lipidomics, <sup>11</sup>Research Pathology, <sup>12</sup>Bioinformatics  
15 and Computational Biology, and <sup>13</sup>Translational Oncology, Genentech, South San  
16 Francisco, CA 94080, USA.

17 <sup>6</sup>MRC Protein Phosphorylation and Ubiquitylation Unit, School of Life  
18 Sciences, University of Dundee, Dundee DD1 5EH, UK.

19 <sup>9</sup>Boston Biochem, Inc. 840 Memorial Drive, Cambridge, MA, USA.

20 <sup>10</sup>Department of Pharmaceutical Chemistry and Small Molecule Discovery Center,  
21 University of California, San Francisco, San Francisco, CA, USA.

22  
23 † These authors contributed equally to this publication.

24 \* To whom correspondence should be addressed.

25  
26 **The ubiquitin system regulates the majority of cellular processes in eukaryotes.**  
27 **Ubiquitin is ligated to substrate proteins as monomers or chains and the topology**  
28 **of ubiquitin modifications regulates substrate interactions with specific proteins.**  
29 **Thus ubiquitination directs a variety of substrate fates including proteasomal**  
30 **degradation<sup>1</sup>. Deubiquitinase enzymes cleave ubiquitin from substrates and are**  
31 **implicated in disease<sup>2</sup>; for example ubiquitin-specific protease-7 (USP7) regulates**  
32 **stability of the p53 tumor suppressor and other proteins critical for tumor cell**  
33 **survival<sup>3</sup>. However, developing selective deubiquitinase inhibitors has been**  
34 **challenging<sup>4</sup> and no co-crystal structures have been solved with small molecule**  
35 **deubiquitinase inhibitors. Here, using nuclear magnetic resonance (NMR)-based**  
36 **screening and structure-based drug design, we describe the development of**  
37 **selective USP7 inhibitors GNE-6640 and GNE-6776. These compounds induce**  
38 **hematopoietic and solid tumor cell death and enhance cytotoxicity with**  
39 **chemotherapeutic agents and targeted compounds, including PIM kinase**  
40 **inhibitors. Structural studies reveal that GNE-6640 and GNE-6776 non-covalently**  
41 **target an interface between the thumb, fingers, and palm regions of the USP7**  
42 **catalytic domain, 12Å distant from the catalytic cysteine. The compounds**  
43 **attenuate ubiquitin binding and thus inhibit USP7 deubiquitinase activity. Within**  
44 **the USP7 thumb region, GNE-6640 and GNE-6776 interact with acidic residues that**  
45 **mediate H-bond interactions with the ubiquitin Lys-48 side-chain<sup>5</sup>, suggesting that**  
46 **USP7 preferentially interacts with and cleaves ubiquitin moieties having free Lys-**  
47 **48 side-chains. We investigated this idea by engineering di-ubiquitin chains**  
48 **containing differential proximal and distal isotopic labels and measuring USP7**  
49 **binding via NMR, a study that substantiated our hypothesis. This preferential**  
50 **binding significantly protracted the depolymerization kinetics of Lys-48-linked**

51 **ubiquitin chains relative to Lys-63-linked chains. In summary, engineering**  
52 **compounds that inhibit USP7 activity by attenuating ubiquitin binding suggests**  
53 **opportunities for developing other deubiquitinase inhibitors and may be a strategy**  
54 **more broadly applicable to inhibiting proteins that require ubiquitin binding for full**  
55 **functional activity.**

56  
57 USP7 is a genetically-validated deubiquitinase for MDM2, a ubiquitin ligase that  
58 promotes degradation of the tumor suppressor p53. Depletion of USP7 enhances  
59 ubiquitination of USP7 substrates, including MDM2. Subsequent MDM2 proteasomal  
60 degradation stabilizes the p53 tumor suppressor, thus promoting cell cycle arrest and  
61 apoptosis. USP7 inhibition enhances ubiquitination of additional USP7 substrates that  
62 also contribute to cell growth inhibition<sup>3,6,7</sup> (Fig. 1a). To identify USP7 inhibitors, we  
63 established a high throughput activity-based screening (HTS) cascade, consisting of a  
64 primary deubiquitinase assay followed by a series of counter-screen assays and  
65 selection filters (Supplementary Information Fig. 1a, 1b). In parallel we developed an  
66 NMR fragment screening cascade to identify fragments that bind the USP7 catalytic  
67 domain at discrete sites (Supplementary Information Fig. 1c). A hit-to-lead selection  
68 cascade was established to guide optimization of HTS and NMR hits into more potent  
69 USP7 inhibitors (Fig. 1b). At the apex of this cascade, deubiquitinase selectivity assays  
70 and structural biology directed medicinal chemistry design. Additionally, assays to  
71 measure total- and ubiquitinated-MDM2 levels were developed as proximal indicators of  
72 USP7 cellular activity, followed by cellular viability assays using inactive compounds  
73 from the same chemical series as negative controls (Fig. 1a, 1b).

74  
75 Progression of HTS and NMR screening hits through the hit-to-lead selection cascade  
76 identified a series of fragment compounds as having the most favorable properties for  
77 on-target efficacy (Supplementary Information Figs. 2-5). Optimization of the parent  
78 compound GNE-2916 yielded GNE-6640 and GNE-6776. These USP7 inhibitors  
79 enhanced endogenous MDM2 ubiquitination while achieving selectivity over USP47, the  
80 most USP7-homologous deubiquitinase, and USP5, a highly-expressed and active  
81 deubiquitinase<sup>8</sup> (Extended Data Fig. 1a). Both compounds accelerated endogenous  
82 MDM2 turnover, that was apparent in combination with cycloheximide, a necessary co-  
83 treatment since MDM2 is a p53 target gene (Fig. 1a, 1c, Extended Data Fig. 1b).  
84 Accordingly, both GNE-6640 and GNE-6776, but not control compounds GNE-2118 and  
85 GNE-6641, promoted endogenous MDM2 ubiquitination with Lys-48 (K48)-linked  
86 polyubiquitin chains that direct proteins for proteasomal degradation<sup>9</sup> (Fig. 1d, Extended  
87 Data Fig. 1c). The active USP7 inhibitors stabilized p53 and upregulated p21 in wild-  
88 type cells, but not in p53-null cells, and did not further elevate p53 and p21 expression in  
89 USP7-null cells (Fig. 1e, Extended data Fig. 1b). These data were corroborated by a  
90 significant dose-dependent decrease in viability of wild-type, but not of USP7-null cells,  
91 treated with either inhibitor at concentrations  $\leq 15\mu\text{M}$  (Extended data Fig. 1d). GNE-6640  
92 also increased p53 and p21 levels and decreased viability to a greater extent in breast  
93 adenocarcinoma and osteosarcoma cell lines compared to normal primary breast  
94 epithelial cells or osteocytes (Extended Data Fig. 2a, 2b). Thus the collective data  
95 indicate that GNE-6640 and GNE-6776 regulate cellular USP7/MDM2/p53 signaling  
96 pathways.

97  
98 A study by Ritorto et al. revealed that previously-reported deubiquitinase inhibitors are  
99 neither potent nor sufficiently selective when evaluated at 1-10 $\mu\text{M}$  in a MALDI-TOF mass  
100 spectrometry-based assay<sup>4</sup>. In this assay, GNE-6640 and GNE-6776 inhibited USP7  
101 cleavage of di-ubiquitin chains and were highly selective against 36 other recombinant

102 deubiquitinases at 10 $\mu$ M (Fig. 2a, Extended Data Fig. 3a). GNE-6776 remained  
103 selective even at 100 $\mu$ M, a >6-fold higher concentration than used in cellular assays,  
104 whereas control compound GNE-6641 had negligible activity at either concentration (Fig.  
105 2a, Extended Data Fig. 3b). Since deubiquitinase activities are regulated by numerous  
106 cellular mechanisms<sup>10</sup> we developed an assay utilizing activity-based probes to evaluate  
107 USP7 inhibitor effects on endogenous deubiquitinases (Heideker et al., manuscript in  
108 preparation). Both GNE-6640 and GNE-6776 significantly inhibited USP7 at 15 $\mu$ M  
109 ( $p=0.0503$  and  $0.0058$ , respectively; adjusted by the Benjamini-Hochberg False  
110 Discovery Rate method) while remaining selective against 44 to 47 other endogenous  
111 detected deubiquitinases (Fig. 2b, Extended Data Fig. 3c, 3d). Thus GNE-6640 and  
112 GNE-6776 are highly selective USP7 inhibitors against both recombinant and  
113 endogenous cellular deubiquitinases. Given these favorable features, we investigated  
114 whether the compounds could be utilized in animal studies. Pharmacodynamic and  
115 pharmacokinetic studies indicated that GNE-6776 is an orally bioavailable compound  
116 that promotes on-target pathway modulation in human hematologic and solid tumor  
117 xenografts (Supplementary Information Fig. 6a-e). Although efficacious drug exposure  
118 was only transiently achieved, GNE-6776 caused modest, though significant, EOL-1  
119 xenograft growth delay (Supplementary Information Fig. 6f). Thus development of USP7  
120 inhibitors having improved drug-like properties will be required in order to demonstrate  
121 the full value of USP7 inhibition *in vivo*.

122

123 USP7 and MDM2 regulate proteins other than p53<sup>3,6,11-16</sup> (Fig. 1a). Having confirmed the  
124 selectivity and on-target cellular potency of GNE-6640 and GNE-6776, we screened 441  
125 cell lines from 15 tumor indications in three-day viability assays to enable an unbiased  
126 analysis of cellular factors that contribute to USP7 inhibitor sensitivity (Extended Data  
127 Fig. 4a). GNE-6641 was inactive in all cell lines whereas GNE-6640 decreased viability  
128 of 108 cell lines with IC<sub>50</sub>  $\leq 10\mu$ M (data not shown). Next, we selected a subset of 181  
129 cell lines from six tumor indications that displayed a range of sensitivities for confirmation  
130 and more extensive analysis (Extended Data Fig. 4a). GNE-6641 remained inactive in a  
131 five-day viability assay, whereas GNE-6640 and GNE-6776 decreased viability of 54 and  
132 six cell lines, respectively, with IC<sub>50</sub>  $\leq 10\mu$ M (Extended Data Fig. 4b). Five-day viability  
133 data and exome sequencing analysis were integrated to identify potential features  
134 associated with compound sensitivity. Acute myeloid leukemia (AML) cell lines were  
135 significantly associated with increased sensitivity to GNE-6640 (Extended Data Fig. 4c,  
136 4e). Loss-of-function mutant TP53 lines were in general less responsive than wild-type  
137 TP53 lines, but the trend was not statistically significant (Extended Data Fig. 4d).  
138 Indeed, the TP53 R175 hotspot was associated with increased sensitivity while the Y220  
139 hotspot was associated with decreased sensitivity (Extended Data Fig. 4c, 4e). To  
140 further investigate the mechanisms by which TP53 status regulates viability in response  
141 to USP7 inhibition, we imaged cellular proliferation and caspase activation in TP53 wild-  
142 type and TP53-null cell lines treated with USP7 inhibitors. Both compounds decreased  
143 proliferation and activated caspases in TP53 wild-type cell lines. These effects were  
144 reduced, but not abolished, in the evaluated TP53-null cell lines (Extended Data Fig. 5a-  
145 5c). Combining GNE-6640 with doxorubicin or cisplatin, DNA-damaging agents that  
146 activate the p53 response<sup>17</sup>, enhanced the efficacy of USP7 inhibitors (Extended Data  
147 Fig. 6a, 6b). Thus immunoblot analysis and cellular viability studies indicate that the  
148 MDM2/p53 pathway is a mediator of GNE-6640 and GNE-6776 cellular activity but is not  
149 the only determinant. These findings corroborate genetic studies crossing *TP53*<sup>-/-</sup> mice  
150 with *USP7*<sup>-/-</sup> mice, that afford only a partial rescue of the *USP7*<sup>-/-</sup> embryonic lethality<sup>7</sup>.

151

152 The enhanced efficacy of GNE-6640 in combination with DNA damaging agents  
153 suggested a strategy to identify cellular signaling pathways that intersect with USP7  
154 inhibition. We therefore screened the EOL-1 AML cell line using a panel of 589  
155 chemotherapeutic and targeted agents in combination with GNE-6640 or GNE-6776.  
156 Top hits for both compounds included inhibitors of PI3K and PIM kinases (Extended  
157 Data Fig. 6c, 6d, Supplementary Information Table 1). PIM kinases are reported to share  
158 substrates with PI3K pathway kinases including TSC1/2 and the pro-apoptotic Bcl-2  
159 family member Bad (Extended Data Fig. 7d)<sup>18</sup>. Given the role of PIM kinases,  
160 particularly PIM2, in hematological malignancies<sup>18</sup>, we confirmed combination efficacy  
161 with Bliss score analysis using PIM inhibitors GDC-0339<sup>19</sup> or GDC-0570 (Fig. 2c,  
162 Extended Data Figures 7a-7c). Both Pim inhibitors share structural similarities and are  
163 highly potent against Pim kinases while remaining selective against other kinases  
164 (manuscripts in preparation). We also investigated cellular mechanisms of combination  
165 efficacy. Whereas GNE-6776 promoted a modest elevation of p21 levels in EOL-1 and  
166 MV-4-11 cell lines, PIM2 levels were reduced. The GNE-6776-induced decrease in  
167 PIM2 protein level was rescued by inhibition of the ubiquitin-activating enzyme UAE1,  
168 that globally blocks ubiquitination of cellular proteins, and the proteasome inhibitor  
169 bortezomib, that inhibits degradation of ubiquitinated proteins. PIM2 levels were also  
170 lower in USP7 null cells and were rescued by proteasome inhibition, collectively  
171 indicating that USP7 stabilizes PIM2 levels via a ubiquitin/proteasome-dependent  
172 mechanism (Extended Data Fig. 7e, 7f). Analysis of a treatment time course with GNE-  
173 6776, the PIM inhibitor GDC-0570, or the two compounds in combination revealed that,  
174 as expected, GDC-0570 reduced phosphorylation of the S6 ribosomal protein and of  
175 Bad, and decreased expression of short-lived proteins including p21 and the pro-survival  
176 Bcl-2 family member Mcl-1. GNE-6776 decreased PIM2 levels over time and  
177 remarkably, also reduced S6 and Bad phosphorylation and total Mcl-1 levels, similar to  
178 PIM inhibitor treatment. In combination, GNE-6776 and GDC-0570 treatments  
179 enhanced the apoptosis indicators cleaved PARP and cleaved caspase-3, confirming  
180 the cell viability combination data (Fig. 2d). We therefore hypothesized that USP7  
181 regulates PIM2 ubiquitination: upon USP7 inhibition, ubiquitin modifications accumulate  
182 on PIM2 that promote PIM2 proteasomal degradation. In support of this idea,  
183 endogenous USP7 associates with PIM2 in cellular lysates and GNE-6776 treatment  
184 enhances PIM2 ubiquitination (Fig. 2e, Extended Data Fig. 7g). Furthermore  
185 recombinant USP7, but not a C223S catalytic mutant, deubiquitinated PIM2 *in vitro*  
186 (Extended Data Fig. 7h). Our data thus reveal a previously undescribed juncture  
187 between USP7 deubiquitinase activity and PIM signaling. This finding expands the  
188 repertoire of USP7-regulated oncogenic signaling pathways beyond MDM2/p53  
189 signaling and merits further investigation in additional cell lines and indications.

190  
191 Given the selectivity and efficacy of GNE-6640 and GNE-6776, it was of interest to  
192 understand the precise molecular mechanisms by which these tool compounds inhibit  
193 USP7. Enzymatic studies utilizing a ubiquitin-AMC substrate verified that the  
194 compounds inhibit intrinsic USP7 catalytic activity ( $k_{cat}$ ) and notably, attenuate substrate  
195 binding ( $K_m$ ) (Extended Data Fig. 8a). NMR analysis confirmed that USP7 inhibitors  
196 weaken USP7 interactions with native ubiquitin (Fig. 3a, Extended Data Fig. 8b, 8c).  
197 Analysis of co-crystal structures revealed that both compounds bind into a pocket  
198 approximately 12Å from the catalytic triad that is located at the interface of the palm,  
199 fingers, and thumb sub-domains (Fig. 3b, Extended Data Fig. 7d, 7e). The phenol-  
200 aminopyridine moieties of both compounds make similar interactions with their phenol  
201 rings buried in the pocket and hydroxyl groups engaged in H-bond interactions with  
202 H403, which is located at the tip of the  $\beta 8$  sheet. The 2-aminopyridine is directed out of

203 the pocket towards solvent with the 2-amino group engaging D349, which is located on  
204 the loop connecting  $\beta 2$  and  $\beta 3$ . The two different chemical moieties at the 5-position of  
205 the aminopyridine, namely the pyridine-carboxamide (GNE-6776) and indazole (GNE-  
206 6440), are largely solvent exposed and lie between the  $\alpha 5$  and  $\alpha 6$  helices. The NH  
207 atoms of the carboxamide of GNE-6776 engages USP7-D305 on the  $\alpha 5$  helix and the  
208 indazole of GNE-6640 makes extensive van der Waals contacts in the crevice between  
209  $\alpha 5$  and  $\alpha 6$  (Fig. 3c, Extended Data Fig. 7d). Comparison of the co-crystal structures of  
210 GNE-6776 and GNE-6640 with the USP7-ubiquitin complex structure (PDB 1NBF)  
211 revealed that the compounds likely sterically inhibit ubiquitin binding and prevent the  
212 transition of the USP7  $\alpha 5$  helix to the active conformation<sup>5</sup> (Fig. 3c, Extended Data Fig.  
213 7d). However, given the extensive interactions between USP7 and ubiquitin<sup>5</sup>, we  
214 investigated the functional significance of residues on the  $\alpha 5$  helix of USP7 that interact  
215 with K48 in the USP7-ubiquitin structure. The K48A mutant of ubiquitin has reduced  
216 affinity for USP7 (Extended Data Fig. 9a). Similarly, recombinant D305A/E308A USP7  
217 catalytic domain failed to cleave tetra-K48- or tetra-K63-linked polyubiquitin conjugated  
218 to a TAMRA-labeled peptide<sup>20</sup> and enzymatic analysis revealed this apparent inactivity  
219 was due to a significantly increased  $K_m$  of 1120  $\mu$ M (Extended Data Fig. 9b, 9c).  
220 Importantly, expression of a D305A/E308A USP7 mutant increased K48-linked  
221 polyubiquitination on endogenous MDM2, similarly to expression of catalytically-inactive  
222 USP7 (Extended Data Fig. 9d), thus demonstrating the importance of ubiquitin-K48 and  
223 USP7-D305/E308 residues for USP7/ubiquitin binding and substrate deubiquitination.

224  
225 The GNE-6640 and GNE-6776 USP7-interaction modes independently implicated the  
226 ubiquitin-K48 side-chain as a key contributor to USP7 binding, suggesting that USP7  
227 preferentially associates with ubiquitin moieties having free K48 side-chains.  
228 Mechanistically this could direct USP7 to distal subunits of K48-linked polyubiquitin,  
229 resulting in sequential distal-to-proximal chain depolymerization (exo-cleavage).  
230 However in non-K48-linked chains, USP7 may bind and cleave proximal to any ubiquitin  
231 moieties having accessible K48 side-chains (exo-, endo-, or base-cleavage) (Extended  
232 Data Fig. 10a). In order to evaluate this idea, it was necessary to engineer K48- and  
233 K63-linked di-ubiquitin with differentially-labeled distal and proximal ubiquitin subunits  
234 using spectroscopically distinct amino acids. To select the ubiquitin residues for isotopic  
235 labeling, we evaluated the chemical shift perturbations induced by USP7 binding  
236 (Extended Data Fig. 10b). The cluster of residues L8, T12, T14, and L15 broaden upon  
237 USP7 binding and are well-resolved in the spectra, thus Leu residues were isotopically  
238 labeled with <sup>15</sup>N in the proximal di-ubiquitin subunit and Thr residues were <sup>15</sup>N-labeled in  
239 the distal subunit (Fig. 4a, Extended Data Fig. 10b, 10c). NMR analysis of these  
240 differentially-labeled di-ubiquitins showed preferential USP7 binding to the distal subunit  
241 of K48-linked di-ubiquitin while USP7 binding was similar to both proximal and distal  
242 K63-linked di-ubiquitin subunits (Fig. 4a, top panels, Extended Data Fig. 10c).  
243 Importantly, both D305A USP7 and D305A/E308A USP7 mutants demonstrated similar  
244 binding to both proximal and distal K48-linked di-ubiquitin subunits (Fig. 4a, bottom  
245 panels). Based on these data, we evaluated whether differential di-ubiquitin binding  
246 impacts the dynamics of ubiquitin chain depolymerization by USP7. A previous study  
247 reported that USP7 cleaves K6-, K11-, K33-, K48-, and K63-linked di-ubiquitins with  
248 similar  $k_{cat}$  and  $K_m$  values, indicating that different isopeptide bond conformations do not  
249 significantly impact cleavage efficiency<sup>21</sup>. Remarkably, our studies reveal that USP7  
250 sequentially depolymerizes tetra-K48-linked ubiquitin from the distal residue (exo-  
251 cleavage) whereas tetra-K63-ubiquitin chains are cleaved via a combination of exo-,  
252 endo-, or base-cleavage, as nearly complete depolymerization occurs within four

253 minutes (Fig. 4b, Extended Data Fig. 10d, 10e). Thus USP7 preferentially binds  
254 ubiquitin moieties that have a free K48 side-chain, resulting in protracted and sequential  
255 depolymerization of K48-linked polyubiquitin.

256

257 Herein we describe the development and characterization of GNE-6640 and GNE-6776,  
258 *bona fide* USP7 inhibitors having clear selectivity against other deubiquitinases and a  
259 structurally-defined, unique mechanism of action. Establishing a compound selection  
260 cascade of biochemical, biophysical, and cellular assays using inactive control  
261 compounds for cross-validation was critical for selecting on-target inhibitors and guiding  
262 their optimization. Additionally, combination studies revealed a previously undescribed  
263 intersection between USP7 deubiquitinase activity and PIM kinases in regulating cell  
264 viability. Co-crystal structures of GNE-6640 and GNE-6776 demonstrate that both  
265 compounds specifically inhibit USP7 deubiquitinase activity by binding into a unique  
266 pocket at the interface of USP7 palm, fingers, and thumb sub-domains and sterically  
267 block ubiquitin binding. These inhibitor binding modes also pointed to the potential  
268 importance of the complementary charged interactions between USP7-D305/E308 and  
269 ubiquitin-K48, which we confirmed via mutational analysis. Notably D305G has been  
270 identified as a somatic loss-of-function mutant in acute lymphoblastic leukemia  
271 patients<sup>22</sup>. Furthermore, NMR analysis of USP7 binding to native monoubiquitin and  
272 differentially-labeled di-ubiquitins revealed that USP7 preferentially interacts with  
273 ubiquitin moieties having free K48 side-chains. Thus, although USP7 cleaves most  
274 ubiquitin-isopeptide linkages non-selectively<sup>21</sup>, USP7 chain depolymerization is markedly  
275 protracted for K48-linked polyubiquitin relative to K63-linked polyubiquitin. It has been  
276 proposed that the inefficiency of some deubiquitinases to depolymerize longer substrate-  
277 conjugated K48-linked chains enables a threshold for proteasome-targeting  
278 polyubiquitination<sup>23</sup>; our studies substantiate this idea and provide a biophysical  
279 mechanism. Numerous proteins including other deubiquitinases, ubiquitin ligases, DNA  
280 repair and endocytosis machinery, and epigenetic regulators are functionally dependent  
281 on ubiquitin binding<sup>24</sup>. Developing selective inhibitors that attenuate ubiquitin binding,  
282 instead of directly targeting active-site residues, is an effective strategy for USP7  
283 inhibition. Our studies demonstrate the feasibility of this approach, that may have  
284 broader applications for inhibiting other classes of ubiquitin-binding proteins.

285

286  
287  
288  
289  
290  
291  
292  
293  
294  
295  
296  
297  
298  
299  
300  
301  
302  
303  
304  
305  
306  
307  
308  
309  
310  
311  
312  
313  
314  
315  
316  
317  
318  
319  
320  
321  
322  
323  
324  
325  
326  
327  
328  
329  
330  
331  
332  
333  
334  
335

## Acknowledgements

The authors thank Wayne Fairbrother, Lauren Frick, Sharon Fong, Tom Hunsaker, Cynthia Lam, Bianca Liederer, Mark Merchant, Jim Nonomiya, Jing Peng, Thin Pham, Linda Rangell, Richard A. Rodriguez, Udi Segal, Raymond Tong, Leslie Wang, and the Genentech Protein Expression group, Cell Central group, gCSI group, and the Boston Biochem, Inc. team for reagents, helpful discussions, and collaborations. DRA and MT are supported by the UK Medical Research Council (grant number MC\_UU\_12016/2).

## References

- 1 Komander, D. & Rape, M. The ubiquitin code. *Annual review of biochemistry* **81**, 203-229, doi:10.1146/annurev-biochem-060310-170328 (2012).
- 2 Clague, M. J., Heride, C. & Urbe, S. The demographics of the ubiquitin system. *Trends Cell Biol* **25**, 417-426, doi:10.1016/j.tcb.2015.03.002 (2015).
- 3 Nicholson, B. & Suresh Kumar, K. G. The multifaceted roles of USP7: new therapeutic opportunities. *Cell Biochem Biophys* **60**, 61-68, doi:10.1007/s12013-011-9185-5 (2011).
- 4 Ritorto, M. S. *et al.* Screening of DUB activity and specificity by MALDI-TOF mass spectrometry. *Nature communications* **5**, 4763, doi:10.1038/ncomms5763 (2014).
- 5 Hu, M. *et al.* Crystal structure of a UBP-family deubiquitinating enzyme in isolation and in complex with ubiquitin aldehyde. *Cell* **111**, 1041-1054 (2002).
- 6 Cummins, J. M. *et al.* Tumour suppression: disruption of HAUSP gene stabilizes p53. *Nature* **428**, 1 p following 486, doi:10.1038/nature02501 (2004).
- 7 Kon, N. *et al.* Inactivation of HAUSP in vivo modulates p53 function. *Oncogene* **29**, 1270-1279.
- 8 Clague, M. J. *et al.* Deubiquitylases from genes to organism. *Physiol Rev* **93**, 1289-1315, doi:10.1152/physrev.00002.2013 (2013).
- 9 Deshaies, R. J. Proteotoxic crisis, the ubiquitin-proteasome system, and cancer therapy. *BMC biology* **12**, 94, doi:10.1186/s12915-014-0094-0 (2014).
- 10 Heideker, J. & Wertz, I. E. DUBs, the regulation of cell identity and disease. *The Biochemical journal* **467**, 191 (2015).
- 11 Fahraeus, R. & Olivares-Illana, V. MDM2's social network. *Oncogene* **33**, 4365-4376, doi:10.1038/onc.2013.410 (2014).
- 12 Song, M. S. *et al.* The deubiquitylation and localization of PTEN are regulated by a HAUSP-PML network. *Nature* **455**, 813-817, doi:10.1038/nature07290 (2008).
- 13 Pozhidaeva, A. K. *et al.* Structural Characterization of Interaction between Human Ubiquitin-specific Protease 7 and Immediate-Early Protein ICP0 of Herpes Simplex Virus-1. *The Journal of biological chemistry* **290**, 22907-22918, doi:10.1074/jbc.M115.664805 (2015).
- 14 Cheng, J. *et al.* Molecular mechanism for USP7-mediated DNMT1 stabilization by acetylation. *Nature communications* **6**, 7023, doi:10.1038/ncomms8023 (2015).
- 15 Tavana, O. *et al.* HAUSP deubiquitinates and stabilizes N-Myc in neuroblastoma. *Nat Med* **22**, 1180-1186, doi:10.1038/nm.4180 (2016).
- 16 Wang, L. *et al.* Ubiquitin-specific Protease-7 Inhibition Impairs Tip60-dependent Foxp3+ T-regulatory Cell Function and Promotes Antitumor Immunity. *EBioMedicine* **13**, 99-112, doi:10.1016/j.ebiom.2016.10.018 (2016).
- 17 Williams, A. B. & Schumacher, B. p53 in the DNA-Damage-Repair Process. *Cold Spring Harb Perspect Med* **6**, doi:10.1101/cshperspect.a026070 (2016).



- 336 18 Nawijn, M. C., Alendar, A. & Berns, A. For better or for worse: the role of Pim  
337 oncogenes in tumorigenesis. *Nat Rev Cancer* **11**, 23-34, doi:10.1038/nrc2986  
338 (2011).
- 339 19 Hodges, A. J. M., M.; Sharpe, A.; Sun, M.; Wang, X.; Tsui, V. H. Pyrazol-4-yl-  
340 heterocycl-yl-carboxamide compounds as Pim kinase inhibitors and their  
341 preparation. PCT Int. Appl. WO2013045461 (2013).
- 342 20 Geurink, P. P., El Oualid, F., Jonker, A., Hameed, D. S. & Ovaa, H. A general  
343 chemical ligation approach towards isopeptide-linked ubiquitin and ubiquitin-like  
344 assay reagents. *Chembiochem : a European journal of chemical biology* **13**, 293-  
345 297, doi:10.1002/cbic.201100706 (2012).
- 346 21 Faesen, A. C. *et al.* The differential modulation of USP activity by internal  
347 regulatory domains, interactors and eight ubiquitin chain types. *Chem Biol* **18**,  
348 1550-1561, doi:10.1016/j.chembiol.2011.10.017 (2011).
- 349 22 Huether, R. *et al.* The landscape of somatic mutations in epigenetic regulators  
350 across 1,000 paediatric cancer genomes. *Nature communications* **5**, 3630,  
351 doi:10.1038/ncomms4630 (2014).
- 352 23 Schaefer, J. B. & Morgan, D. O. Protein-linked ubiquitin chain structure restricts  
353 activity of deubiquitinating enzymes. *The Journal of biological chemistry* **286**,  
354 45186-45196, doi:10.1074/jbc.M111.310094 (2011).
- 355 24 Husnjak, K. & Dikic, I. Ubiquitin-binding proteins: decoders of ubiquitin-mediated  
356 cellular functions. *Annual review of biochemistry* **81**, 291-322,  
357 doi:10.1146/annurev-biochem-051810-094654 (2012).
- 358 25 Reverdy, C. *et al.* Discovery of specific inhibitors of human USP7/HAUSP  
359 deubiquitinating enzyme. *Chem Biol* **19**, 467-477,  
360 doi:10.1016/j.chembiol.2012.02.007 (2012).
- 361 26 Yu, M. *et al.* A resource for cell line authentication, annotation and quality control.  
362 *Nature* **520**, 307-311, doi:10.1038/nature14397 (2015).
- 363 27 Wertz, I. E. *et al.* Phosphorylation and linear ubiquitin direct A20 inhibition of  
364 inflammation. *Nature* **528**, 370-375, doi:10.1038/nature16165 (2015).
- 365 28 Haverty, P. M. *et al.* Reproducible pharmacogenomic profiling of cancer cell line  
366 panels. *Nature* **533**, 333-337, doi:10.1038/nature17987 (2016).
- 367 29 Bett, J. S. *et al.* Ubiquitin C-terminal hydrolases cleave isopeptide- and peptide-  
368 linked ubiquitin from structured proteins but do not edit ubiquitin homopolymers.  
369 *The Biochemical journal* **466**, 489-498, doi:10.1042/BJ20141349 (2015).
- 370 30 Iwasaki, T. *et al.* Dissection of hydrogen bond interaction network around an iron-  
371 sulfur cluster by site-specific isotope labeling of hyperthermophilic archaeal  
372 Rieske-type ferredoxin. *J Am Chem Soc* **134**, 19731-19738,  
373 doi:10.1021/ja308049u (2012).
- 374  
375

376 **Figure Legends**

377

378 **Figure 1: Identification and characterization of USP7 inhibitors.** **a.** Schematic of  
379 USP7-regulated signaling. USP7 inhibition increases substrate ubiquitination, leading to  
380 proteasome-mediated substrate degradation. Increased ubiquitination and subsequent  
381 degradation of the MDM2 ubiquitin ligase stabilizes the p53 tumor suppressor, resulting  
382 in cell cycle arrest or cell death. MDM2 is also a p53-target gene. **b.** A schematic of the  
383 USP7 inhibitor hit-to-lead selection cascade. See text for more details. **c.** Left panels:  
384 western blot analysis of MDM2 turnover upon USP7 inhibition. MCF7 cells were treated  
385 with cycloheximide (CHX) for the indicated times with DMSO vehicle or the indicated  
386 compounds. See Extended Data Fig. 1b for corresponding USP7, p53, and p21 western  
387 blots. Right panel: graph showing actin-normalized MDM2 levels from western blots of  
388 three experiments, error bars indicate SD. **d.** Analysis of endogenous MDM2  
389 polyubiquitinated with K48-linked chains. Top panel: denatured lysates from HCT-116  
390 cells treated for 8 hours with the indicated compounds were immunoprecipitated with a  
391 K48 polyubiquitin linkage-specific antibody and immunocomplexes were western blotted  
392 with an anti-MDM2 antibody. Western blot analysis of whole cell lysates for the indicated  
393 proteins are shown below. **e.** Western blot analysis of p53-pathway proteins in wild-type,  
394 USP7 null, or p53-null HCT116 cells after 24-hour treatment with 15 $\mu$ M of the indicated  
395 USP7 inhibitors or inactive controls. At least three experimental replicates were  
396 performed for panels **c.** - **e.**

397

398 **Figure 2: Selectivity of USP7 inhibitors and mechanism of synergy with PIM**  
399 **kinase inhibition.** **a.** An activity heatmap of a panel of deubiquitinases incubated with  
400 USP7 inhibitors. Deubiquitinases at the indicated concentrations were treated with  
401 10 $\mu$ M of the indicated USP7 inhibitor compounds, incubated with di-ubiquitin substrates,  
402 and analyzed by MALDI-TOF mass spectrometry. Detection of monoubiquitin was used  
403 to quantitate deubiquitinase activity, shown in a gradient of white (0% inhibition) to dark  
404 red (100% inhibition). **b.** Volcano plots summarizing activity-based profiling data of  
405 endogenous deubiquitinases treated with USP7 inhibitors. Benjamini-Hochberg False  
406 Discovery Rate-adjusted *p*-values are plotted vs. normalized log<sub>2</sub> fold change in  
407 deubiquitinase activity in 293T cells treated in experimental triplicates (left graph) or  
408 quadruplicates (right graph) with the indicated USP7 inhibitors compared to the indicated  
409 controls. **c.** Bliss analysis of 9x9 dose response matrix with PIM inhibitor GDC-0570 and  
410 GNE-6776 in EOL-1 cells. Left panel: curve fitted viability values at each dose across  
411 the matrix. Zero represents no effect whereas 100 indicates complete loss of viability.  
412 Right panel: the difference in observed versus predicted values using the Bliss  
413 independence model. Positive values indicate a greater than predicted decrease in  
414 viability. **d.** Time course study of EOL-1 cells treated with 2 $\mu$ M GNE-6776, 0.02 $\mu$ M GDC-  
415 0570, or a combination of the two compounds. Cells were collected at the indicated time  
416 points and the indicated proteins were examined by immunoblotting cell lysates. \*\*  
417 indicates uncleaved PARP; \* indicates cleaved PARP. **e.** Analysis of endogenous PIM2  
418 polyubiquitinated with K48-linked chains. Top panel: denatured lysates from EOL-1  
419 cells treated for the indicated times with GNE-6776 were immunoprecipitated with a K48  
420 polyubiquitin linkage-specific antibody and immunocomplexes were western blotted with  
421 an anti-PIM2 antibody. Western blot analysis of whole cell lysates for the indicated  
422 proteins are shown below.

423

424 **Figure 3: USP7 inhibitors compete with ubiquitin binding to USP7.** **a.** Overlay of a  
425 region of the 2D <sup>1</sup>H/<sup>15</sup>N transverse relaxation optimized spectroscopy (TROSY) spectrum  
426 of the USP7 catalytic domain (orange) highlighting changes induced by binding of

427 ubiquitin in the absence (left, blue) and presence of GNE-6776 (middle, dark grey). The  
428 right panel shows the effect of GNE-6776 on labeled USP7 in the absence of ubiquitin in  
429 light gray. Individual peaks stemming from residues E371 and Q287 are highlighted.  
430 Three experimental replicates were performed. **b.** Left panel: crystal structure of USP7  
431 catalytic domain in complex with GNE-6776. The catalytic domain is shown as an  
432 orange cartoon, the ligand as yellow sticks, and the catalytic triad residues are shown as  
433 green sticks with individual atoms colored following CPK color convention. Right panel:  
434 GNE-6776 compound structure. **c.** Left panel: depiction of the USP7 catalytic  
435 domain/ubiquitin complex PDB 1NBF (green and cyan cartoons, respectively) with the  
436 K48 residue side chain in ubiquitin and the acidic patch D305 and E308 in USP7  
437 represented as sticks. Binding interactions are shown as gray dashed lines. Right  
438 panel: the structure of USP7/GNE-6776 (orange cartoon and residue side chains and  
439 yellow sticks, respectively) and the structure of ubiquitin (cyan) modeled in from PDB  
440 1NBF. GNE-6776 sterically blocks the binding of ubiquitin and prevents the hydrogen  
441 bond interaction between ubiquitin-K48 and USP7-D305. The E308 side chain is also  
442 oriented away from ubiquitin-K48.

443

444 **Figure 4: USP7 preferentially binds and cleaves ubiquitin moieties with free K48**  
445 **side-chains. a.** Schematic diagrams of differentially labeled di-ubiquitins (also see  
446 Extended Data Fig. 10b, 10c) and representative 2D  $^1\text{H}/^{15}\text{N}$  SOFAST spectra overlays,  
447 and 1D traces extracted from the  $^1\text{H}$  dimension at the peak maximum. In both K48- and  
448 K63-linked di-ubiquitin schematics, the distal (dist.) ubiquitin has isotopically-labeled  $^{15}\text{N}$ -  
449 Thr residues and the proximal (prox.) ubiquitin has  $^{15}\text{N}$ -Leu residues, marked with  
450 asterisks. Top left panel: K48-linked di-ubiquitin spectra and 1D traces. Di-ubiquitin  
451  $^{15}\text{N}$ -Thr or  $^{15}\text{N}$ -Leu peaks are shown in green; the same peaks after addition of unlabeled  
452 USP7-C223A catalytic domain are overlaid in orange. Top right panel: K63-linked di-  
453 ubiquitin spectra and 1D traces. Di-ubiquitin  $^{15}\text{N}$ -Thr or  $^{15}\text{N}$ -Leu peaks are shown in  
454 purple; the same peaks after addition of unlabeled USP7-C223A catalytic domain are  
455 overlaid in orange. Bottom panels: the SOFAST experiments with K48-linked di-  
456 ubiquitin  $^{15}\text{N}$ -Thr or  $^{15}\text{N}$ -Leu peaks shown in green and the effect of adding the USP7  
457 catalytic domain double mutant C223A/D305A (left) or triple mutant  
458 C223A/D305A/E308A (right) overlaid in orange. The concentration ratios for the top two  
459 experiments were 1:1 at 70 $\mu\text{M}$  ubiquitin, the bottom left was 1:1.5 at 65 $\mu\text{M}$  ubiquitin and  
460 the bottom right was 1:2 at 60 $\mu\text{M}$  ubiquitin. **b.** Time course analysis of peptide-  
461 conjugated tetra-ubiquitin chains cleaved by full-length USP7 (above) and corresponding  
462 densitometry plots (below). Left panels: time course of USP7-mediated  
463 depolymerization of K48-linked tetra-ubiquitin conjugated to a TAMRA-labeled peptide.  
464 Right panels: time course of USP7-mediated depolymerization of K63-linked tetra-  
465 ubiquitin conjugated to a TAMRA-labeled peptide. At least three experimental replicates  
466 were performed.

467

468

469

470

471

472 **Extended Data Figure Legends**

473

474 **Extended Data Figure 1: Deubiquitinase inhibition and cellular activity of**  
475 **optimized fragment compounds.**

476 **a.** A table summarizing deubiquitinase biochemical assay data and ubiquitin-MDM2  
477 assay data from optimized fragment compounds and inactive controls. Fragment  
478 compound structures are shown below. **b.** Western blot analysis of USP7, p53, p21  
479 levels from the cycloheximide (CHX)-chase study of MDM2 turnover shown in Fig. 1c.  
480 **c.** Analysis of endogenous MDM2 polyubiquitinated with K48-linked chains. Top panel:  
481 denatured lysates from MCF7 cells treated for 8 hours with the indicated compounds  
482 were immunoprecipitated with a K48 polyubiquitin linkage-specific antibody and  
483 immunocomplexes were western blotted with an anti-MDM2 antibody. Western blot  
484 analysis of whole cell lysates for the indicated proteins are shown below. **d.** Cell viability  
485 of wild-type and USP7-null HCT116 colon adenocarcinoma cells, treated as indicated,  
486 and analyzed using the CellTiter-Glo assay. Data normalized to vehicle control are  
487 plotted as a function of compound concentration. Two-sided t-tests were used to  
488 calculate *p*-values between wild-type HCT-116 and USP7-null cells treated with GNE-  
489 6640. 7.5 $\mu$ M *p* = 0.01, 10 $\mu$ M *p* = 0.041, 12.5 $\mu$ M *p* = 0.009, 15 $\mu$ M *p* = 0.011, 20 $\mu$ M *p* =  
490 0.017. **e.** Cell viability of wild-type and USP7-null HCT116 colon adenocarcinoma cells,  
491 treated and analyzed as in **d.** with the indicated doses of GNE-6776. 1 $\mu$ M *p* = 0.023,  
492 2.5 $\mu$ M *p* = 0.003, 5 $\mu$ M *p* = 0.001, 7.5 $\mu$ M *p* = 0.003, 10 $\mu$ M *p* = 0.007, 12.5 $\mu$ M *p* = 0.001,  
493 15 $\mu$ M *p* = 0.007, 17.5 $\mu$ M *p* = 0.001, 20 $\mu$ M *p* = 0.008. At least two experimental  
494 replicates were performed.

495

496 **Extended Data Figure 2: Effects of USP7 inhibitors in human primary cells and**  
497 **tumor cell lines.**

498 **a.** Top panels: representative western blots of p53-pathway proteins and tubulin loading  
499 controls in lysates of tumor cell lines and tissue-matched primary cells after 24 hour  
500 treatment with USP7 inhibitors. Lower graphs: bands from p53, p21, and tubulin  
501 immunoblots were quantified and p53 and p21 expression was normalized to tubulin.  
502 The tubulin-normalized p53 or p21 ratio of the DMSO-treated sample in the relevant  
503 primary cell line was arbitrarily set to a value of one. The average relative ratios of  
504 tubulin-normalized p53 or p21 expression levels are plotted for four (breast cell lines) or  
505 three (osteo-cell lines) biological replicate experiments. Asterisks indicate *p*<0.05, two-  
506 sided t-test. **b.** Cell viability of tumor cell lines and tissue-matched primary cells, treated  
507 as indicated, and analyzed using the CellTiter-Glo assay. Data normalized to vehicle  
508 control are plotted as a function of compound concentration. At least three experimental  
509 replicates were performed for panels a and b.

510

511 **Extended Data Figure 3: Selectivity and cellular efficacy of USP7 inhibitors.**

512 **a.** GNE-6776 dose-dependent inhibition of di-ubiquitin cleavage by USP7 measured by  
513 MALDI-TOF and plotted using SigmaPlot v.12.5. **b.** Percent inhibition of the indicated  
514 deubiquitinases for cleaving di-ubiquitins after treatment with 100 $\mu$ M of the indicated  
515 USP7 inhibitor compounds. Deubiquitinase concentrations and di-ubiquitin substrates  
516 are as in Fig. 2a. **c.** Supporting western blots for Fig. 2b, left panel. HEK-293T cell  
517 lysates were treated with the indicated USP7 inhibitors (0.1% DMSO control = 0 $\mu$ M  
518 compound) and endogenous deubiquitinases were reacted with the HA-ubiquitin-  
519 vinylsulfone activity-based probe (HA-Ub-VS). Reacted cell lysates were immunoblotted  
520 with the indicated antibodies. \* indicates unreacted deubiquitinases, \*\* indicates probe-  
521 reacted deubiquitinases, the arrowhead points to a band identified by anti-HA  
522 immunoblotting that runs at the expected molecular weight of USP7 and is diminished in

523 lysates treated with GNE-6640. **d.** Supporting western blots for Fig. 2b, right panel.  
524 HEK-293T cell lysates were treated with the indicated USP7 inhibitors, endogenous  
525 deubiquitinases were reacted with the HA-Ub-VS activity-based probe, and reacted cell  
526 lysates were immunoblotted with the indicated antibodies. \* indicates unreacted  
527 deubiquitinases, \*\* indicates probe-reacted deubiquitinases.

528

529 **Extended Data Figure 4: Bioinformatics analysis of USP7 inhibitor cell viability**  
530 **screens.**

531 **a.** Schematic of the cellular viability assay workflow and bioinformatics analysis. The six  
532 tumor cell line indications included leukemias, lymphomas, lung carcinomas, and breast,  
533 colon, and prostate adenocarcinomas. **b.** Histogram of IC<sub>50</sub> values of GNE-6640, GNE-  
534 6446, and GNE-6641 in 181 cell lines. Mean viability is calculated as the arithmetic  
535 average of the fitted viabilities at each tested dose of GNE-6640 or GNE-6446  
536 normalized to the mean viability of GNE-6641. **c.** Univariate analysis of features  
537 associated with viability differences. The x-axis represents the fold change (log<sub>2</sub>) in  
538 normalized mean viability between cell lines present or absent for a given feature. The  
539 y-axis represents the nominal *p*-value (-log<sub>10</sub> scale). Features with *q*-values less than  
540 0.05 and absolute log<sub>2</sub> fold change greater than 0.1 are colored in red. Features with  
541 only absolute log<sub>2</sub> fold change greater than 0.1 are colored in gold. *P*-values were  
542 determined using the two-sided Student's t-Test and *q*-values were determined by  
543 correcting resulting *p*-values for multiple hypothesis testing using the Benjamini and  
544 Hochberg approach. The size of each point corresponds to the number of cell lines  
545 present with the feature. **d, e.** Boxplots of selected features and their respective  
546 associations with normalized mean viability. The respective *p*- and *q*-values are  
547 indicated below.

548 **Extended Data Figure 5: Live cell imaging of USP7 inhibitor-treated cells.**

549 Graphs showing cell confluence as a function of time (top rows) and normalized caspase  
550 activity (bottom rows) in cells treated with the indicated USP7 inhibitors. **a.** TP53 wild-  
551 type or TP53 null HCT116 colon adenocarcinoma cells. **b.** TP53 wild-type MCF7 or  
552 TP53 null MDA-MB157 breast adenocarcinoma cells. **c.** TP53 wild-type U2OS cells or  
553 TP53 null SaOS osteosarcoma cells. At least three experimental replicates were  
554 performed for all experiments.

555

556 **Extended Data Figure 6: Viability of USP7 inhibitor-treated cells in combination**  
557 **with chemotherapeutic and targeted agents.**

558 Graphs showing cell confluence as a function of time (top rows) and normalized caspase  
559 activity (bottom rows) in cells treated with the indicated USP7 inhibitors and/or  
560 chemotherapeutics. **a.** MCF7 breast adenocarcinoma cells treated with GNE-6640 or  
561 doxorubicin alone or in combination. **b.** U2OS osteosarcoma cells treated with GNE-  
562 6640 or cisplatin alone or in combination. At least three experimental replicates were  
563 performed for all experiments. **c.** A pie chart illustrating the distribution of compound  
564 classes in the Genentech Chemical Genomics Compound library, comprising 589  
565 compounds. NHR = nuclear hormone receptor, GEF = guanine nucleotide exchange  
566 factor, DNA = DNA damaging agent. **d.** Bar plot visualizing the -log<sub>10</sub> transformed *p*-  
567 value from the Wilcoxon rank sum test evaluating the enrichment of a given compound  
568 target over all concentrations of USP7 inhibitors vs. DMSO experiments in EOL-1 cells.  
569 Only compound targets with 3 or more compounds in the screen were visualized. Higher  
570 values indicate synergy with USP7 inhibitors and were followed up by Bliss analysis.  
571 Compounds common to certain signaling pathways including PI3K/PIM, RTK/MAPK,  
572 epigenetic regulation, and DNA damage are color-coded as indicated.

573 **Extended Data Figure 7: Mechanism of action studies with USP7 inhibitor and PIM**  
574 **inhibitor combinations.** **a.** Compound structure of GDC-0339. **b.** PIM inhibitor  
575 viability curves at different fixed doses of GNE-6676 in EOL-1 cells. **c.** Bliss analysis of  
576 9x9 dose response matrix with PIM inhibitor GDC-0339 and GNE-6776 in EOL-1 cells.  
577 Left panel: curve-fitted viability values at each dose across the matrix. Zero represents  
578 no effect whereas 100 indicates complete loss of viability. Right panel: the difference in  
579 observed versus predicted values using the Bliss independence model. Positive values  
580 indicate a greater than predicted decrease in viability. **d.** A schematic of the PI3K  
581 signaling pathway and regulation by PIM kinases. PIM and AKT kinases regulate Bad  
582 and TSC1/2 phosphorylation status. Phospho-proteins highlighted in yellow were  
583 profiled in cellular studies shown in Figure 2d. **e.** Immunoblot analysis of cell lysates  
584 from the indicated cell lines treated with GNE-6776 (2 $\mu$ M for 18 hours), a UAE1 inhibitor  
585 MLN-7243 (5 $\mu$ M for 45 minutes) or the proteasome inhibitor bortezomib (5 $\mu$ M for 45  
586 minutes). **f.** Immunoblot analysis of cell lysates from the indicated cell lines, either  
587 untreated or treated with the proteasome inhibitor bortezomib (5 $\mu$ M for 45 minutes). **g.**  
588 Immunoprecipitation of cellular lysates using an anti-USP7 antibody or an isotype-  
589 matched control antibody indicates a specific interaction between endogenous USP7  
590 and PIM2. **h.** Wild-type recombinant USP7, but not a catalytically inactive USP7 mutant,  
591 deubiquitinates endogenous polyubiquitinated PIM2 that was immunoprecipitated from  
592 proteasome inhibitor-treated MV-4-11 cells.

593

594 **Extended Data Figure 8: Enzymatic analysis and supporting structural biology**  
595 **data for USP7 inhibitors and USP7.**

596 **a.** Michaelis-Menten kinetic analysis of USP7 and a series of ubiquitin-AMC substrate  
597 titrations with the indicated USP7 inhibitors. Initial rate of substrate hydrolysis was  
598 determined using the Magellan software on a Tecan Safire2 plate reader and kinetic  
599 parameters were modeled using nonlinear regression analysis with GraphPad Prism  
600 software. Standard error was calculated from at least 3 experimental replicates. **b.**  
601 Affinity values of ubiquitin binding to USP7 catalytic domain in the absence and  
602 presence of USP7 inhibitors. The values were determined by titration of unlabeled  
603 ubiquitin to labeled USP7 catalytic domain and the NMR chemical shift changes were  
604 fitted as described in the methods. Standard error was calculated from at least 3  
605 experimental replicates. **c.** Overlay of a region of the 2D  $^1\text{H}/^{15}\text{N}$  transverse relaxation  
606 optimized spectroscopy (TROSY) spectrum of the USP7 catalytic domain (orange)  
607 highlighting changes induced by binding of ubiquitin in the absence (left, blue) and  
608 presence of GNE-6640 (right, black). Individual peaks stemming from residues E371  
609 and Q387 are highlighted. Three experimental replicates were performed. **d.**  
610 Comparison of the crystal structure of USP7 catalytic domain in complex with GNE-6640  
611 (cyan) and GNE-6776 (yellow). The catalytic domain is shown as an orange cartoon and  
612 the side chains of the residues in proximity to the inhibitor binding sites are shown as  
613 orange sticks. GNE-6640 and GNE-6776 compound structures are indicated above. **e.**  
614 Data collection and refinement statistics for GNE-6440 and GNE-6776 crystal structures  
615 with the USP7 catalytic domain.

616

617 **Extended Data Figure 9: Analysis of the functional significance of the interactions**  
618 **between ubiquitin-K48 and USP7-D305, -E308 residues.**

619 **a.** Titration curves showing the effect of unlabeled wild-type ubiquitin (top) and ubiquitin  
620 K48A (bottom) addition to [ $^2\text{H}/^{15}\text{N}$ ] labeled USP7 catalytic domain. The weighted  
621 combined  $^1\text{H}/^{15}\text{N}$  chemical shift change is plotted against the ubiquitin concentration for  
622 5 well-resolved peaks stemming from E371, Q387, A381, D342 and Y339 residues in the  
623  $^{15}\text{N}$  TROSY spectrum. Standard error was calculated from at least three experimental

624 replicates. **b.** Time course analysis of peptide-conjugated tetra-ubiquitin chains reacted  
625 with the USP7 catalytic domain D305A/E308A mutant. **c.** Michaelis-Menten analysis of  
626 USP7 catalytic domain D305A/E308A mutant showing the results of three independent  
627 experiments. **d.** Evaluation of endogenous MDM2 ubiquitination status upon expression  
628 of wild-type, C223A, or D305A/E308A full-length USP7. Top panel: denatured lysates  
629 from MCF7 cells transfected with the indicated USP7 expression constructs were  
630 immunoprecipitated with a K48 linkage-specific antibody and immunocomplexes were  
631 blotted with an MDM2 antibody. Western blot analysis of whole cell lysates for the  
632 indicated proteins are shown below. Three experimental replicates were performed.

633

634 **Extended Data Figure 10: Analysis of differential USP7 binding to K48- and K63-**  
635 **linked poly-ubiquitin and depolymerization kinetics.**

636 **a.** Schematic diagrams of substrate-bound K48-linked polyubiquitin chains (left) and  
637 K63-linked chains (right), and proposed USP7 interactions. Dashed lines indicate  
638 residue side-chains and the • symbol indicates an isopeptide bond between the ubiquitin  
639 C-terminus and a Lys residue side chain. The proximal ubiquitin subunits (ligated to the  
640 substrate) and their K48 or K63 side-chains are indicated with “a” subscripts, the next  
641 most distal ubiquitin subunits and side-chains are indicated with “b” subscripts, etc.  
642 Preferential USP7 binding to free K48 side-chains would direct USP7 to the distal  
643 ubiquitin subunit of K48 polyubiquitin and promote sequential exo-cleavage, whereas  
644 USP7 would bind all subunits of K63-polyubiquitin and promote exo-, endo-, and base-  
645 cleavage. **b.** The  $^1\text{H}/^{15}\text{N}$  SOFAST spectrum of labeled ubiquitin (cyan), superimposed  
646 with the spectrum of a 1:1 molar ration of labeled ubiquitin in the presence of unlabeled  
647 USP7-catalytic domain (orange). Ubiquitin residues affected by the USP7 interaction,  
648 that results in exchange broadening of the residue cross peaks, are labeled with grey or  
649 blue text and correspond to the residues depicted in Extended Data Fig. 10c. The K48  
650 and K63 residues are labeled with red font; the L43 and L50 residues labeled with green  
651 font do not broaden upon USP7 binding and serve as internal controls. The box  
652 highlights the region depicted in Fig. 4a. **c.** Structure depictions by ribbon diagrams of  
653 the covalent complex between USP7 catalytic domain (orange) with ubiquitin (cyan);  
654 (PDB code 1NBF) [top panel], K48 linked di-ubiquitin (green; PDB code 2KDE) [lower left  
655 panel], and K63 linked di-ubiquitin (purple; PDB code 2RR9) [lower right panel]. In all  
656 diagrams, highlighted spheres are the residues in ubiquitin that are broadened in the  
657  $^1\text{H}/^{15}\text{N}$  SOFAST spectrum of  $^1\text{H}/^{15}\text{N}$  labeled protein by addition of unlabeled USP7  
658 catalytic domain (see Extended Data Fig. 10b for more details). Leu or Thr residues  
659 colored in blue show well-resolved peaks and were amenable to selective  $^{15}\text{N}$  labeling of  
660 di-ubiquitin, highlighted with asterisks in the corresponding schematic diagrams. Lysine  
661 side chains of K48 and K63 are indicated as sticks in red. **d.** Time course analysis of  
662 peptide-conjugated tetra-ubiquitin chains cleaved by the USP7 catalytic domain (above)  
663 and corresponding densitometry plots (below). Left panels: time course of USP7  
664 catalytic domain-mediated depolymerization of K48-linked tetra-ubiquitin conjugated to a  
665 TAMRA-labeled peptide. Right panels: time course of USP7 catalytic domain-mediated  
666 depolymerization of K63-linked tetra-ubiquitin conjugated to a TAMRA-labeled peptide.  
667 **e.** A shorter 0 – 7 minute time-course analysis of TAMRA peptide-K63 tetra-ubiquitin  
668 conjugate depolymerization by full-length USP7 (top gel) and the corresponding  
669 densitometry plot (below). At least three experimental replicates were performed.

670 **Supplementary Information figure legends and summary**

671  
672 **Supplementary Information Figure 1: Screening cascades for USP7 inhibitors.**

673 **a.** High-throughput activity-based screening cascade to identify USP7  
674 inhibitors. Screening stages are identified in bold print. Numbers of compounds at each  
675 stage are provided to the right of each box. Criteria for progression to the next stage are  
676 highlighted in italics to the left of each arrow. **b.** Confirmed hits from USP7  
677 screen. Structures and assay results are provided for 5 of the 101 confirmed  
678 actives. The compounds were clustered by structural similarity. IC<sub>50</sub> values and Hill  
679 slopes were determined from 10-point dose titrations with n=2. **c.** Fragment NMR  
680 screen diagram. Screening stages are identified in bold print. Numbers of compounds  
681 at each stage are provided to the right of each box. Criteria for progression to the next  
682 stage are highlighted in italics to the left of each arrow. Protein Saturation Transfer  
683 Difference (STD) experiments were performed at 283K. Primary USP7 catalytic domain  
684 binders were selected based on the signal to noise (S/N) of the respective compound  
685 with a cut-off of greater than 5. All primary binders were re-measured as single  
686 compounds under otherwise identical conditions and confirmed binders selected having  
687 a S/N of greater than 10. Hits were further tested for specific binding to USP7 catalytic  
688 domain by measurement of <sup>1</sup>H<sup>15</sup>N TROSY protein spectra. Positive hits were defined as  
689 compounds that induced chemical shift perturbations. Perturbations were classified by  
690 the chemical shift patterns and selected compounds passed onto X-ray soaking  
691 experiments.

692  
693 **Supplementary Information Figure 2: Hit-to-lead selection assay data summary**  
694 **for lead USP7 inhibitors.**

695 A table summarizing the hit-to-lead assay results of the lead compounds identified by the  
696 high throughput screening and NMR fragment screening campaigns. Compound series  
697 are grouped in columns and hit-to-lead selection assay data are listed in the indicated  
698 rows. See Fig. 1b and text for more details.

699  
700 *Indole tricyclic compounds including GNE-8735 increased total MDM2 levels and*  
701 *inhibited cathepsin-B, indicating poor selectivity and induction of general cell stress by*  
702 *this chemical series (see also Supplementary Information Fig. 3a and 3b). Indole*  
703 *tricyclics also precipitated caspase-3, although they passed dynamic light scattering*  
704 *(DLS) analysis (see also Supplementary Information Fig. 4a). The peptidomimetic*  
705 *compounds had weaker biochemical potency, poor selectivity, and covalently modified*  
706 *USP7 cysteine (Cys) residues other than the catalytic Cys (data not shown). Given*  
707 *these data, and because optimization of indole tricyclic and peptidomimetic compounds*  
708 *proved challenging, these series were discontinued. The tetrahydroacridine and*  
709 *fragment compounds were relatively potent, selective, and enhanced cellular MDM2*  
710 *ubiquitination without significantly increasing total MDM2 (see also Supplementary Fig.*  
711 *3a and 3b). Tetrahydroacridine compounds passed cathepsin-B inhibition assays,*  
712 *demonstrating additional protease selectivity. Neither tetrahydroacridine nor fragment*  
713 *compounds showed evidence of USP7 aggregation in DLS or in NMR studies (see*  
714 *Supplementary Fig. 4a and data not shown). Tetrahydroacridine compounds, including*  
715 *GNE-6831, covalently modified USP7, consistent with a previous report describing a*  
716 *similar series*<sup>25</sup> *(see also Supplementary Information Fig. 4b).*



720 **Supplementary Information Figure 3: Analysis of total- and ubiquitin-MDM2 levels**  
721 **in cells.**

722 **a.** Cellular MDM2 immunofluorescence studies. HCT-116 human colorectal carcinoma  
723 cells were treated with a range of concentrations of the indicated USP7 inhibitors or  
724 DMSO vehicle for 24 hours and endogenous MDM2 protein levels were detected by  
725 immunofluorescence imaging. Depicted images show cells treated with 10  $\mu$ M of the  
726 indicated compounds or DMSO vehicle control. The graph shows the quantified mean  
727 nuclear MDM2 protein levels per cell over a range of concentrations of GNE-8735 and  
728 GNE-2916 (error bars represent standard deviation). The half maximal effective  
729 concentration ( $EC_{50}$ ) for the elevation in MDM2 caused by GNE-8735 was 2.9  $\mu$ M. **b.**  
730 Quantitation of total- and ubiquitinated-MDM2 (Ub-MDM2) in USP7 inhibitor-treated  
731 cells. SJSA-1 human osteosarcoma cells were treated with a range of concentrations of  
732 the indicated USP7 inhibitors or DMSO vehicle control for 24 hours and the level of  
733 ubiquitinated-MDM2 and total MDM2 were measured using a multiplexed Mesoscale  
734 immunoassay. Representative graphs show the quantified level of either total MDM2  
735 (right column, red), ubiquitinated MDM2 (central column, blue) or the ratio of the  
736 ubiquitinated-MDM2 signal and the total MDM2 signal (left column, orange). All data are  
737 shown as percentage change in each value, relative to DMSO vehicle-treated samples.  
738 The maximal extent of the increase in the ubiquitinated-MDM2/total MDM2 ratio varied  
739 between compounds and in most cases did not reach a plateau. In order to compare the  
740 potency of the on the increase in the ratio of ubiquitinated-MDM2/total MDM2 between  
741 compounds, the top level was set to 100% and was universally applied to calculate a  
742 value for the half maximal effective concentration ( $EC_{50}$ ) of the percent change in this  
743 ratio relative to DMSO (shown in the left column). At least two experimental replicates  
744 were performed.

745  
746 **Supplementary Information Figure 4: Biophysical analysis of selected USP7**  
747 **inhibitors.**

748 **a.** The DLS autocorrelation functions are shown for 100 $\mu$ M Rottlerin (red), full-length  
749 USP7 with 100 $\mu$ M GNE-8735 (blue), full-length USP7 with 100 $\mu$ M GNE-2090 (brown)  
750 and full-length USP7 with 0.1% DMSO vehicle control (black). The percent aggregate by  
751 mass is shown in the table. **b.** USP7 full-length protein was incubated overnight with  
752 excess of GNE-6831 and analyzed by LC-MS. Unmodified and covalently modified  
753 USP7 are represented in the top and bottom panels, respectively. Three experimental  
754 replicates were performed.

755  
756 **Supplementary Information Figure 5: Deubiquitinase inhibition, ubiquitin-MDM2,**  
757 **and cellular viability data for tetrahydroacridine and fragment compounds.**

758 **a.** A table of active and inactive tetrahydroacridine compounds with structures. Hit-to-  
759 lead selection assay data are listed in the indicated rows. See Fig. 1b and text for more  
760 details. **b.** A table of active and inactive fragment compounds with structures. Hit-to-lead  
761 selection assay data are listed in the indicated rows. See Fig. 1b and text for more  
762 details. **c.** Cell viability assays in AMO-1 cells treated as indicated with the  
763 tetrahydroacridine compounds (top graph; purple lines are inactive controls and the  
764 green line is the active compound) and fragment compounds (bottom graph; red lines  
765 are inactive controls and the blue line is the active compound). Data normalized to  
766 vehicle control are plotted as a function of compound concentration. **d.** Cell viability  
767 assays in KMS12-PE cells treated as indicated with the tetrahydroacridine compounds  
768 (top graph; purple lines are inactive controls and the green line is the active compound)  
769 and fragment compounds (bottom graph; red lines are inactive controls and the blue line

770 is the active compound). Data normalized to vehicle control are plotted as a function of  
771 compound concentration. At least two experimental replicates were performed.

772

773 *Tetrahydroacridine compounds GNE-6831 and GNE-2090 decreased viability of KMS12-*  
774 *PE and AMO1 multiple myeloma cell lines but this activity was not differentiated from*  
775 *control compounds GNE-0956, -2143 and -2148. In contrast, the fragment compound*  
776 *GNE-2916 decreased multiple myeloma cell viability significantly more than control*  
777 *compounds GNE-2917, -2931, and -9603. Thus work on tetrahydroacridine series was*  
778 *discontinued and we focused on optimizing the fragment series.*

779

780 **Supplementary Information Figure 6: *in vitro* and *in vivo* drug metabolism and**  
781 **pharmacokinetic (DMPK) profiling, pharmacodynamic effects, and xenograft**  
782 **growth inhibition studies with GNE-6776.**

783 **a.** *In vitro* pharmacokinetic assessment of USP7 inhibitors. Calculated drug properties  
784 are indicated: molecular weight (MW), lipophilicity at pH 7.4 ( $\text{LogD}_{7.4}$ ), total polar surface  
785 area (tPSA), stability in hepatic microsomes (LM  $\text{CL}_{\text{hep}}$ ) or hepatocytes (Hep  $\text{CL}_{\text{hep}}$ ) from  
786 human/rat/mouse/dog/cyno (h/r/m/d/c) species, percent plasma protein binding (PPB %) and permeability across an MDCK cell monolayer from basolateral to apical (B to A) or apical to basolateral (A to B) directions. **b.** EOL-1 cell line viability in response to GNE-6776 as measured in a five-day CellTiterGlo assay performed in triplicate. **c.** *In vivo* pharmacokinetic analysis of GNE-6776. Mice (3 per group) were dosed PO with 100 mg/kg or 200 mg/kg of GNE-6776. Plasma concentrations of GNE-6776 were measured at the indicated time points and plotted as a function of time. Exposure metrics relating to the free fraction EC50 for EOL-1 cells are also indicated, where target exposure = (EOL-1 IC50)/(1 - %PPB) =  $1.54\mu\text{M}/0.066 = 23.33\mu\text{M}$ . **d.** Western blot analysis of MCF7-Ser xenografted tumors. Mice harboring MCF7-Ser xenograft tumors were treated with vehicle or 200 mg/kg GNE-6776 at 0 and 4 hours; 8 hours after the initial treatment tumors were excised and the indicated proteins were examined by immunoblotting tumor lysates. **e.** Pharmacodynamic analysis of USP7 inhibitor-treated EOL-1 xenografted tumors. Mice growing EOL-1 xenograft tumors were dosed by mouth with vehicle or 200 mg/kg GNE-6776 at 0 and 4 hours; 8 hours after the initial treatment tumors were excised and the indicated proteins were examined by immunoblotting tumor lysates. **f.** EOL-1 xenograft growth inhibition study of mice treated PO with vehicle or the indicated doses of GNE-6776.  $n = 7$  mice per group,  $p$ -values were calculated using Dunnett's multiple comparison test. Asterisks indicate significant growth inhibition relative to vehicle-treated mice. Day 4 100 mg/kg  $p = 0.0163$ , Day 4 200 mg/kg  $p = 0.0138$ , Day 6 200 mg/kg  $p = 0.0344$ .

807

808 **Supplementary Table 1**

809 This table summarizes the results of the compound library combination screen  
810 performed in EOL-1 cells in the presence of either DMSO or varying concentrations of  
811 GNE-6776 or GNE-6640. Column headers denote compound used and concentration  
812 used (ie. 1000nM\_6776 indicates 1000 nM of GNE-6776 treatment in combination with  
813 each compound). For each compound treatment, two summary statistics are listed that  
814 are derived from 9-point dose response curves: IC50 is the determined IC50 value of  
815 the dose response curve. This is set to the highest concentration applied if no IC50 was  
816 attained. Mean viability is the mean over all 9 dose viability measures. For each non-  
817 DMSO treatment two values are calculated to indicate synergy between the library  
818 compound and the USP7 inhibitor tested: mvdif indicates the difference in mean  
819 viability between the DMSO treatment and the USP7 inhibitor. Positive values indicate a  
820 lower viability in the USP7-treated condition, which indicates synergism. Log2fc

821 indicates the log2 ratio between the IC50 value of the DMSO treatment and the USP7  
822 treatment. Negative values indicate lower IC50s for the USP7 treatment, also signaling  
823 synergism. All unique compounds are assigned an internal gcgcid (Genentech Chemical  
824 Genomics Compound ID) for tracking purposes. Common drug names are shown in the  
825 compound\_name column and either protein or functional targets of the compound,  
826 where known, are listed in the target\_name column.  
827

828 **Methods**

829

830 ***High-throughput screen (HTS) and counterscreen assays***

831 *USP7 UbA10 TR-FRET activity assay.* Potential inhibitors of USP7 were identified in a  
832 TR-FRET-based enzyme activity assay with UbA10 as substrate. UbA10 is a fragment  
833 of the naturally occurring ubiquitin precursor, Ub52; it retains the 10 amino acid segment  
834 of Ub52 that extends beyond the ubiquitin C-terminus. The primary screening assay is a  
835 novel TR-FRET based activity assay that measures cleavage by full-length USP7 of a  
836 doubly-tagged peptide substrate. The peptide is tagged with GST on the N-terminus  
837 and with eight histidine residues on the C-terminus (GST-UbA10-His). The tags are  
838 detected by anti-GSH-d2 (TR-FRET acceptor) and anti-His-europium (TR-FRET donor),  
839 respectively. Cleavage of this substrate by USP7 at the ubiquitin C-terminus results in  
840 separation of these two tags and loss of TR-FRET signal. Compounds were dispensed  
841 into 1536-well black plates (MaKO, Aurora Microplates, Whitefish, MT) followed by 2 $\mu$ L  
842 full-length recombinant USP7 in assay buffer (50 mM HEPES pH 7.5, 0.1% Prionex  
843 [Pentapharm, Basel, CH], 0.01% Triton X-100, and 10 mM DTT). After a 10-minute  
844 incubation, the reaction was started by the addition of 2 $\mu$ L GST-UbA10-His substrate in  
845 assay buffer. After 75 minutes of reaction, 2 $\mu$ L of a detection antibody reagent,  
846 containing anti-His-europium (Life Technologies, Carlsbad, CA) and anti-GST-d2  
847 (CISbio, Bedford, MA) in assay buffer were added. After 60 minutes, the fluorescence at  
848 618 nm and 671 nm with excitation at 340 nm was read on a ViewLux reader  
849 (PerkinElmer, Waltham, MA). Cleavage of the doubly-tagged substrate resulted in loss  
850 of TR-FRET signal, while inhibition of USP7 by compound restored the signal. The TR-  
851 FRET ratio was calculated as fluorescence at 671 nm/ fluorescence at 618 nm. TR-  
852 FRET ratios were normalized to controls to determine percent inhibition for the single  
853 concentration screen. For confirmation in concentration-response mode (10 points with  
854 N = 2), percent inhibition was plotted against compound concentration, and the data  
855 were fit to a 4-parameter curve with Screener Assay Analyzer (Genedata, Basel, CH) to  
856 determine IC<sub>50</sub> values. The assay buffer was optimized to maintain enzyme stability and  
857 to maximize assay signal to background: Triton X-100 was included to prevent  
858 nonspecific adsorption of the enzyme and/or substrate to the assay plate and/or to  
859 compound aggregates, Prionex carrier protein was included to help stabilize the enzyme  
860 and to prevent nonspecific adsorption to container and tubing surfaces as well as to  
861 minimize nonspecific inhibition by library compounds, and DTT served to maintain good  
862 USP7 activity and minimize the impact of inhibitors that act through redox cycling.  
863 Reagent concentrations were optimized for good assay performance at approximately  
864 50% substrate conversion in the signal decrease assay with a key aim of minimizing the  
865 required concentration of USP7. The GST-UbA10-His concentration was adjusted to  
866 maximize assay signal, anti-GST-d2 concentration was adjusted approximately in  
867 parallel with that of the substrate, and anti-His-europium was used at a concentration  
868 that represented a minimum that is compatible with robust detection on the ViewLux  
869 plate reader. Time course evaluations were conducted to confirm that the enzyme  
870 concentration (10 nM) and reaction time (75 minutes) were in the linear range of enzyme  
871 activity. Additionally, extended time courses for the detection reaction were used to  
872 demonstrate that the 60-minute incubation was sufficient to reach equilibrium. Under the  
873 final assay conditions, reagent stability studies indicated greater than 20 hours of  
874 acceptable performance. Over the course of the screen, Z' values averaged 0.76.

875

876 *USP7 di-ubiquitin FRET activity assay.* Potential USP7 inhibitors were confirmed in an  
877 orthogonal activity assay with an internally quenched K63-linked di-ubiquitin substrate  
878 (U-310, Boston Biochem, Cambridge, MA). Conditions were similar to those used for the

879 UbA10 TR-FRET activity assay. Compounds dispensed into 1536-well plates were  
880 preincubated with full-length recombinant USP7 in assay buffer for 10 minutes, and the  
881 reaction was started by the addition of 2 $\mu$ L of the di-ubiquitin substrate. During the 60-  
882 minute incubation, cleavage of the substrate by USP7 resulted in the release of  
883 quenching of the TAMRA tag by the QXL tag and thus an increase in fluorescence. The  
884 fluorescence intensity was read with excitation at 540 nm and emission at 585 nm.  
885 Concentration-response assay methods and data analyses were conducted as for the  
886 UbA10 TR-FRET assay.

887

888 *USP7 Ubiquitin/Rho110 activity assay.* Potential USP7 inhibitors were also confirmed in  
889 an orthogonal activity assay with ubiquitin/rhodamine-110 as substrate. Compounds  
890 were preincubated for 10 minutes with 2 $\mu$ L full-length recombinant USP7 in assay buffer,  
891 and the reaction was started by the addition of 2 $\mu$ L of ubiquitin/rhodamine-110 (U-555,  
892 Boston Biochem). After a 60-minute reaction in which USP7 cleaves the rhodamine-110  
893 from the ubiquitin and thus increases fluorescence, the fluorescence intensity was read  
894 with excitation at 485 nm and emission at 535 nm. General assay conditions and data  
895 analyses were as described above.

896

897 *USP7 di-ubiquitin cleavage assay with mass spectrometric detection.* To further validate  
898 compounds that met the initial HTS confirmation criteria, the ability of compounds to  
899 inhibit di-ubiquitin cleavage was assessed by monitoring the conversion to ubiquitin by  
900 mass spectrometry. Compounds were dispensed into 384-well polypropylene plates  
901 (Greiner Bio-One, Kremsmunster, AT), and 10 $\mu$ L USP7 were added and allowed to  
902 incubate for 10 minutes. The reaction was started by the addition of 10 $\mu$ L of K48-linked  
903 di-ubiquitin substrate (UC-200, Boston Biochem) and allowed to progress for 70 minutes;  
904 then it was stopped by addition of 20 $\mu$ L 2% formic acid. The assay plates were stored  
905 frozen at -80 °C until analysis by mass spectrometry at Agilent Technologies (Wakefield,  
906 MA). Prior to quantitation, the enzyme reaction was passed over a RapidFire cartridge  
907 to remove buffer components. Both di-ubiquitin substrate consumption and ubiquitin  
908 product formation were monitored by mass spectrometry using multiple reaction  
909 monitoring (MRM) in positive ion mode with parent ion/daughter ion transitions of  
910 1142.1/260.1 and 770.8/817.7, respectively. Percent conversion of substrate was  
911 plotted as a function of compound concentration to generate the IC<sub>50</sub> values as indicated  
912 above.

913

#### 914 ***NMR screen and binding studies***

915 All NMR spectra were recorded on Bruker Avance-600 and 800 MHz spectrometers  
916 operating at 14.1 and 18.8 Tesla using triple resonance cryogenic probes optimized for  
917 proton detection. All two-dimensional spectra were acquired with a spectral width of 16  
918 ppm and 2048 (TROSY) or 954 (SOFAST) data points in the direct proton dimension  
919 and 28 ppm and 192 sample points in the <sup>15</sup>N dimension with echo-antiecho (TROSY) or  
920 States-TPPI (SOFAST) type selection. The resulting free induction decay resolution was  
921 12.52 and 19.05 Hz point for the TROSY and 20.08 and 17.10 Hz/data point for the  
922 SOFAST spectra respectively. All spectra were recorded at 300 K. The pH was adjusted  
923 to 7.2 without correction due to isotope shifts. For data processing NMRPipe/NMRDraw  
924 and the BRUKER software package TOPSPIN 3.2 were used. All data evaluation was  
925 done in NMR view and CCPN. Visualization and presentation of the 3D tertiary USP7-as  
926 well as related protein structures from the RSCB Protein Database was done in Pymol  
927 (The PyMOL Molecular Graphics System, Version 1.7.4 Schrödinger, LLC). The  
928 sequential assignment of USP7 has been deposited in the Biological Magnetic  
929 Resonance Bank and can be retrieved with the accession number 26766. All samples

930 contained 137 mM NaCl, 10 mM Na<sub>2</sub>HPO<sub>4</sub>, 27 mM KCl and 1.8 mM KH<sub>2</sub>PO<sub>4</sub> adjusted to  
931 a pH of 7.2 and contained 7% (w/w) <sup>2</sup>H<sub>2</sub>O and 0.5 μM NaN<sub>3</sub>. Ubiquitin titration  
932 experiments were done by addition of purified bovine ubiquitin (from erythrocytes,  
933 Sigma) from a stock solution of 20mM in the same buffer. All proton chemical shifts were  
934 referenced to internal DSS (50 μM) and <sup>15</sup>N referenced indirectly using the <sup>1</sup>H chemical  
935 shift of the methyl group in DSS by multiplication with a factor of 0.101329118.

936  
937 *NMR screening conditions.* The primary fragment screen was performed on 4871  
938 fragments in mixtures of 5. The individual compound concentration was 500μM, the  
939 concentration of unlabeled USP7-CD was 7μM. Binders were identified by the presence  
940 of signals stemming from the individual ligand in the proton saturation transfer difference  
941 spectra recorded at 284K. The criterion used to identify a binder was a signal to noise  
942 ratio above 5. All primary binders were re-measured as a single compound to confirm  
943 binding. Confirmed binders were defined as compounds with an STD signal to noise  
944 ratio above 10. All confirmed binders were tested again, at 2-2.5mM, by protein  
945 observed <sup>1</sup>H/<sup>15</sup>N TROSY experiments in the presence of <sup>15</sup>N USP7-CD at 220-340uM.

946  
947 *NMR binding studies.* The concentration-dependent NMR shift perturbations caused by  
948 the interaction of unlabeled ubiquitin with labeled USP7 catalytic domain in the absence  
949 and presence of USP7 inhibitors were fit to the function for a two state fast exchanging  
950 equilibrium:

951  $(\Delta\delta = \Delta\delta_{max} \frac{K_d + [P] + [L] - \sqrt{(K_d + [P] + [L])^2 - 4[P][L]}}{2[P]})$  where  $\Delta\delta$  is the chemical shift change at  
952 various protein/ligand ratios,  $\Delta\delta_{max}$  is the chemical shift change at saturation,  $K_d$  is the  
953 dissociation constant, and [L] and [P] are the ligand and protein concentrations,  
954 respectively. The chemical shift change is the root mean square of the <sup>1</sup>H and <sup>15</sup>N values  
955 scaled by 1 and 0.15 respectively. Seven ubiquitin concentrations were measured (0,  
956 100, 250, 500, 750, 1000, 2500uM). USP7 inhibitors were added at 1mM. The mean  
957 values and standard deviation were calculated by averaging the values obtained for  
958 eight well-resolved cross peaks: Y339, S341, D342, G375, A381, G382, D412, and  
959 I419. Data were visualized using GraphPad Prism.

960

### 961 **Compound synthesis**

962 *Synthesis of GNE-6640 is representative of the syntheses for GNE-6776, GNE-6641,*  
963 *GNE-2931, GNE-2917, and GNE-2916.*

964 **3,5-Dibromo-4-ethylpyridin-2-amine:** Into a 500-mL 3-necked round-bottom flask  
965 purged and maintained with an inert atmosphere of nitrogen was placed 4-ethylpyridin-2-  
966 amine (10 g, 81.85 mM), tetrahydrofuran (200 mL), and NBS (29 g, 162.94 mmol) at 0  
967 °C. The resulting solution was stirred at room temperature for 15 min and then  
968 concentrated under vacuum. The residue was purified on a silica gel column eluting with  
969 DCM/MeOH (100:1-20:1) to afford 18 g (79%) of the title compound. <sup>1</sup>H NMR (400 MHz,  
970 CDCl<sub>3</sub>) δ 8.04 (s, 1H), 7.33 – 7.23 (m, 0H), 4.93 (s, 2H), 2.93 (q, *J* = 7.5 Hz, 2H), 1.60 (s,  
971 0H), 1.17 (t, *J* = 7.5 Hz, 3H). LCMS (ESI M/Z): 264.1 (M + H<sup>+</sup>).

972 **3-Bromo-4-ethylpyridin-2-amine:** Into a 500-mL 3-necked round-bottom flask purged  
973 and maintained with an inert atmosphere of nitrogen was placed 3,5-dibromo-4-  
974 ethylpyridin-2-amine (18 g, 64.29 mmol) in tetrahydrofuran (300 mL). To this was added  
975 a solution of n-BuLi (in hexane) (58 mL, 2.2 mol/L) at -78 °C. The resulting solution was  
976 stirred at -78°C for 1 h, quenched by the addition of 450 mL NH<sub>4</sub>Cl and then extracted  
977 with ethyl acetate (2 x 500 mL). The combined organic layers were washed with brine (2  
978 x 500 mL), dried over anhydrous sodium sulfate and concentrated under vacuum. The  
979 crude product was purified by Flash-Prep-HPLC to afford 12 g (93%) of the title

980 compound as a white solid. <sup>1</sup>H NMR (400 MHz, CDCl<sub>3</sub>) δ 7.89 (d, *J* = 5.1 Hz, 1H), 6.60 –  
981 6.48 (m, 1H), 4.93 (s, 2H), 2.69 (q, *J* = 7.6 Hz, 2H), 1.33 – 1.14 (m, 5H). LCMS (ESI  
982 M/Z): 264.1 (M + H<sup>+</sup>).

983 **4-Ethyl-3-(4-methoxyphenyl)pyridin-2-amine**: Into a 500-mL 3-necked round-bottom  
984 flask purged and maintained with an inert atmosphere of nitrogen was placed a solution  
985 of 3-bromo-4-ethylpyridin-2-amine (12 g, 59.68 mmol) in CH<sub>3</sub>CN (100 mL), (4-  
986 methoxyphenyl)boronic acid (11 g, 72.39 mmol), Na<sub>2</sub>CO<sub>3</sub>(120 mL, sat.), and Pd(dppf)Cl<sub>2</sub>  
987 (1.2 g, 1.64 mmol). The resulting solution was stirred at 110 °C for 1 h, diluted with of  
988 500 mL of EA and then extracted with of ethyl acetate (2 x 500 mL). The combined  
989 organic layers were washed with brine (3 x 200 mL), dried over anhydrous sodium  
990 sulfate and concentrated under vacuum. The residue was purified on a silica gel column  
991 eluting with ethyl acetate/petroleum ether (1:100-1:10) to afford 10 g (73%) of the title  
992 compound. <sup>1</sup>H NMR (400 MHz, CDCl<sub>3</sub>) δ 8.06(d, *J* = 5.1 Hz, 1H), 7.21 – 7.11 (m, 2H),  
993 7.06 – 6.97 (m, 2H), 6.64 (d, *J* = 5.4 Hz, 1H), 4.48 (s, 2H), 3.86 (s, 3H), 2.31 (q, *J* = 7.6  
994 Hz, 2H), 1.11 – 0.88 (m, 3H). LCMS (ESI M/Z): 264.1 (M + H<sup>+</sup>).

995 **5-Bromo-4-ethyl-3-(4-methoxyphenyl)pyridin-2-amine**: Into a 250-mL 3-necked  
996 round-bottom flask purged and maintained with an inert atmosphere of nitrogen was  
997 placed 4-ethyl-3-(4-methoxyphenyl)pyridin-2-amine (10 g, 43.80 mmol), THF (100 mL),  
998 followed by NBS (7.8 g, 43.83 mmol) at 0 °C. The resulting solution was stirred at room  
999 temperature for 15 min, diluted with 500 mL EtOAc and 500 mL H<sub>2</sub>O. The resulting  
1000 solution was extracted with ethyl acetate (2 x 500 mL). The organic layers were  
1001 combined, washed with brine (2 x 500 mL) and concentrated under vacuum. The residue  
1002 was purified on a silica gel column eluting with ethyl acetate/petroleum ether (1:20-1:10)  
1003 to afford 8 g (59%) of the title compound. <sup>1</sup>H NMR (400 MHz, CDCl<sub>3</sub>) δ 8.09 (s, 1H), 7.22  
1004 – 7.09 (m, 2H), 7.09 – 6.98 (m, 2H), 4.55 (s, 2H), 2.47 (q, *J* = 7.5 Hz, 2H), 1.10 – 0.84  
1005 (m, 3H). LCMS (ESI M/Z): 264.1 (M + H<sup>+</sup>).

1006 **4-(2-Amino-5-bromo-4-ethylpyridin-3-yl)phenol**: Into a 250-mL 3-necked round-  
1007 bottom flask purged and maintained with an inert atmosphere of nitrogen was placed 5-  
1008 bromo-4-ethyl-3-(4-methoxyphenyl)pyridin-2-amine as a white solid (8 g, 26.04 mmol),  
1009 dichloromethane (100 mL), followed by tribromoborane (19.6 g, 78.24 mmol) at 0 °C.  
1010 The resulting solution was stirred at room temperature for 1 h and then quenched by the  
1011 addition of 100 mL of NaHCO<sub>3</sub> (1 M) at 0 °C. The solids were collected by filtration and  
1012 then washed with 100 mL H<sub>2</sub>O and 300 mL of EA/PE (1:1) to afford 6.3 g (83%) of the  
1013 title compound as a white solid. <sup>1</sup>H NMR (400 MHz, CDCl<sub>3</sub>) δ 8.09 (s, 1H), 7.22 – 7.09  
1014 (m, 2H), 7.09 – 6.98 (m, 2H), 4.55 (s, 2H), 2.47 (q, *J* = 7.5 Hz, 2H), 1.10 – 0.84 (m, 3H).  
1015 LCMS (ESI M/Z): 264.1 (M + H<sup>+</sup>).

1016 **4-[2-Amino-4-ethyl-5-(1H-indazol-5-yl)-3-pyridyl]phenol (GNE-6640)**: Into a 250-mL  
1017 3-necked round-bottom flask purged and maintained with an inert atmosphere of  
1018 nitrogen was placed 4-(2-amino-5-bromo-4-ethylpyridin-3-yl)phenol (1.0 g, 3.41 mmol),  
1019 6-(tetramethyl-1,3,2-dioxaborolan-2-yl)-2H-indazole (880 mg, 3.41 mmol), potassium  
1020 carbonate (3.3 g, 23.88 mmol), water (30 mL), 1,4-dioxane (25 mL), and Pd(dppf)Cl<sub>2</sub>  
1021 (200 mg, 0.3 mmol). The resulting solution was stirred at 80 °C for 16 h, diluted with 500  
1022 mL H<sub>2</sub>O and 500 mL ethyl acetate. The organic layer was washed 30 with brine (2 x 250  
1023 mL) and concentrated under vacuum. The residue was purified on a silica gel column  
1024 eluting with DCM/CH<sub>3</sub>OH (20:1-10:1) to afford the titled compound. <sup>1</sup>H NMR (400 MHz,  
1025 DMSO-*d*<sub>6</sub>) δ 13.07 (s, 1H), 9.52 (s, 1H), 8.07 (d, *J* = 1.0 Hz, 1H), 7.74 (s, 1H), 7.65 (dd, *J*  
1026 = 1.6, 0.8 Hz, 1H), 7.56 (dt, *J* = 8.6, 0.9 Hz, 1H), 7.28 (dd, *J* = 8.5, 1.6 Hz, 1H), 7.10 –  
1027 7.04 (m, 2H), 6.92 – 6.86 (m, 2H), 4.94 (s, 2H), 2.26 (q, *J* = 7.4 Hz, 2H), 0.60 (t, *J* = 7.4  
1028 Hz, 3H). LCMS (ESI M/Z): 331.1 (M+H). HRMS *m/e* 331.1533. (M + H<sup>+</sup>, C<sub>20</sub>H<sub>19</sub>ON<sub>4</sub>  
1029 requires 331.1653)

1030 **5-[6-Amino-4-ethyl-5-(4-hydroxyphenyl)-3-pyridyl]-N-methyl-pyridine-2-**  
1031 **carboxamide (GNE-6776):** <sup>1</sup>H NMR (400 MHz, DMSO-*d*<sub>6</sub>) δ 9.56 (s, 1H), 8.80 (q, *J* =  
1032 4.7 Hz, 1H), 8.59 (dd, *J* = 2.3, 0.9 Hz, 1H), 8.07 (dd, *J* = 8.0, 0.9 Hz, 1H), 7.96 (dd, *J* =  
1033 8.0, 2.2 Hz, 1H), 7.79 (s, 1H), 7.11 – 7.02 (m, 2H), 6.94 – 6.86 (m, 2H), 5.19 (s, 2H),  
1034 2.84 (d, *J* = 4.8 Hz, 3H), 2.26 (q, *J* = 7.4 Hz, 2H), 0.62 (t, *J* = 7.4 Hz, 3H). HRMS *m/e*  
1035 349.1659. (M + H<sup>+</sup>, C<sub>20</sub>H<sub>21</sub>O<sub>2</sub>N<sub>4</sub> requires 349.1650)

1036 **4-[2-Amino-4-ethyl-5-(2-methylindazol-6-yl)-3-pyridyl]phenol (GNE-6641).** <sup>1</sup>H NMR  
1037 (400MHz, DMSO-*d*<sub>6</sub>) δ 9.54 (s, 1H), 7.81 (dd, *J* = 7.3, 1.5Hz, 2H), 7.77 – 7.52 (m, 4H),  
1038 7.13 – 7.01 (m, 2H), 6.93 – 6.85 (m, 2H), 5.10 (s, 2H), 3.28 (s, 2H), 2.24 (q, *J* = 7.4Hz,  
1039 2H), 0.60 (t, *J* = 7.5Hz, 3H). HRMS *m/e* 345.1710. (M + H<sup>+</sup>, C<sub>21</sub>H<sub>21</sub>ON<sub>4</sub> = 345.1650)

1040 **4-[2-Amino-4-ethyl-5-(2-methoxyphenyl)-3-pyridyl]phenol (GNE-2931).** <sup>1</sup>H NMR (400  
1041 MHz, DMSO-*d*<sub>6</sub>) δ 9.54 (s, 1H), 8.00 (s, 2H), 7.90 – 7.77 (m, 3H), 7.73 (s, 1H), 7.54 –  
1042 7.40 (m, 2H), 7.39 – 7.34 (m, 1H), 7.12 – 7.00 (m, 2H), 6.94 – 6.82 (m, 2H), 3.03 (s, 3H),  
1043 2.91 (q, *J* = 4.4 Hz, 2H), 1.71 (t, *J* = 4.4 Hz, 3H). HRMS *m/e* 321.1598 (M + H<sup>+</sup>,  
1044 C<sub>20</sub>H<sub>21</sub>O<sub>2</sub>N<sub>2</sub> requires 321.1650)

1045 **3-[6-Amino-4-ethyl-5-(4-hydroxyphenyl)-3-pyridyl]benzamide (GNE-2917).** <sup>1</sup>H NMR  
1046 (400 MHz, DMSO-*d*<sub>6</sub>) δ 9.52 (s, 1H), 8.48 (s, 2H), 7.58 (s, 1H), 7.34 (ddd, *J* = 8.2, 7.3,  
1047 1.8 Hz, 1H), 7.13 (dd, *J* = 7.4, 1.8 Hz, 1H), 7.10 – 6.94 (m, 6H), 6.88 (d, *J* = 7.6 Hz, 2H),  
1048 2.91 (q, *J* = 4.4 Hz, 2H), 1.71 (t, *J* = 4.4 Hz, 3H). HRMS *m/e* 334.1550 (M + H<sup>+</sup>,  
1049 C<sub>20</sub>H<sub>20</sub>O<sub>2</sub>N<sub>3</sub> requires 334.1700)

1050 **4-[6-Amino-4-ethyl-5-(4-hydroxyphenyl)-3-pyridyl]benzamide (GNE-2916).** <sup>1</sup>H NMR  
1051 (400 MHz, DMSO-*d*<sub>6</sub>) δ 9.53 (s, 1H), 7.97 (s, 1H), 7.95 – 7.87 (m, 1H), 7.72 (s, 3H), 7.43  
1052 – 7.35 (m, 1H), 7.33 (s, 1H), 7.12 – 7.00 (m, 2H), 6.93 – 6.83 (m, 2H), 5.04 (s, 2H), 2.27  
1053 (q, *J* = 7.4 Hz, 2H), 0.61 (t, *J* = 7.5 Hz, 3H). LCMS (ESI) *m/z* 334.2 [M+H<sup>+</sup>]  
1054 *Synthesis of GNE-6831 is representative of the syntheses for GNE-2090, GNE-2143,*  
1055 *and GNE-2148.*

1056 **Synthesis of 9-chloro-N-(5-chloro-2,4-dimethoxy-phenyl)-N-(cyanomethyl)-5,6,7,8-**  
1057 **tetrahydroacridine-3-carboxamide (GNE-6831).** 9-chloro-5,6,7,8-tetrahydroacridine-3-  
1058 carboxylic acid ( 100 mg, 0.38 mmol) was dissolved in 2 mL of DMF and charged with  
1059 HATU (144 mg, 0.38 mmol). After stirring at RT for minutes, the mixture was then  
1060 charged with 3-((5-chloro-2,4-dimethoxyphenyl)amino)propanenitrile ( 91 mg, 0.38  
1061 mmol). The resulting solution was stirred at 110 °C for 1 h, diluted with of 50 mL of EA  
1062 and then extracted with ethyl acetate (2 x 100 mL). The combined organic layers were  
1063 washed with brine (3 x 200 mL), dried over anhydrous sodium sulfate and concentrated  
1064 under vacuum. The residue was purified on a silica gel column eluting with ethyl  
1065 acetate/petroleum ether (1:100-1:10) to afford the title compound (110 mg, 0.30 mmol,  
1066 78% yield) of the title compound. <sup>1</sup>H NMR (400 MHz, DMSO-*d*<sub>6</sub>) δ 8.02 (d, *J* = 8.7 Hz,  
1067 1H), 7.82 (d, *J* = 1.7 Hz, 1H), 7.65 – 7.56 (m, 2H), 6.67 (s, 1H), 4.84 (s, 2H), 3.79 (s,  
1068 3H), 3.73 (s, 3H), 2.92 (m, 4H), 1.85 (m, 4H). HRMS *m/e* 470.1033 (M + H<sup>+</sup>,  
1069 C<sub>24</sub>H<sub>22</sub>O<sub>3</sub>N<sub>3</sub>Cl<sub>2</sub>, requires 470.1029)

1070 **9-Chloro-N-(5-chloro-2,4-dimethoxy-phenyl)-N-(2,3-dihydroxypropyl)-5,6,7,8-**  
1071 **tetrahydroacridine-3-carboxamide (GNE-2090):** <sup>1</sup>H NMR (400 MHz, DMSO-*d*<sub>6</sub>) δ 7.96  
1072 (dd, *J* = 8.6, 3.4 Hz, 2H), 7.77 – 7.68 (m, 2H), 7.66 – 7.47 (m, 1H), 6.56 (d, *J* = 14.2 Hz,  
1073 1H), 4.99 (d, *J* = 5.2 Hz, 1H), 4.54 (tt, *J* = 15.4, 5.8 Hz, 2H), 3.46 – 3.33 (m, 4H), 2.91  
1074 (m, 4H), 1.85 (m, 4H). LCMS (ESI) *m/z* 505.2 [M + H<sup>+</sup>].

1075 **9-Chloro-N-(2-hydroxyethyl)-N-methyl-5,6,7,8-tetrahydroacridine-3-carboxamide**  
1076 **(GNE-2143):** <sup>1</sup>H NMR (400 MHz, DMSO-*d*<sub>6</sub>) δ 8.16 (d, *J* = 8.2 Hz, 1H), 7.95 (d, *J* = 8.2  
1077 Hz, 1H), 7.7 (m, 1H), (3.66 (s, 3H), 3.57 (s, 1H), 1.90 (td, *J* = 3.8, 1.8 Hz, 4H). HRMS  
1078 *m/e* 319.1208(M + H<sup>+</sup>, C<sub>17</sub>H<sub>20</sub>O<sub>2</sub>N<sub>2</sub>Cl requires 319.1500)

1079 **9-Chloro-N-methyl-N-(2-morpholino-2-oxo-ethyl)-5,6,7,8-tetrahydroacridine-3-**  
1080 **carboxamide (GNE-2148):** <sup>1</sup>H NMR (400 MHz, DMSO-*d*<sub>6</sub>) δ 8.21 (d, *J* = 8.6 Hz, 1H),



1081 8.16 (d,  $J = 8.6$  Hz, 1H), 7.96 – 7.90 (m, 1H), 4.40 (s, 1H), 3.62 (s, 4H), 3.54 – 3.41 (m,  
1082 4H), 3.15 (s, 3H), 3.00 (t, 20.9 Hz, 4H), 1.94 – 1.86 (m, 4H). HRMS  $m/e$  402.1579 ( $M +$   
1083  $H^+$ ,  $C_{21}H_{25}O_3N_3Cl$  requires 402.1725)

1084

1085 **Synthesis of (1S)-1-(5-bromo-1H-indol-2-yl)-N-(2-phenylethyl)ethanamine (GNE-**  
1086 **0300).** 1-(5-bromo-1H-indol-2-yl)ethan-1-one (90 mg, 0.38 mmol) was dissolved in 2 mL  
1087 of DMF and charged with (S)-phenethylamine (46 mg, 0.38 mmol). After stirring at RT  
1088 for 30 minutes, the mixture was diluted with 50 mL ethyl acetate and 50 mL water. The  
1089 mixture was partitioned and the organic was collected. The aqueous was then extracted  
1090 with ethyl acetate (2 x 100 mL). The combined organic layers were washed with brine  
1091 (3 x 200 mL), dried over anhydrous sodium sulfate and concentrated under vacuum. The  
1092 residue was purified on a silica gel column eluting with ethyl acetate/petroleum ether  
1093 (1:100-1:10) to afford the title compound (120 mg, 0.35 mmol, 92% yield) of the titled  
1094 compound.  $^1H$  NMR (400 MHz,  $DMSO-d_6$ )  $\delta$  11.05 (s, 1H), 7.59 (d,  $J = 1.9$  Hz, 1H), 7.30  
1095 – 7.19 (m, 3H), 7.20 – 7.06 (m, 4H), 6.21 (d,  $J = 1.8$  Hz, 2H), 3.93 (q,  $J = 6.6$  Hz, 1H),  
1096 2.77 – 2.56 (m, 4H), 1.36 (d,  $J = 6.6$  Hz, 3H). LCMS (ESI)  $m/z$  343.9 [ $M + H^+$ ]

1097

1098 *Synthesis of GDC-0570 follows similar procedures as described for GDC-0339 as below.*

1099 **(Z)-2,3,6,7-Tetrahydro-1H-azepine hydrochloride:** 4N Hydrogen chloride in 1,4-  
1100 dioxane (250 mL; 1 mol) was added over 5 minutes to a stirred, ice cooled solution of  
1101 (Z)-*tert*-butyl 2,3,6,7-tetrahydro-1H-azepine-1-carboxylate (50 g; 0.254 mol) in methanol  
1102 (250 mL). On complete addition, the ice bath was removed and stirring continued at  
1103 room temperature for 3.75 h. Volatiles were removed under reduced pressure and the  
1104 residue triturated twice with diethyl ether (300 mL) to afford (Z)-2,3,6,7-tetrahydro-1H-  
1105 azepine hydrochloride as a pale pink solid (32.3 g; 95%).  $^1H$ -NMR ( $DMSO-d_6$ , 400 MHz)  
1106  $\delta$  9.54 (br s, 2H), 6.40-6.25 (m, 2H), 3.15-3.05 (m, 4H), 2.55-2.40 (m, 4H).

1107

1108 **(Z)-1-(1-Methyl-4-nitro-1H-pyrazol-5-yl)-2,3,6,7-tetrahydro-1H-azepine:** A mixture of  
1109 (Z)-2,3,6,7-tetrahydro-1H-azepine hydrochloride (32.3 g; 0.24 mol), 5-chloro-1-methyl-4-  
1110 nitro-1H-pyrazole (37.2 g; 0.23 mol), potassium fluoride (56.24 g; 0.96 mol) and  
1111 diisopropylethylamine (64 mL; 0.362 mol) in anhydrous DMSO (650 mL) was heated at  
1112 75 °C for 21 h. On cooling, the mixture was poured into water (1500 mL), extracted with  
1113 ethyl acetate (4 x 500 mL) and the combined organics washed with water (2 x 400 mL),  
1114 brine (300 mL) and dried ( $MgSO_4$ ). The solvent was removed under reduced pressure  
1115 to afford (Z)-1-(1-methyl-4-nitro-1H-pyrazol-5-yl)-2,3,6,7-tetrahydro-1H-azepine as a light  
1116 brown solid (50.74 g; 99%).  $^1H$ -NMR ( $CDCl_3$ , 400 MHz)  $\delta$  8.00 (s, 1H), 5.95-5.85 (m,  
1117 2H), 3.80 (s, 3H), 3.30-3.20 (m, 4H), 2.45-2.35 (m, 4H). LCMS (ESI  $M/Z$ ): 223.1 [ $M +$   
1118  $H^+$ ].

1119

1120 **4-(1-Methyl-4-nitro-1H-pyrazol-5-yl)-8-oxa-4-azabicyclo[5.1.0]octane:** 77% meta-  
1121 Chloroperbenzoic acid (77 g; 0.343 mol) was added portion-wise over 10 minutes to a  
1122 stirred, ice cooled solution of (Z)-1-(1-methyl-4-nitro-1H-pyrazol-5-yl)-2,3,6,7-tetrahydro-  
1123 1H-azepine (50.74 g; 0.23 mol) in dichloromethane (1000 mL). Ice bath used to control  
1124 minor exotherm observed during a smaller scale reaction. On complete addition, the ice  
1125 bath was removed and stirring continued at room temperature for 18 h. The reaction  
1126 mixture was washed with saturated sodium hydrogen carbonate (750 mL), 1N sodium  
1127 hydroxide (2 x 500 mL) and brine (350 mL). The organics were dried ( $MgSO_4$ ) and the  
1128 solvent removed under reduced pressure to afford 4-(1-methyl-4-nitro-1H-pyrazol-5-yl)-  
1129 8-oxa-4-azabicyclo[5.1.0]octane as a pale yellow solid (55.6 g).  $^1H$ -NMR ( $CDCl_3$ , 400  
1130 MHz)  $\delta$  7.98 (s, 1H), 3.75 (s, 3H), 3.50-3.35 (m, 2H), 3.30-3.20 (m, 2H), 2.95-2.80 (m,  
1131 2H), 2.35-2.15 (m, 4H). LCMS (ESI  $M/Z$ ): 239.2 [ $M + H^+$ ].

1132

1133 **rel-(4R,5R)-5-Azido-1-(1-methyl-4-nitro-1H-pyrazol-5-yl)azepan-4-ol:** To a stirred  
1134 solution of 4-(1-methyl-4-nitro-1H-pyrazol-5-yl)-8-oxa-4-azabicyclo[5.1.0]octane (29.28 g)  
1135 in methanol (350 mL) and water (90 mL) was added ammonium chloride (16.5 g; 0.308  
1136 mol) followed by sodium azide (20 g; 0.307 mol). The mixture was heated behind a blast  
1137 screen at 70 °C for 22 h, cooled then concentrated to 100 mL under reduced pressure at  
1138 40 °C. The concentrated solution was poured into water (1300 mL), extracted with  
1139 dichloromethane (4 x 400 mL) and the combined organics dried (MgSO<sub>4</sub>). Evaporation  
1140 under reduced pressure at 35 °C gave rel-(4R,5R)-5-azido-1-(1-methyl-4-nitro-1H-  
1141 pyrazol-5-yl)azepan-4-ol (anti-isomer and a racemic mixture) as a pale yellow oil (34.5 g;  
1142 96% over 2 steps). <sup>1</sup>H-NMR (CDCl<sub>3</sub>, 400 MHz) δ 8.03 (s, 1H), 3.85-3.77 (m, 1H), 3.77  
1143 (s, 3H), 3.65-3.55 (m, 1H), 3.45-3.15 (m, 4H), 2.85-2.70 (m, 1H), 2.25-2.10 (m, 2H),  
1144 2.05-1.85 (m, 2H). LCMS (ESI M/Z): 282.1 [M + H<sup>+</sup>].

1145

1146 **rel-(4R,5R)-4-Azido-5-fluoro-1-(1-methyl-4-nitro-1H-pyrazol-5-yl)azepane:** 50%  
1147 Deoxofluor in THF (111 mL; 0.307 mol) was added slowly over 20 minutes to a stirred,  
1148 ice cooled solution of rel-(4R,5R)-5-azido-1-(1-methyl-4-nitro-1H-pyrazol-5-yl)azepan-4-  
1149 ol (32.5 g; 0.115 mol) in dichloromethane (500 mL). On complete addition, the ice bath  
1150 was removed and stirring continued at room temperature for 20 h. The reaction mixture  
1151 was re-cooled in an ice bath and saturated sodium hydrogen carbonate (400 mL) added  
1152 dropwise (effervescence!). After stirring for 30 minutes the layers were separated and  
1153 the aqueous layer extracted with dichloromethane (2 x 500 mL). Pooled organics were  
1154 dried (MgSO<sub>4</sub>) and the solvent removed under reduced pressure. Flash column  
1155 chromatography on silica eluting with 0 – 100% ethyl acetate in isohexane gradient  
1156 afforded rel-(4R,5R)-4-azido-5-fluoro-1-(1-methyl-4-nitro-1H-pyrazol-5-yl)azepane as a  
1157 pale orange oil (26 g; 80%). <sup>1</sup>H-NMR (CDCl<sub>3</sub>, 400 MHz) δ 8.03 (s, 1H), 4.90-4.65 (m,  
1158 1H), 4.00-3.85 (m, 1H), 3.77 (s, 3H), 3.40-3.10 (m, 4H), 2.35-2.05 (m, 3H), 1.95-1.75 (m,  
1159 1H). LCMS (ESI M/Z): 284.3 [M + H<sup>+</sup>].

1160

1161 **rel-(4R,5R)-5-Fluoro-1-(1-methyl-4-nitro-1H-pyrazol-5-yl)azepan-4-amine:** A mixture  
1162 of rel-(4R,5R)-4-azido-5-fluoro-1-(1-methyl-4-nitro-1H-pyrazol-5-yl)azepane (26 g; 91.8  
1163 mmol) and triphenylphosphine (24.1 g; 92 mmol) in tetrahydrofuran (400 mL) and water  
1164 (80 mL) was heated at 60 °C for 20 h, cooled and concentrated to approximate 80 mL  
1165 under reduced pressure. Ethyl acetate (500 mL) was added and the mixture extracted  
1166 with 1N HCl (4 x 125 mL). Pooled acidic extracts were washed with ethyl acetate (500  
1167 mL), basified to pH 14 with 6N NaOH and extracted with dichloromethane (3 x 400 mL).  
1168 Combined extracts were dried (MgSO<sub>4</sub>) and the solvent removed under reduced  
1169 pressure to give rel-(4R,5R)-5-fluoro-1-(1-methyl-4-nitro-1H-pyrazol-5-yl)azepan-4-amine  
1170 as a pale yellow oil (22 g; 93%). <sup>1</sup>H-NMR (CDCl<sub>3</sub>, 400 MHz) δ 8.03 (s, 1H), 4.60-4.40  
1171 (m, 1H), 3.77 (s, 3H), 3.45-3.10 (m, 5H), 2.35-1.90 (m, 3H), 1.80-1.65 (m, 1H), 1.60 (br  
1172 s, 2H). LCMS (ESI M/Z): 258.3 [M + H<sup>+</sup>].

1173

1174 **tert-Butyl (4R,5R)-5-fluoro-1-(1-methyl-4-nitro-1H-pyrazol-5-yl)azepan-4-  
1175 ylcarbamate:** Di-*tert*-butyl dicarbonate (28 g; 128.3 mmol) was added to a stirred, ice  
1176 cooled solution of rel-(4R,5R)-5-fluoro-1-(1-methyl-4-nitro-1H-pyrazol-5-yl)azepan-4-  
1177 amine (22 g; 85.6 mmol) and diisopropylethylamine (22.4 mL; 128.6 mmol) in  
1178 dichloromethane (600 mL). On complete addition, the ice bath was removed and stirring  
1179 continued at room temperature for 20 h. The reaction mixture was washed with  
1180 saturated sodium hydrogen carbonate (500 mL) and the aqueous layer re-extracted with  
1181 dichloromethane (2 x 300 mL). Pooled organics were dried (MgSO<sub>4</sub>) and the solvent  
1182 removed under reduced pressure. Flash column chromatography on silica eluting with 0

1183 – 100% ethyl acetate in isohexane gradient afforded a pale yellow solid (29.7 g; 97%).  
1184 Chiral separation of the racemic mixture by supercritical fluid chromatography (SFC)  
1185 using Chiralpak IA column with an isocratic mobile phase of 15% methanol (with 0.1%  
1186 NH<sub>4</sub>OH) in carbon dioxide gave the desired product (second peak) as a single  
1187 enantiomer. <sup>1</sup>H-NMR (CDCl<sub>3</sub>, 400 MHz) δ 8.04 (s, 1H), 5.05 (m, 1H), 4.80-4.55 (m, 1H),  
1188 4.15-4.05 (m, 1H), 3.79 (s, 3H), 3.45-3.10 (m, 4H), 2.35-2.05 (m, 3H), 1.95-1.80 (m, 1H),  
1189 1.47 (s, 9H). LCMS (ESI M/Z): 358.3 [M + H<sup>+</sup>].

1190  
1191 **tert-Butyl (4R,5R)-5-fluoro-1-(4-amino-1-methyl-1H-pyrazol-5-yl)azepan-4-**  
1192 **ylcarbamate:** To a stirred solution of *tert*-butyl (4R,5R)-5-fluoro-1-(1-methyl-4-nitro-1H-  
1193 pyrazol-5-yl)azepan-4-ylcarbamate (15.0 g; 42 mmol) in ethanol (1000 mL) and water  
1194 (100 mL) was added ammonium chloride (11.34 g; 210 mmol) and iron powder (9.4 g;  
1195 168 mmol). The mixture was heated at 99 °C for 2.75 h, cooled, filtered through Celite®  
1196 and evaporated to approximately 100 mL. The concentrate was diluted with water (1000  
1197 mL) and extracted with ethyl acetate (2 x 500 mL). The pooled extracts were washed  
1198 with water (200 mL), dried (MgSO<sub>4</sub>) and the solvent removed under reduced pressure to  
1199 give *tert*-butyl (4R,5R)-5-fluoro-1-(4-amino-1-methyl-1H-pyrazol-5-yl)azepan-4-  
1200 ylcarbamate as a pale brown solid (12.6 g; 91%). <sup>1</sup>H-NMR (CDCl<sub>3</sub>, 400MHz) δ 7.13 (s,  
1201 1H), 6.35-6.20 (m, 1H), 4.85-4.65 (m, 1H), 4.35-4.15 (m, 1H), 3.66 (s, 3H), 3.45-3.30 (m,  
1202 2H), 3.15-2.90 (m, 2H), 2.65 (s, 2H), 2.30-2.15 (m, 1H), 2.15-1.95 (m, 2H), 1.90-1.80 (m,  
1203 1H), 1.45 (s, 9H). LCMS (ESI M/Z): 327.2 [M + H<sup>+</sup>].

1204  
1205 **tert-Butyl (4R,5R)-1-(4-(5-*tert*-butoxycarbonylamino-2-(2,6-difluorophenyl)thiazole-**  
1206 **4-carboxamido)-1-methyl-1H-pyrazol-5-yl)-5-fluoroazepan-4-ylcarbamate:** A mixture  
1207 of *tert*-butyl (4R,5R)-5-fluoro-1-(4-amino-1-methyl-1H-pyrazol-5-yl)azepan-4-ylcarbamate  
1208 (12.6 g, 38.5 mmol), 5-(*tert*-butoxycarbonylamino)-2-(2,6-difluorophenyl)thiazole-4-  
1209 carboxylic acid (14.4 g, 40.4 mmol), diisopropylethylamine (13.4 mL, 77 mmol) and  
1210 PyBOP (26.1 g, 50 mmol) in dichloromethane (400 mL) was stirred at room temperature  
1211 for 48 h. Saturated sodium hydrogen carbonate (600 mL) was added and stirring  
1212 continued for 0.5 h. The mixture was filtered, the layers separated and the aqueous  
1213 extracted with dichloromethane (500 mL). The pooled organics were dried (MgSO<sub>4</sub>) and  
1214 the solvent removed under reduced pressure. Flash column chromatography on silica  
1215 eluting with 0 – 100% ethyl acetate in isohexane gradient afforded *tert*-butyl (4R,5R)-1-  
1216 (4-(5-*tert*-butoxycarbonylamino-2-(2,6-difluorophenyl)thiazole-4-carboxamido)-1-methyl-  
1217 1H-pyrazol-5-yl)-5-fluoroazepan-4-ylcarbamate as a pale yellow solid (2.5 g, 9.8%).  
1218 Further elution with 0-10% methanol in ethyl acetate, then 10% methanol in  
1219 dichloromethane, evaporation of relevant fractions under reduced pressure and  
1220 trituration of the residue with cold diethyl ether gave a further 7.61g (30%) of product. <sup>1</sup>H-  
1221 NMR (CDCl<sub>3</sub>, 400MHz) δ 10.34 (s, 1H), 8.75 (s, 1H), 7.89 (s, 1H), 7.40-7.25 (m, 1H),  
1222 7.15-7.00 (m, 2H), 4.95-4.85 (m, 1H), 4.85-4.65 (m, 1H), 4.15-4.00 (m, 1H), 3.77 (s, 3H),  
1223 3.45-3.30 (m, 2H), 3.25-3.00 (m, 2H), 2.35-2.10 (m, 3H), 1.95-1.75 (m, 1H), 1.55 (s, 9H),  
1224 1.43 (s, 9H).

1225  
1226 **5-Amino-N-(5-((4R,5R)-4-amino-5-fluoroazepan-1-yl)-1-methyl-1H-pyrazol-4-yl)-2-**  
1227 **(2,6-difluorophenyl)thiazole-4-carboxamide (GDC-0339):** *tert*-butyl (4R,5R)-1-(4-(5-  
1228 *tert*-butoxycarbonylamino-2-(2,6-difluorophenyl)thiazole-4-carboxamido)-1-methyl-1H-  
1229 pyrazol-5-yl)-5-fluoroazepan-4-ylcarbamate (10.11 g, 15.2 mmol) in 4N HCl in dioxane  
1230 (200 mL) and methanol (200 mL) was stirred at room temperature for 20 h. Evaporation  
1231 under reduced pressure afforded a pale brown solid which was dissolved in 50%  
1232 methanol in dichloromethane and added to an SCX cartridge (strong cation exchange  
1233 chromatography). After washing with dichloromethane and methanol, elution with 1N

1234 ammonia in methanol and evaporation of the eluent under reduced pressure afforded 5-  
1235 amino-*N*-(5-((4*R*,5*R*)-4-amino-5-fluoroazepan-1-yl)-1-methyl-1*H*-pyrazol-4-yl)-2-(2,6-  
1236 difluorophenyl)thiazole-4-carboxamide as the free base (6.3 g, 89%). <sup>1</sup>H-NMR (DMSO-  
1237 *d*<sub>6</sub>, 400MHz) δ 8.92 (s, 1H), 7.65-7.50 (m, 4H), 7.40-7.25 (m, 2H), 4.60-4.45 (m, 1H),  
1238 3.70 (s, 3H), 3.35-3.05 (m, 5H), 2.30-1.60 (m, 6H). LCMS (ESI M/Z): 466.1 [M + H<sup>+</sup>].  
1239

#### 1240 **Hit-to-lead selection cascade assays**

1241 *Biochemical deubiquitinase assays.* Biochemical deubiquitinase assays used Ubiquitin-  
1242 Rho110 as a substrate to enable kinetic monitoring of reactions for USP7, USP7  
1243 catalytic domain, USP5, and USP47. The deubiquitinase proteins and their  
1244 concentrations that were used in biochemical reactions were as follows: USP7, full-  
1245 length N-terminal His-tag, native C-Terminus: 0.18 nM (Genentech, Hs\_USP7 2-1102);  
1246 USP7 catalytic domain N-terminal His-tag: 40 nM (Genentech, Hs\_USP7.K208-K554);  
1247 USP5; full-length: 0.5 nM (Boston Biochem cat # E-322, lot 02010210); USP47, full-  
1248 length N-terminal His-tag: 0.8 nM (Genentech Hs\_USP47.M1-D1287). Substrate Km  
1249 values for USP proteins were: USP7, full-length, 2 μM; USP5, full-length, 0.33 μM;  
1250 USP47 full-length, 0.175 μM. The final assay conditions were as follows: The Reaction  
1251 Buffer consisted of 50 mM Tris (pH 7.5), 0.01%(v/v) Triton X-100, 2.5 mM Dithiothreitol,  
1252 0.1% (w/v) bovine gamma globulin (Sigma cat # G5009-25G). The final substrate  
1253 Ubiquitin-Rho110 (Boston Biochem cat # U-555) concentration used for reactions was  
1254 1μM. Reactions were carried out for 1 hour at room temperature, in black 20μL volume  
1255 polystyrene ProxiPlate 384 F Plus (PerkinElmer cat # 6008260). Test compounds,  
1256 including a control USP7 inhibitor (Ub-aldehyde, Boston Biochem cat # U-201) were  
1257 serially diluted in DMSO, in 384-well clear V-bottom polypropylene plates (Greiner cat #  
1258 781280). Compounds in DMSO were diluted 10-fold into Reaction Buffer, to achieve 3-  
1259 fold the final desired concentration. The substrate, Ubiquitin-Rho110 (Boston Biochem  
1260 cat # U-555), was prepared at 3μM (3-fold the final concentration) and 5μL was  
1261 dispensed into the reaction plate. Five μL of the compounds (diluted in Reaction Buffer  
1262 at 3-fold the final concentration) were transferred to the reaction plate. Five μL of DUB  
1263 protein, which was diluted in Reaction Buffer at 3-fold the final concentration, was  
1264 transferred to the reaction plate to initiate the reaction. After 1 hour incubation at room  
1265 temperature the reaction was quenched by the addition of 5μL of 400mM acetic acid, in  
1266 the case of an endpoint reaction. The enzymatic product was measured by quantifying  
1267 the fluorescence signal of cleaved Rhodamine-110 using excitation at 485 nm and  
1268 emission at 535nm. When pre-incubation of DUB with compounds was required, the  
1269 order of addition of reagents was modified to pre-mix the compounds with DUB (with a 1  
1270 hour incubation period), prior to the addition of the substrate and the initiation of the  
1271 reaction period. Percentage inhibition values were calculated relative to a no enzyme  
1272 control and an uninhibited enzyme control. Curve fitting and IC<sub>50</sub> calculations were  
1273 carried out using Genedata Screener software. Conversion between IC<sub>50</sub> and Ki values  
1274 were carried out using the Cheng-Prusoff equation.  
1275

1276 *Cellular ubiquitin-MDM2 assay.* HCT116 colon cancer cells or SJSA-1 osteosarcoma  
1277 cells were seeded at a density of 150,000 cell per well in 90μl (RPMI 1640 media, 10%  
1278 FBS (or 0.5% FBS for low serum conditions), 1X GlutaMAX™ from Gibco) in 96-well  
1279 black clear bottom, TC-treated (Greiner, Cat# 655090), and incubated for 2 hours at  
1280 37°C, 5% CO<sub>2</sub> in a tissue culture incubator. Compounds were prepared in a serial  
1281 dilution in DMSO at 200x the final desired concentration in a 96-well polypropylene V-  
1282 bottom (Greiner, Cat# 651261), then diluted 1:20 in RPMI tissue culture medium and  
1283 10μl transferred to each well of the cell plate. Cell plates were incubated overnight for 20

1284 hours, 37°C, 5% CO<sub>2</sub>. Twenty µl of a 120 µM stock (in RPMI) of the proteasome  
1285 inhibitor, MG132 (Cayman Chemical, Cat# 10012628), was added to each well. Cells  
1286 were incubated for 1 hour at 37°C, 5% CO<sub>2</sub>. Quantitation of ubiquitin-MDM2 was carried  
1287 out using Ub/Total MDM2 whole cell lysate kit (MSD, Cat# K15168D-2). Cells were lysed  
1288 by adding 15µl of 5x MSD lysis buffer (containing additives: 10mM NaF, 10mM beta-  
1289 glycerophosphate, 1.5mM Na<sub>3</sub>VO<sub>4</sub>, protease inhibitor cocktail (Sigma, P8340) to each  
1290 well and incubated at 4°C for 30 minutes with shaking. One hundred µl of lysate was  
1291 transferred to each well of the MSD 96-well plate, incubated at room temperature for 1  
1292 hour while shaking (650 RPM) in the dark. The MSD plates were washed 3 times in Tris  
1293 buffered saline (50 mM Tris-Cl, pH 7.5. 150 mM NaCl) using a Biotek EL405 plate  
1294 washer. Three mL of detection antibody solution was prepared per plate (1 mL of block  
1295 buffer A, 1.82ml 1X Tris wash buffer, 150µl 2% Blocker D-M, 30µl 10% Blocker D-R,  
1296 60µl 50X anti-total MDM2 antibody). Twenty-five µl of detection antibody solution was  
1297 added per well and incubated for 1 hour at room temperature (650RPM) in the dark.  
1298 Plates were washed 3 times in Tris buffered saline using a Biotek EL405 plate washer.  
1299 MSD read buffer was prepared according to manufacturer's instructions and 150 µl  
1300 added per well. Plates were read using a MSD Sector Reader. The final measurement  
1301 was the ratio of ubiquitinated MDM2 / total MDM2. Percentage increase in ubiquitin-  
1302 MDM2 was calculated relative to DMSO controls using Genedata Screener software.  
1303

1304 *Total MDM2 immunofluorescence.* HCT-116 cells were seeded at a density of  
1305 40,000/well in 50µL/well in 384 well tissue culture plates (Greiner #781091) in RPMI,  
1306 10% FBS, 2mM L-glutamine, and incubated overnight. Test compounds were prepared  
1307 in a 20-point serial dilution (1:2-fold) in DMSO using a Biomek FX in a 384 well Labcyte-  
1308 approved polypropylene plate (Labcyte P05525). Compounds were acoustically  
1309 dispensed into the cell plates using a Labcyte Echo (final total volume transferred was  
1310 50nL (DMSO final concentration was 0.1%v/v). Cell plates were incubated at 37°C 5%  
1311 CO<sub>2</sub>, for 24 hours. Cells were fixed by addition of 15µL of 16% paraformaldehyde  
1312 (Electron Microscopy Sciences #15710-S) directly to the 50µL cell culture medium in  
1313 each well. Plates were incubated for 30 minutes at room temperature. The well contents  
1314 was aspirated using the Biotek EL406 and 50µL/well of Permeabilization / Block buffer  
1315 added (Phosphate buffered saline (PBS, pH 7.5), Triton X100 0.5% (v/v), BSA 0.5%  
1316 (w/v), proclin 15ppm). Plates were incubated for 30 minutes then washed 3 times with  
1317 100µL/well of PBS. Twenty-five µL/well of anti-MDM2 (rabbit polyclonal, AbCam  
1318 #ab58530 diluted 1:500 in PBS, BSA 0.5% (w/v), Triton X100 0.1% (v/v)) was dispensed  
1319 into each well. Plates were incubated 2 hours at room temperature then washed 4 times  
1320 with 100uL/well of PBS using a Biotek EL406. Twenty-five µL/well of Alexafluor 555  
1321 conjugated anti-rabbit IgG (Life Technologies #A31572, diluted 1:1000 and Hoechst  
1322 33342 1µg/mL diluted in PBS, BSA 0.5% (w/v), Triton X100 0.1% (v/v)) was dispensed  
1323 into each well. Plates were incubated for 2 hours at room temperature then washed 4  
1324 times with 100µL/well of PBS using a Biotek EL406. Fluorescence images of the  
1325 samples (Channel 1: 386-23\_BGRFRN\_BGRFRN (DNA); Channel 2: 549-  
1326 15\_BGRFRN\_BGRFRN (MDM2)) were acquired using a Celloomics XTI Arrayscan with  
1327 the Bioapplication "Compartmental Analysis". Channel 1 was used to define the nuclear  
1328 region. Measurements were made of "Mean\_CircAvgIntCh2", which is the Alexafluor 555  
1329 fluorescence intensity (MDM2) within the nuclear region measured on a per cell basis  
1330 and averaged over all the measured cells. Data analysis and EC<sub>50</sub> calculation was  
1331 carried out in GraphPad Prism using non-linear four parameter curve fitting.  
1332

1333 *Cathepsin-B protease assay.* Cathepsin-B proteolytic activity is quantitated by an  
1334 LC/MS, MRM-based detection method. Briefly, varying concentrations of experimental  
1335 compound are incubated with 0.5 nM human liver Cathepsin-B (EMD Millipore, #219364)  
1336 and Benzoyloxycarbonyl-Arg-Arg-7-amino-4-methylcoumarin (Cbz-RR-AMC) fluorogenic  
1337 substrate in buffer containing 10 mM MES pH 6.0 and 1 mM DTT. The reaction is  
1338 incubated for 5 minutes at room temperature, followed by quenching with the addition of  
1339 an equal volume of 2% formic acid in water. Free AMC liberated by Cathepsin-B is  
1340 quantitated on a Sciex 5500 QTRAP mass spectrometer (Sciex, Framingham, MA)  
1341 equipped with a Biocius Rapidfire high-throughput LC system (Agilent, Santa Clara, CA).  
1342 AMC product is captured on an Agilent C18 Rapidfire cartridge, desalted with a 0.1%  
1343 formic acid wash, and then eluted with 80% acetonitrile, 0.1% formic acid. Measured  
1344 MRM AUC for AMC is plotted against compound concentration using GraphPad Prism  
1345 (GraphPad Software, La Jolla, CA) and fitted for IC50 using four parameter fitting. MRM  
1346 parameters for AMC: ESI positive mode, Q1=233.1, Q3=175.2, collision energy=16.

1347

1348 *Caspase-3 protease assay.* Caspase-3 proteolytic activity is quantitated by an LC/MS,  
1349 MRM-based detection method. Briefly, varying concentrations of experimental  
1350 compound are incubated with 0.025 nM of recombinant Caspase-3 (cloned and purified  
1351 in-house) and 1  $\mu$ M (Z-DEVD)<sub>2</sub>-Rho110 fluorogenic substrate in buffer containing 25  
1352 mM Hepes, pH 7.2 and 5 mM DTT. The reaction is incubated for 20 minutes at room  
1353 temperature, followed by quenching with the addition of an equal volume of 2% formic  
1354 acid in water. Free Z-DEVD liberated by Caspase-3 is quantitated on a Sciex 5500  
1355 QTRAP mass spectrometer (Sciex, Framingham, MA) equipped with a Biocius Rapidfire  
1356 high-throughput LC system (Agilent, Santa Clara, CA). Z-DEVD product is captured on  
1357 an Agilent C18 Rapidfire cartridge, desalted with a 0.1% formic acid wash, and then  
1358 eluted with 80% acetonitrile, 0.1% formic acid. Measured MRM AUC for Z-DEVD is  
1359 plotted against compound concentration using GraphPad Prism (GraphPad Software, La  
1360 Jolla, CA) and fitted for IC50 using four parameter fitting. MRM parameters for Z-DEVD:  
1361 ESI negative mode, Q1=609.2, Q3=440.2, collision energy=-35.

1362

1363 *USP7 aggregation analysis.* Aggregation of full-length USP7 was confirmed by dynamic  
1364 light scattering (DLS) using a Wyatt DynaPro Plate Reader. DLS data were acquired at  
1365 37°C, with Dynamics V7 software, with a 10 second acquisition time, 10 acquisitions per  
1366 measurement in auto-attenuation mode. Compounds were present at 100 $\mu$ M in a buffer  
1367 containing 50mM HEPES pH 7.2, 150mM NaCl, 0.01% Triton X-100, 1mM TCEP, 0.1%  
1368 DMSO. Full-length USP7 was present at 1 mg/ml with all compounds except Rottlerin.  
1369 Aggregate is defined here as having a hydrodynamic radius greater than 10 nm.

1370

1371 *USP7 covalent modification and LC-MS analysis.* To evaluate potential covalent  
1372 modification of the proteins, full-length USP7 full-length was incubated with excess  
1373 compound at room temperature overnight and covalent modification was evaluated by  
1374 LC-MS using standard methods.

1375

### 1376 **Cell culture and cell treatments**

1377 HCT-116 parental, USP7 null (HD R02-028), and HCT-116 p53 null (Horizon; HD 104-  
1378 001) cell lines were purchased from Horizon. Normal cells were purchased from the  
1379 following vendors: normal mammary cells (Life Technologies; HMEC A10565), normal  
1380 osteoblasts (Lonza; CC-2538) and were cultured in the vendor-specified media. All  
1381 other cell lines were obtained from Genentech's repository and were cultured in standard  
1382 conditions in RPMI media containing 10% FBS (solid tumor cell lines) or 20% FBS  
1383 (hematopoietic cell lines), 1% penicillin/streptomycin, and 1% L-Glutamine. All cell lines

1384 were mycoplasma-tested and cell line identity was by STR and SNP profiling as  
1385 described<sup>26</sup>. For studies evaluating cellular effects of compound treatments, 2,500-5,000  
1386 cells were seeded in 1-well of a 96-well plate (Corning; 3904). The following day, the  
1387 media was changed from normal (10%) to low serum (0.5%) containing vehicle (DMSO)  
1388 or compounds. Sixteen to 24 hours later FBS was added to each well to bring serum  
1389 levels back to 10%. Cells were then allowed to grow for two additional days. All  
1390 treatments were done in triplicate. For degradation rescue studies, the proteasome  
1391 inhibitor bortezomib (Selleckchem) or the UAE inhibitor MLN7243 (Active Biochem) were  
1392 added at 5 $\mu$ M 30-45 minutes prior to harvest.

1393

#### 1394 **Cycloheximide chase studies**

1395 MCF-7 cells were treated for a total of 7 hours with DMSO or 15 $\mu$ M of the indicated  
1396 compounds. During the 7 hours of compound treatment, 50 $\mu$ M cycloheximide was  
1397 added for the indicated times prior to harvest. Cell lysates were subsequently processed  
1398 for western blot analysis.

1399

#### 1400 **Antibodies and reagents**

1401 Antibodies to the indicated proteins were purchased from the following vendors: USP7  
1402 (ab84098), USP5 (ab84695) [AbCam] or (4833) [Cell Signaling Technology]; MDM2  
1403 (Santa Cruz sc-965 or EMD Millipore 07-575); tubulin (LICOR 926-42211); tubulin-HRP  
1404 (5346), actin-HRP (12620), GAPdH-HRP (8884), caspase-3 (9662), PARP (9441), total  
1405 S6 (2217), phospho-S235/236-S6 (2945), Mcl-1 (4572), PIM2 (2730), cleaved-caspase-3  
1406 (2664), phospho-S112-Bad (5284), p21 (2947) [Cell Signaling Technology]; K48  
1407 polyubiquitin (Genentech); USP47 (Bethyl A301190A); UCHL1 (Invitrogen 38-1000); HA-  
1408 HRP (clone HA-7) and FLAG (A8592) [Sigma]; p53 (Thermo Scientific MS738-P1); p21  
1409 (Millipore 05-655), Bad (AF819) [R&D]. Secondary antibodies were purchased from  
1410 LICOR Biosciences or Jackson Immunoresearch. Full-length human USP7 was cloned  
1411 into a pRK5 mammalian expression construct with a C-terminal FLAG-tag and mutations  
1412 were introduced by QuickChange site-directed mutagenesis as instructed by the  
1413 manufacturer (Agilent).

1414

#### 1415 **Western blotting, quantitation, immunoprecipitations, and deubiquitinase assays**

1416 Cells were treated with compounds as detailed above prior to lysis for Western Blot  
1417 analysis. Primary antibodies were diluted 1:1000 and incubated 1 hour at room  
1418 temperature or 4°C overnight. Secondary antibodies were diluted 1:10,000 and  
1419 incubated 30-60 minutes at room temperature. Blots were either imaged using a  
1420 chemiluminescent reagent (Pierce) or were scanned and bands were quantified using  
1421 LICOR Odyssey instrumentation and software, respectively. Immunoprecipitations with  
1422 ubiquitin-specific antibodies were performed as described<sup>27</sup> and immunoprecipitates and  
1423 corresponding cell lysates were analyzed by immunoblot analysis as previously  
1424 described<sup>27</sup> using the antibodies detailed above. For *in vitro* deubiquitination of PIM2,  
1425 ubiquitinated PIM2 was captured by treating MV-4-11 cells for 45 minutes with the  
1426 proteasome inhibitor MG-132 (SelleckChem). Cells were washed, lysed in a 6M urea  
1427 lysis buffer, and anti-K48 polyubiquitin immunoprecipitates were washed and  
1428 deubiquitinated with 250nM wild-type or C223S full length recombinant USP7 following a  
1429 similar protocol as described<sup>27</sup>.

1430

#### 1431 **Cell viability studies**

1432 *IncuCyte live cell analysis.* One day after cell seeding, 10% cell culture media was  
1433 changed to 0.5% serum media containing 2 $\mu$ M CellEvent Caspase 3/7 reagent (Life  
1434 Technologies; C10423) and compounds. The plates were placed in an IncuCyte live cell

1435 imager and scanning was started within 15-20 minutes. Images were taken every 2  
1436 hours for 68-72 hours, using a 10X objective. Phase contrast was used to measure cell  
1437 confluency/density while green fluorescence was used to measure caspase activity. The  
1438 images were analyzed using IncuCyte software (Basic Analysis parameters) and a ratio  
1439 of caspase activity to cell density/count was determined. For combination experiments,  
1440 MCF7 cells were treated with 15 $\mu$ M USP7 inhibitors or 0.1 $\mu$ M doxorubicin alone or in  
1441 combination. Similarly, U2OS cells were treated with 15 $\mu$ M USP7 inhibitors or 1 $\mu$ M  
1442 cisplatin alone or in combination.

1443  
1444 *CellTiter-Glo assays (Extended Data Figures 1d, 1e, 2b)*. Seventy-two hours after  
1445 compounds were added, CellTiter-Glo (CTG, Promega) reagent was added following the  
1446 vendor protocol. Three times more USP7 null HCT-116 cells were plated per well than  
1447 wild-type HCT-116 cells (7,500 vs. 2,500 cells), given the slower proliferation of USP7  
1448 null cells. For studies with multiple myeloma cell lines, cells were seeded in 0.5% serum  
1449 and treated with compounds immediately. Twenty-four hours later, serum was added  
1450 back to normal levels. CTG assay was done 24 hours later, i.e. 48 hours after  
1451 compounds were added instead of 72 hours later for the adherent cells.

1452  
1453 *Tumor cell line panel viability studies*. GNE-6640 and GNE-6641 were profiled across  
1454 441 cell lines as previously described<sup>28</sup>. In brief, compounds were screened in 9-point  
1455 dose response using a 3-fold dilution. Cells were seeded into 384 well plates 24 hours  
1456 prior to compound addition. Cells were then incubated with compound for 72 hours or  
1457 120 hours before assaying viability (CellTiter-Glo, Promega). Assays were performed in  
1458 biological triplicate. Cells were incubated (37 °C, 5% CO<sub>2</sub>) in RPMI-1640, 2.5% FBS (72  
1459 hour assay) or 5% FBS (120 hour assay), and 2 mM glutamine throughout the assay.  
1460 The reported IC<sub>50</sub> and mean viability metrics are as follows: IC<sub>50</sub> is the dose at which the  
1461 estimated inhibition is 50% relative to untreated wells (i.e. absolute IC<sub>50</sub>). The mean  
1462 viability statistic is the arithmetic average of the fitted viabilities at each tested dose.  
1463 Mean viability is equivalent to the area under the log-dose/viability curve divided by the  
1464 total number of tested doses, and is thus on an interpretable percentage scale.

1465  
1466 *Exome-Seq pipeline*. FASTQ reads were aligned to the human reference genome  
1467 (GRCh38) using GSNAP (PMID:20147302, 27008021) version '2013-10-10' using the  
1468 following parameters: -M 2 -n 10 -B 2 -i 1 --pairmax-dna=1000 --terminal-threshold=1000  
1469 --gmap-mode=none --clip-overlap. Duplicate reads in the resulting BAM file were  
1470 marked using PicardTools, and indels realigned using the GATK IndelRealigner tool.  
1471 Variations were called using the Bioconductor package VariantTools version 1.9.4. using  
1472 default options except for two exceptions: 1) no variants were called in repeat regions as  
1473 defined by the annotation Dust, Satellite repeats, and Tandem repeats in Ensembl 77  
1474 and 2) the avgNborCount post filter was configured using all SNPs from dbSNP version  
1475 138.

1476 *Mean viability analysis*. We determined genomic and non-genomic features that were  
1477 associated with differences in compound sensitivity. Mean viability is calculated as the  
1478 arithmetic average of the fitted viabilities at each tested dose, as previously described<sup>28</sup>.  
1479 For this analysis, normalized mean viabilities of GNE-6640 and GNE-6446 were  
1480 determined by normalizing the mean viabilities of each compound by the mean viability  
1481 of GNE-6641. Cancer type, cell histology, loss-of-function and hotspot mutations were  
1482 assessed for statistical association with changes in normalized mean viability. Loss-of-  
1483 function protein coding mutations include: 1) insertions, 2) deletions, and 3) substitutions  
1484 resulting in predicted truncating, splice site, translational start site, or non-stop mutations



1485 present in greater than 90% of reads sequenced (> 90% variant allele frequency).  
1486 Hotspot missense mutations assessed here were previously reported as significantly  
1487 recurrent mutations in a pan-cancer analysis (PMID: 26619011). Features present in at  
1488 least 3 cell lines were assessed. Statistical significance was determined using two-sided  
1489 Student's t-Test. Q-values were determined by correcting resulting p-values for multiple  
1490 hypothesis testing using Benjamini and Hochberg.

1491 *Primary combination screen.* A compound library comprising 589 compounds arrayed in  
1492 9 point dose response was screened in the absence or presence of fixed doses of GNE-  
1493 6776 (0 nM, 125 nM, 250 nM, 500 nM, 1000nM, and 2000 nM) or GNE-6640 (400 nM).  
1494 Briefly, 5,000 EOL-1 cells were seeded into 384 well plates, and compound was added  
1495 24 h later. Cell viability was determined 120 h post-compound addition (CellTiter Glo).  
1496 Curves were fitted, and both IC<sub>50</sub> and mean viability metrics were calculated. The IC<sub>50</sub> is  
1497 the dose at which inhibition is 50% relative to untreated wells. The mean viability is the  
1498 average of the fitted viabilities at each tested dose. Mean viability is equivalent to the  
1499 area under the log-dose/viability curve divided by the total number of tested doses.  
1500 Mean viability values were used for the analysis described in Extended Data Figure 6d.  
1501 All data were fitted using Genedata Screener (GDS) software.

1502 *Primary combination screen analysis.* We determined normalized mean viabilities in the  
1503 EOL-1 cell line for 574 compounds with a known protein or mechanistic target either in  
1504 the presence of DMSO or increasing concentrations of GNE-6776 (100 nM, 250 nM, 500  
1505 nM, 1000 nM or 2000 nM) or 400 nM of GNE-6640. For each compound we assessed  
1506 the difference in mean viability between USP7-inhibitor treatment versus the DMSO  
1507 treatment. For targets targeted by 3 or more compounds we calculated the enrichment  
1508 of high mean viability difference for each concentration of USP7 inhibitor by using the  
1509 Wilcoxon rank sum test. For visualization purposes we combine the results of all  
1510 concentrations by taking the mean of the -log<sub>10</sub> transformed p-values for each target.

1511 *Bliss Analysis.* PIM inhibitors were tested in a 9-point dose response matrix with GNE-  
1512 6676 in the same manner as described for the compound library screen. Inhibitors were  
1513 screened in 3-fold dilution using a top concentration of 10 μM for PIM inhibitors and 20  
1514 μM for GNE-6676. Bliss calculations were performed in GDS.

1515

#### 1516 ***Deubiquitinase selectivity analysis***

1517 *Recombinant deubiquitinase di-ubiquitin mass spec cleavage assay.* The MALDI-TOF  
1518 DUB assay was performed using the indicated concentrations of recombinant  
1519 deubiquitinases, di-ubiquitin substrates, and USP7 inhibitor compounds as previously  
1520 described<sup>4</sup>. The inhibition efficiency for GNE-6640 and GNE-6776 against the UCHL  
1521 family members was monitored on an alternative substrate, Ub-Ube2W (Ub-E2), since  
1522 UCHL1, -3, and -5 and BAP1 are inactive against ubiquitin dimers of all linkage types<sup>29</sup>.

1523

1524 *Endogenous deubiquitinase activity-based probe assay.* 293T cells at 80% confluency  
1525 were harvested by rinsing the plate once with 10 mL PBS followed by scraping. Cells  
1526 were cleared by spinning them for 3 min at 350 g at 4°C and cell pellets were flash-  
1527 frozen in liquid nitrogen and stored at -80 °C until lysis. Frozen pellets were lysed by  
1528 quickly re-thawing them in Buffer A (50 mM Tris-HCl pH 7.5, 250 mM Sucrose, 1x  
1529 Phosphatase STOP, 2.5 mM TCEP, 2 mM ATP, 50 μM phenylmethylsulfonyl fluoride  
1530 (PMSF), 120 mM NaCl, 5 mM MgCl<sub>2</sub>) and the lysate was cleared by centrifugation by  
1531 spinning at 18,000 g at 4°C. The protein concentration was adjusted to 5 mg/mL, and 5  
1532 mg (1 mL) each of this cell lysate was incubated with indicated compounds or DMSO at

1533 the indicated concentrations for 20 min at 900 rpm, 25 °C in a Thermomixer®  
1534 (Eppendorf AG). After compound incubation, 300 ng recombinant viral DUB was added  
1535 and lysates were incubated with 6.6 µg/mL of the indicated activity-based DUB probe,  
1536 1250 rpm, at 25°C, for the indicated times. The reaction was terminated by adding a  
1537 20% SDS solution to a final concentration of 0.4% for at least 30 min at room  
1538 temperature, rotating. Subsequently, the lysate was diluted 10x with Buffer B (50mM  
1539 Tris-HCl pH 7.5, 150 mM NaCl, 5 mM EDTA, protease inhibitor cocktail EDTA-free  
1540 (Roche, Mannheim, Germany), 50 µM PMSF, 0.5 % NP-40) into 15 mL conical tubes. ~  
1541 120 µL slurry of pre-equilibrated anti-HA affinity matrix (Roche, Mannheim, Germany)  
1542 was added and HA-tagged proteins were immunopurified with this matrix by rotating the  
1543 samples overnight at 4 °C. The beads were then washed 1 mL of ice-cold Buffer B (3x),  
1544 Buffer B without NP-40 (1x), and TEAB (15 mM Triethylammonium bicarbonate, pH 8.5)  
1545 (3x). Spins between washes were performed at 2000 g at 4°C. To elute the  
1546 immunopurified material 330 µL of Buffer C (1 mg/mL HA peptide (Thermo Scientific,  
1547 Waltham, MA), 15 mM TEAB, 0.02 % Rapigest® (Waters, Milford, MA)) was added and  
1548 the samples were incubated at 37°C for 30 min at 1100 rpm shaking in a Thermomixer®  
1549 (Eppendorf AG). The eluted material was cleared from the beads by spinning at 2600 g.  
1550 The cleared material was stored at -80 °C until mass spectrometry preparation and  
1551 analysis. For DUB identifications the eluted proteins were digested with trypsin using  
1552 filter-aided sample preparation (FASP). Eluents were added to Microcon-30K filtration  
1553 devices (Millipore, Billerica, MA) and briefly washed by 0.2 mL of 8 M urea in 200 mM  
1554 TEAB, pH 8.5. In between each step, liquid was cleared by centrifugation at 14,000 xg,  
1555 except if noted. Proteins were reduced by Dithiothreitol (DTT) for 20 minutes at 60°C  
1556 and subsequently alkylated by iodoacetamide (IAA) for 15 minutes in the dark. The  
1557 membrane was further washed by 8 M urea once and 200 mM TEAB three times.  
1558 Trypsin (Promega, Madison, WI) was added at 1:40 enzyme/substrate ratio. Devices  
1559 were briefly centrifuged at 100 xg for 30 seconds and incubated overnight at 37°C.  
1560 Tryptic peptides were recovered by centrifugation at 14,000 xg for 4 minutes. An  
1561 additional 60 µL of 200 mM TEAB, pH 8.5 was added to the devices and centrifuged as  
1562 an additional elution step. This eluent was combined with the previous for further  
1563 processing. Ten percent of the eluents were dried in speedvac and desalted with a C18  
1564 STAGE tip (Proxeon, Thermo Fisher) before injected onto the mass spectrometer for LC-  
1565 MS/MS acquisition.

1566

1567 *Deubiquitinase identification by mass spectrometry.* Peptides were loaded onto an  
1568 Acuity UPLC® BEH130 C18 column (1.7 µm, 12Å, 100 µm x 100 mm) at a flow rate of  
1569 1.5 µL/min in solvent A (98% water/2% MeCN/0.1% formic acid) using a NanoAcquity  
1570 UPLC system (Waters, Milford, MA). Separation was achieved with a linear gradient of  
1571 2% Solvent B (98% MeCN/2% water/0.1% formic acid) to 25% Solvent B over 45  
1572 minutes. Eluted peptides were injected onto an Orbitrap Elite mass spectrometer  
1573 (Thermo Fisher, San Jose, CA) using an Advance CaptiveSpray source (Bruker, Auburn,  
1574 CA) at a voltage of 1.2kV. Full MS scans were collected in the orbitrap at 60,000  
1575 resolution and the top 15 most abundant ions were selected in a data dependent mode  
1576 and fragmented with CID and ms/ms were collected in the ion trap. MS/MS spectra  
1577 were searched using Mascot (v.2.3.02) against a human proteome database (Uniprot  
1578 Dec. 2011) with known contaminants along with all decoy sequences. Search  
1579 parameters included trypsin cleavage allowing up to 2 missed cleavage events, a  
1580 precursor ion tolerance of 50 ppm, and a fragment ion tolerance of 0.8 Da. Searches  
1581 also permitted variable modifications of methionine oxidation (+15.9949 Da), and two  
1582 cysteine modifications of either (+57.0215) for carbamidomethylation or (+192.0569 Da)  
1583 for reacted DUB probe remnant, Peptide spectra matches were filtered with a false

1584 discovery rate (FDR) of 5% on the peptide level and subsequently at 2% on the protein  
1585 level. Each identified peptide-spectrum match (PSM) was quantified using the area  
1586 under curve and same quantification event was extended to other runs where such  
1587 peptide was not identified by an ms/ms spectrum, based on exact precursor m/z and  
1588 retention time matching.

1589  
1590 *Statistical analysis of deubiquitinase activity data.* Detected and quantified area-under-  
1591 curve (AUC) measures from label-free mass spectrometry were logarithmically (base 2)  
1592 rescaled. Changes between inhibitor- and control-treated lysate were compared via a  
1593 linear mixed effects model with fixed effects for treatments and random effects for  
1594 peptide species and mass-spec run. Computations were performed in R, version 3.3.0  
1595 using the R package *lme4*, with error degrees of freedom estimated via the Kenward-  
1596 Roger method using the R package *pbkrtest*. For each protein, log<sub>2</sub> fold change in  
1597 activity was normalized to that observed in a spiked-in viral DUB or BSA control protein.  
1598 Statistical significance of the observed “inhibitor-vs-control” differences in log<sub>2</sub> fold  
1599 change between each DUB and the control protein was then assessed via a t-statistic  
1600 with Satterthwaite-estimated degrees of freedom, and corrected for multiplicity via the  
1601 Benjamini-Hochberg False-Discovery Rate method (FDR) set at 0.10.

1602

### 1603 **Animal use and care**

1604 All animal work followed the recommendations of the Guide for Care and Use of  
1605 Laboratory Animals with respect to restraint, husbandry, surgical procedures, feed and  
1606 fluid regulation, and veterinary care. The animal care and use program at Genentech is  
1607 accredited by the Association for Assessment and Accreditation of Laboratory Animal  
1608 Care International (AAALAC), which assures compliance with accepted standards for the  
1609 care and use of laboratory animals. Studies were tailored to minimize the number of  
1610 animals used, yet sufficient numbers to address any variability in drug exposure or  
1611 biomarker response. Due to the need to monitor potential adverse effects with first in-  
1612 life assessment of novel compounds, no study was conducted under blinded conditions.

1613

### 1614 **DMPK analysis**

1615 *In vitro* DMPK studies were performed using standard protocols. GNE-6776 was  
1616 formulated as a suspension in 0.5% methylcellulose/0.2% Tween-80 (MCT) and was  
1617 administered at 200 mg/kg by oral gavage to female *C.B-17 SCID* mice, age 12 – 16  
1618 weeks (Charles River Labs; n=3 per time point). At 0.5, 1, 2, 4, 8 and 24 hours post-  
1619 dose, blood samples were collected by terminal cardiac puncture into anticoagulant  
1620 tubes (EDTA). Clarified plasma was then transferred to a fresh tube and snap frozen.  
1621 GNE-6776 plasma concentrations were determined by LC/MS-MS.

1622

### 1623 **In vivo pharmacodynamic response**

1624 For EOL1 acute myeloid leukemia xenograft studies, immunodeficient *C.B-17 SCID* mice  
1625 (Charles River Labs), aged 12 - 16 weeks, were inoculated subcutaneously on the right  
1626 flank with five million cells in a 50:50 suspension of HBSS:Matrigel (BD Biosciences; 100  
1627 µL). When tumor volumes reached between ~285-500 mm<sup>3</sup>, mice were distributed into  
1628 volume-matched cohorts (n=4). For MCF7 breast cancer xenograft studies,  
1629 immunodeficient *nu/nu* mice (Charles River Labs), aged 6-8 weeks, were implanted with  
1630 0.36 mg estrogen pellets (Innovative Research of America) via trochar 1-3 days prior to  
1631 tumor cell inoculation. Ten million MCF7-Ser cells, an *in vivo*-optimized MCF7 variant,  
1632 were injected orthotopically into the 2/3 mammary fat pad of each mouse in a 50:50  
1633 suspension of HBSS:Matrigel (BD Biosciences) in a total volume of 100 µL. When tumor  
1634 volumes reached between ~285-450 mm<sup>3</sup>, mice were distributed into volume-matched

1635 cohorts (n=4). GNE-6776 was formulated as a suspension in 0.5%  
1636 methylcellulose/0.2% Tween-80 (MCT) and was administered at 200 mg/kg by oral  
1637 gavage at zero and four hours. MCT control or GNE-6776-treated samples were  
1638 collected at eight hours following the first dose and excised tumors were flash-frozen on  
1639 dry ice. Tumors were lysed in RIPA buffer containing protease inhibitors (Roche) and  
1640 300 mM NaCl using a Qiagen Tissuelyser. Samples were incubated on ice for 15  
1641 minutes and then centrifuged at 20,000 x g at 4°C for 10 minutes. Protein levels in  
1642 clarified lysates were quantified using a Pierce BCA assay kit and concentrations were  
1643 normalized with sample buffer. Samples were run on gels and proteins were transferred  
1644 to membranes and western blotted as described above.

1645

#### 1646 ***In vivo efficacy study***

1647 For EOL1 acute myeloid leukemia xenograft studies, immunodeficient *C.B-17 SCID* mice  
1648 (Charles River Labs), aged 12 - 16 weeks, were inoculated subcutaneously on the right  
1649 flank with five million cells in a 50:50 suspension of HBSS:Matrigel (BD Biosciences; 100  
1650  $\mu$ L). When tumors became established (150 – 300  $\text{mm}^3$ ), mice were distributed into  
1651 tumor volume-matched cohorts (n=7, mean tumor volume  $\sim$ 250  $\text{mm}^3$ ). GNE-6776 was  
1652 formulated as a suspension in 0.5% methylcellulose/0.2% Tween-80 (MCT) and was  
1653 administered at 100 or 200 mg/kg by oral gavage on a once or twice daily schedule.  
1654 Tumor volume measurements, body weight and condition data was collected 2-3 times  
1655 per week.

1656

#### 1657 ***USP7 enzymatic analysis***

1658 Michaelis-Menten kinetic measurements with full-length USP7 were carried out using 1  
1659 nM USP7 with a series of ubiquitin-AMC substrate titrations with at least three technical  
1660 replicates. Initial rate of substrate hydrolysis was determined using the Magellan  
1661 software on a Tecan Safire2 plate reader and kinetic parameters modeled using  
1662 nonlinear regression analysis with GraphPad Prism software. Standard error was  
1663 calculated from multiple experimental replicates. For studies using the USP7  
1664 D305/E308 mutant, samples were reacted in a buffer consisting of 50 mM HEPES (pH  
1665 7.5), 100 mM NaCl, 2.5 mM Dithiothreitol, 0.1% (w/v) bovine gamma globulin (Sigma cat  
1666 # G5009-25G). The starting substrate concentration of Ubiquitin-Rho110 (Boston  
1667 Biochem cat # U-555) used for the Michaelis-Menten analysis was 100  $\mu$ M serial diluted  
1668 to 781 nM. Reactions were carried out for 1 hour at room temperature with a final  
1669 enzyme concentration of 100 nM (three independent experiments, see symbols in plot),  
1670 in a black 100  $\mu$ L volume 96 well half area plates (Corning cat # 3993). The enzymatic  
1671 activity was calculated by fitting the data using the initial velocity using the linear  $V_0$   
1672 values measured by analyzing the fluorescence signal of cleaved Rho-110 using  
1673 excitation at 485 nm and emission at 535 nm.

1674

#### 1675 ***X-Ray crystallography***

1676 Crystals were grown by the hanging-drop method by mixing the USP7 catalytic domain  
1677 (residues 208–554) at 15 mg/ml with an equal volume of reservoir solution containing  
1678 100 mM Tris,-HCl, pH 7.0, and 20% PEG1000 (v/v). Co-structures with compounds were  
1679 obtained by soaking crystals with 1 mM of compound overnight. Crystals were  
1680 cryoprotected with reservoir solution supplemented with 20% glycerol (v/v) and flash  
1681 frozen in liquid nitrogen. Data collection and refinement statistics are detailed in  
1682 Extended Data Fig. 7d.

1683

#### 1684 ***Generation of isotopically-labeled di-ubiquitins***

1685 Ubiquitin was cloned into a peT3a vector and transformed into the auxotrophic strains  
1686 RF2 and ML2 (a kind gift from Robert Gennis and Toshio Iwasaki)<sup>30</sup> and expressed  
1687 with the following modifications: Bacterial cultures were grown at 37°C in M9 media  
1688 supplemented with NH<sub>4</sub>Cl (2 g/L), C<sub>6</sub>-glucose (4 g/L). Strain RF2 was additionally  
1689 supplemented with 6mM <sup>15</sup>N L-Thr (Cambridge Isotopics Cat#NLM-142-PK) and ML2  
1690 were supplemented with 6mM <sup>15</sup>N L-Leu (Cambridge Isotopics Cat#NLM-142-1) and 6  
1691 mM unlabeled Ile and Tyr (Sigma-Aldrich Cat# I2752 and Cat# T3754). After reaching  
1692 an OD of 0.6 the cells were induced with 1 mM IPTG and further grown for 6 hours.  
1693 Protein purification was performed at room temperature. Cells were harvested and  
1694 lysed in lysis buffer (50 mM HEPES 7.0). The cleared lysate was subjected to affinity  
1695 chromatography using DEAE sepharose Fast Flow (GE Cat# 17-0709-01). Ubiquitin  
1696 was collected in the flow through and dialyzed overnight into NaOAc pH 4.5. Dialyzed  
1697 material was clarified by centrifugation at 35K and ubiquitin was subjected to ion  
1698 exchange chromatography (IEX) using a MonoS column (GE Healthcare, Cat# 17-  
1699 5169-01). The following enzymes were obtained from Boston Biochem Cambridge,  
1700 UBE1 (Cat# E-305), UBE2K and UBE2N/UBE2V1 complex (Cat# E2-602 and Cat# E2-  
1701 664) respectively. K63- and K48-linked di-ubiquitin chains were generated and purified  
1702 as follows: In separate reactions incubating 250 nM E1 enzyme, 5 μM UBE2K (K48  
1703 linked) or 5 μM UBE2N/UBE2V1 complex (K63 linked) with equal molar ratios of 1 mM  
1704 ubiquitin and 1 mM ubiquitin, 10 mM ATP, 50 mM HEPES (pH 8.0), 10 mM MgCl<sub>2</sub> in a  
1705 10 mL reaction at 37 °C. After 2 hours, the reaction was acidified with 2 mL of 17.4 M  
1706 Glacial Acetic Acid. Obtained di-ubiquitins (K63- or K48-linked) were purified by cation  
1707 exchange using a MonoS column (GE Healthcare, Cat# 17-5169-01). All purified di-  
1708 ubiquitin chains were buffer exchanged into 1x PBS buffer and proteins were flash  
1709 frozen in liquid nitrogen prior to storage at -80°C.

#### 1710 **Generation of 5-TAMRA-peptide/tetra-ubiquitin conjugates**

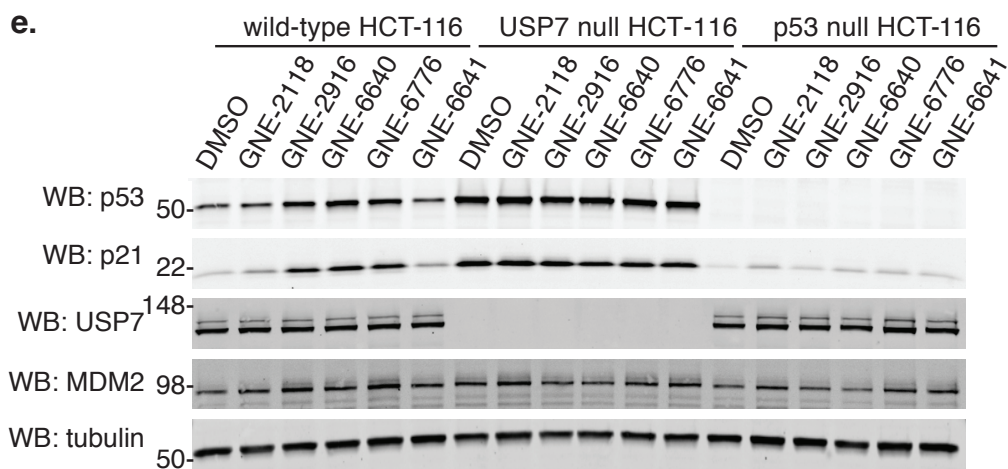
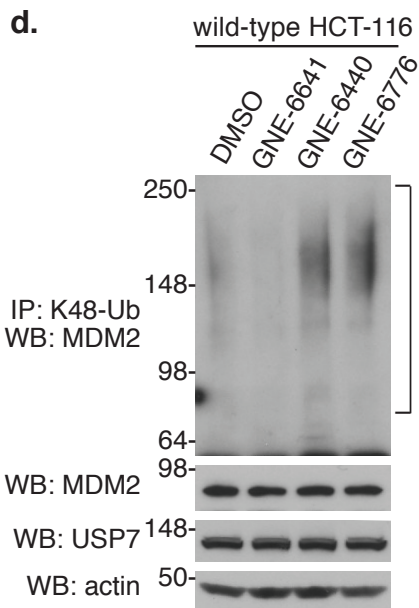
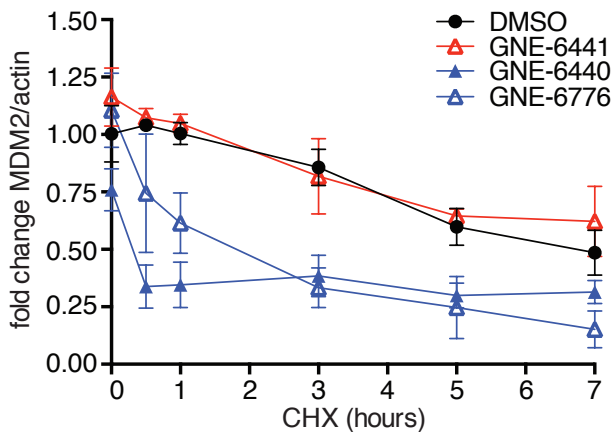
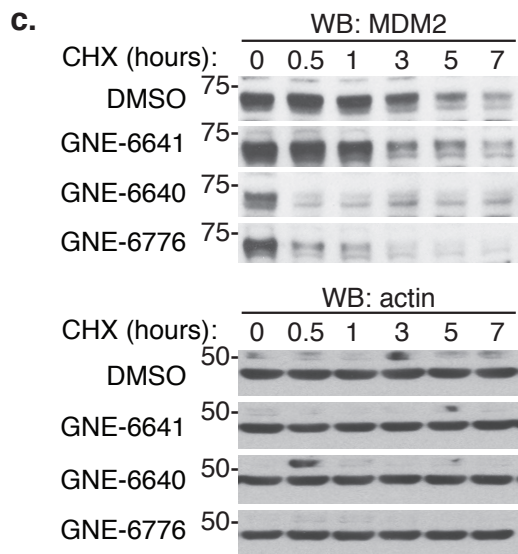
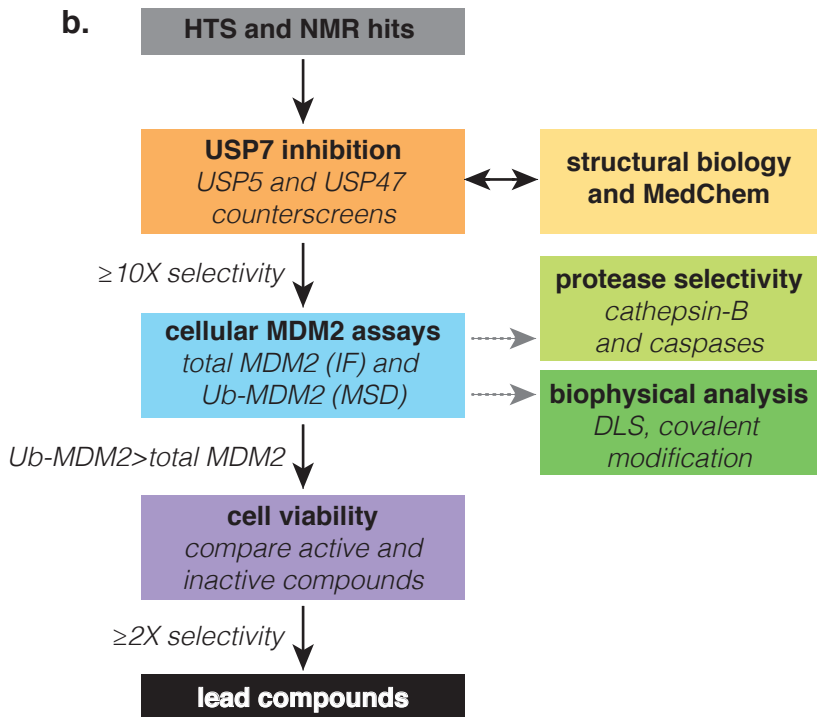
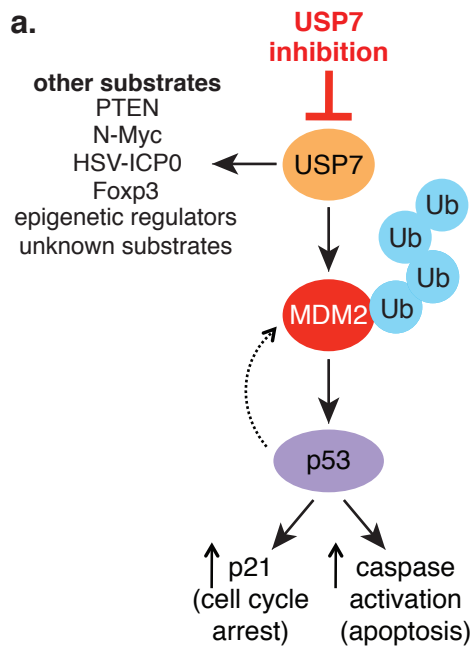
1711 K63- and K48-linked tetra-ubiquitin chains were obtained from Boston Biochem  
1712 Cambridge, K63-linked (Cat# UC-310B), K48-linked (Cat# UC-210B). The 5-TAMRA  
1713 (5-Carboxytetramethylrhodamine) peptide was generated by CPC-Scientific consisting of  
1714 the sequence 5-TAMRA-YPYDVPDYAIREIVSRNKRRYQEDG<sup>20</sup>. K63 or K48 tetra-  
1715 ubiquitin chains were conjugated to the peptide as follows: (1) Generation of tetra-  
1716 ubiquitin-MESNA; incubating 250 nM E1, 10 mM MgCl<sub>2</sub>, 10 mM MgATP, 1 mM tetra-  
1717 ubiquitin, 100 mM MESNA (Sigma Aldrich, Cat# 63705), in 20 mM Na<sub>2</sub>HPO<sub>4</sub> at pH 8.0 at  
1718 37°C overnight. Dialyzed into 0.4% TFA and tetra-ubiquitin-MESNA was lyophilized. (2)  
1719 Lyophilized tetra-ubiquitin was dissolved in DMSO at a concentration of 0.5 mM and 2  
1720 mg of peptide were added until all components were dissolved, reaction volume 1 mL.  
1721 The reaction was initiated by adding (final concentrations) NHS 27.5 mM, AgNO<sub>3</sub> 3.3  
1722 mM, and 22 μl DIPEA and incubated at RT overnight. The reaction was diluted 10X with  
1723 ddH<sub>2</sub>O and desalted into PBS pH 7.5. Non-conjugated peptide was removed by size  
1724 exclusion (SEC) chromatography. In a second step non-conjugated tetra-ubiquitin was  
1725 removed by IEX chromatography as described above and buffer exchanged into 1x PBS  
1726 (pH 7.5). The concentration of the purified final conjugate was determined by  
1727 absorbance using an extinction coefficient for 5-TAMRA at 80,000 cm<sup>-1</sup>M<sup>-1</sup>.

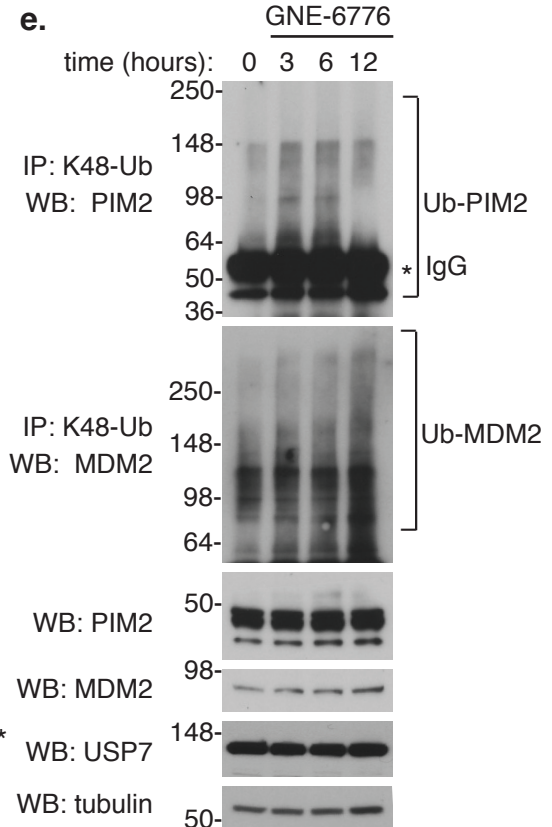
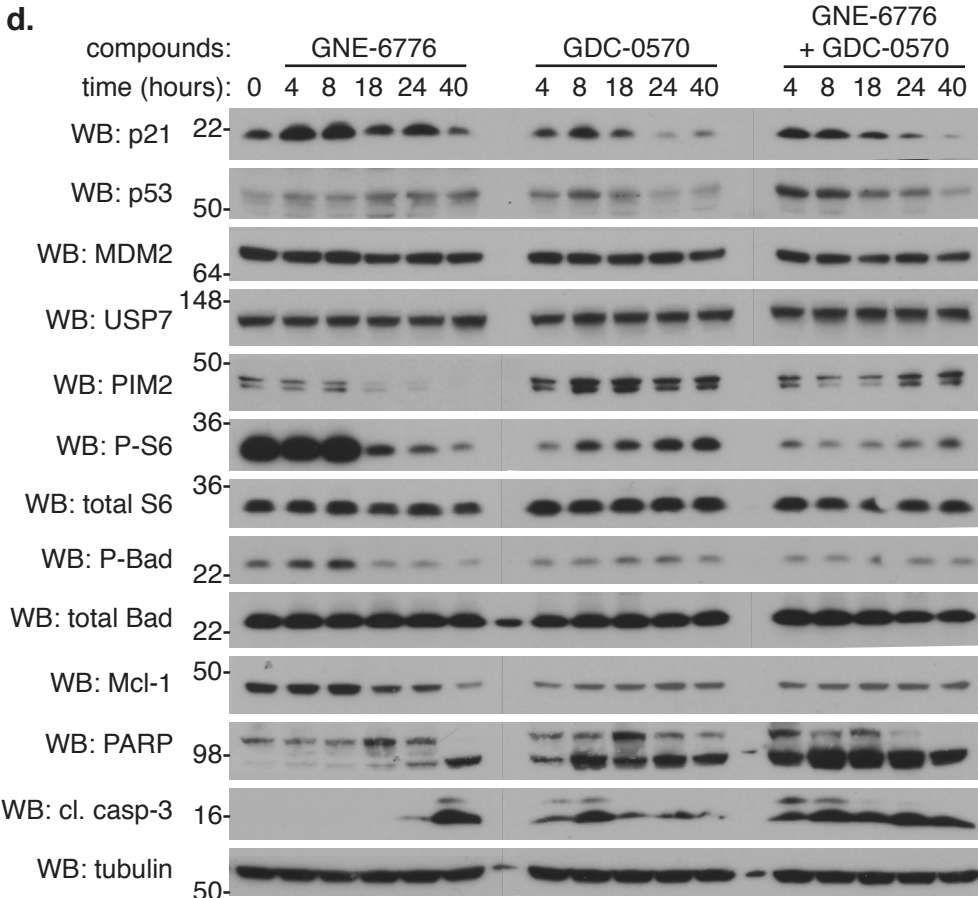
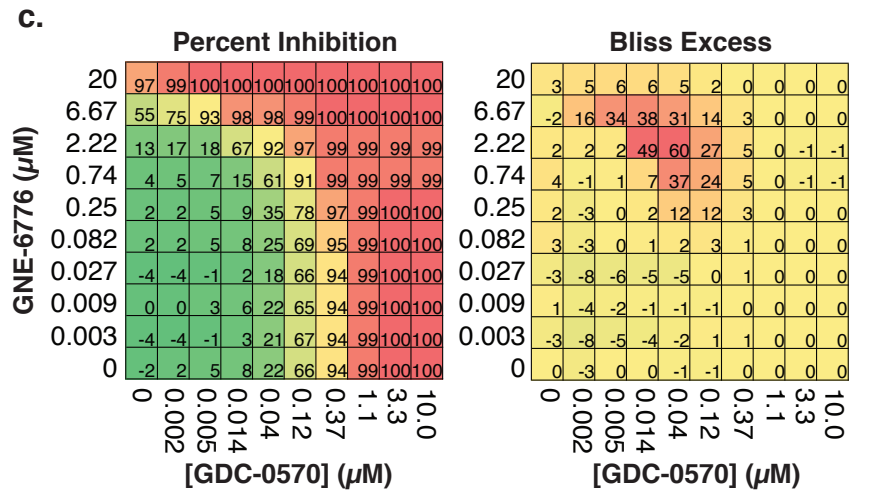
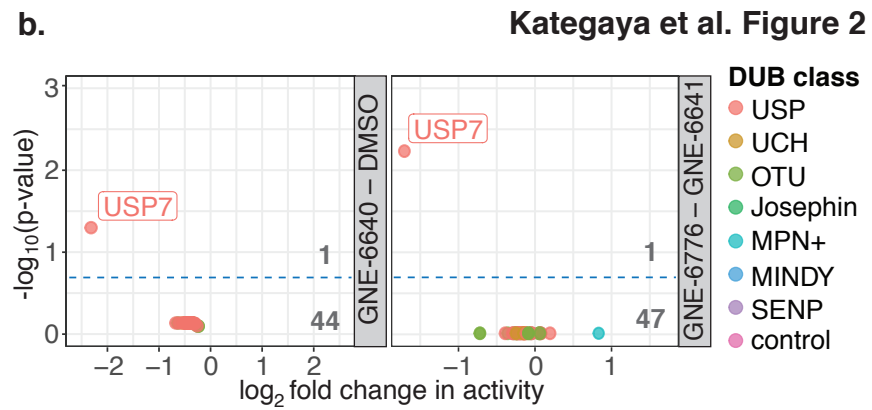
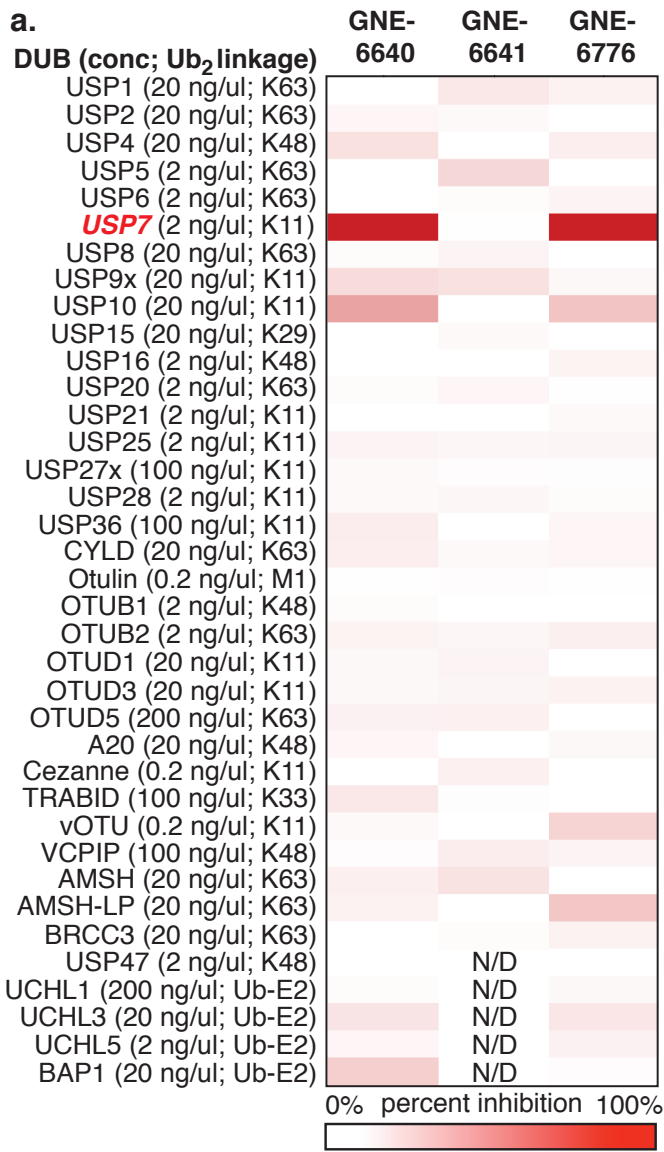
1728

#### 1729 **TAMRA-peptide/tetra-ubiquitin conjugate depolymerization studies**

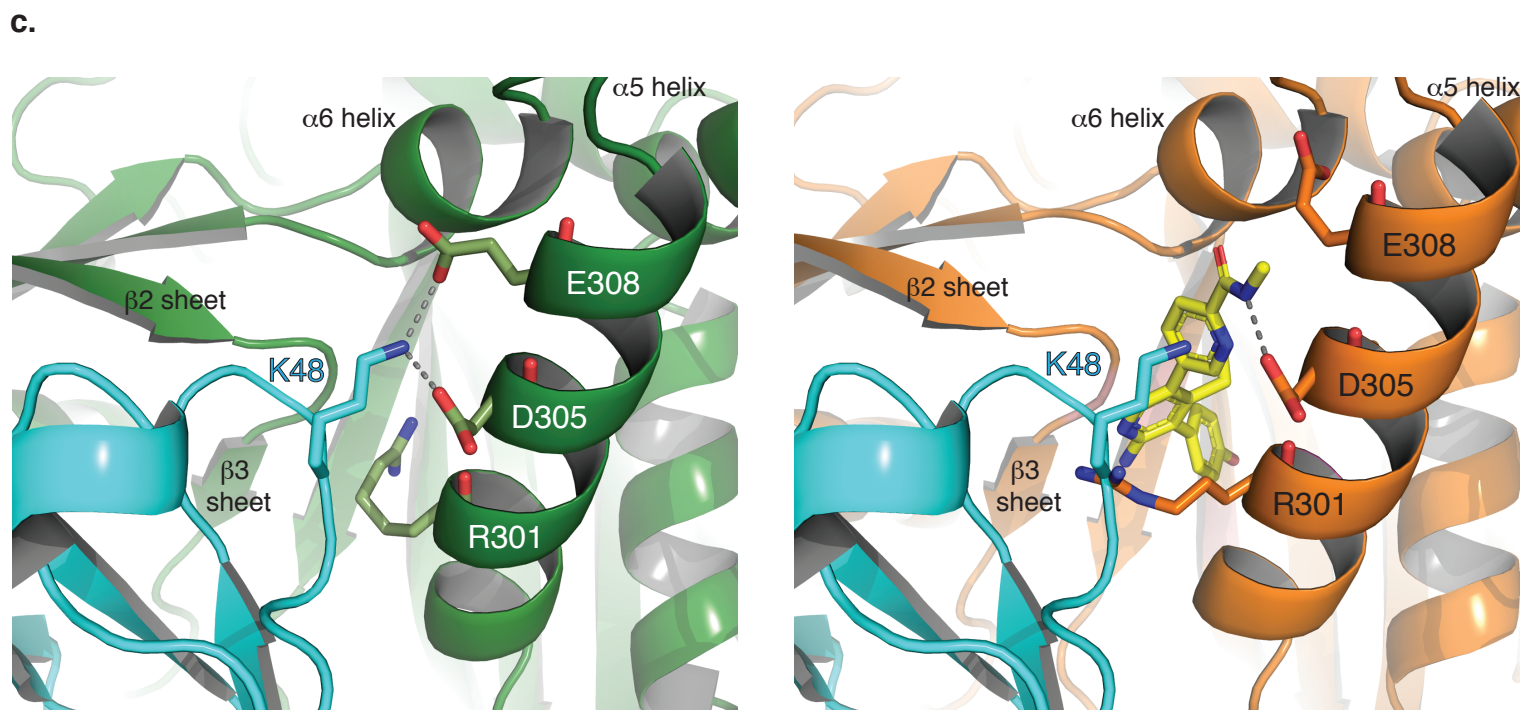
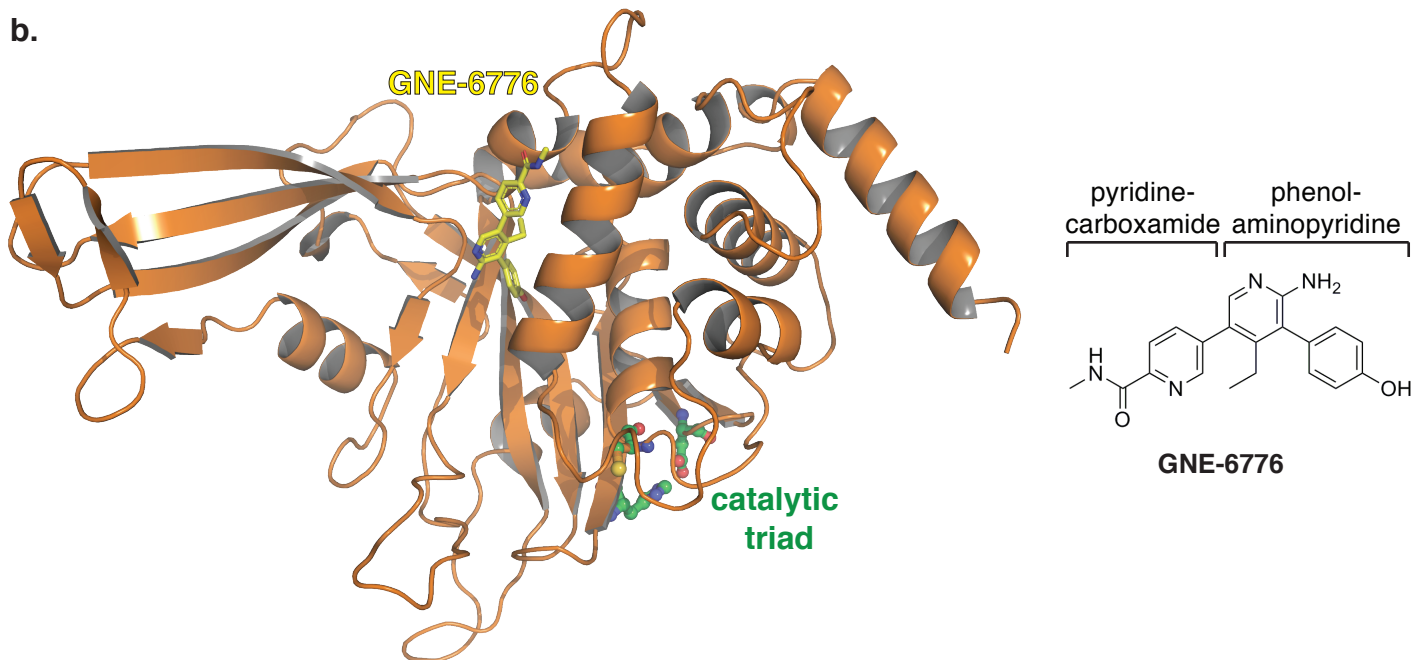
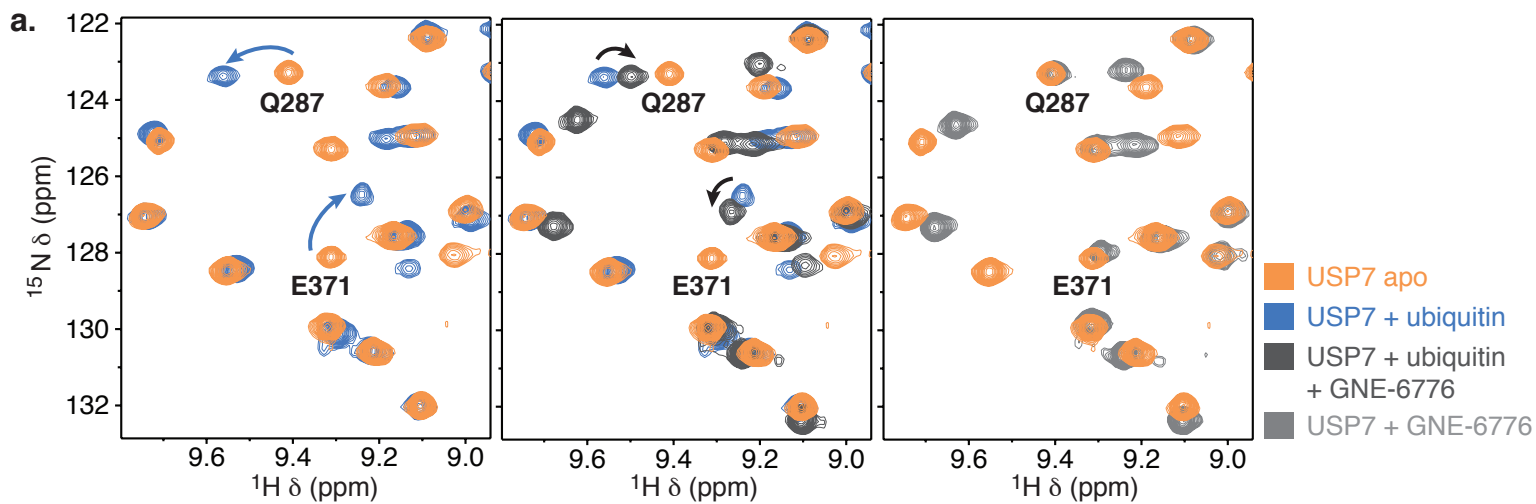
1730 For depolymerization assays, 100 nM USP7 (cat# E-519, lot#09939314) or 100 nM  
1731 USP7 catalytic domain N-terminal His-tag (Genentech, Hs\_USP7.K208-K554) were  
1732 diluted in 1x PBS buffer (pH 7.5) containing 5 mM DTT to generate 10x stock solutions in  
1733 respect to the final concentration and preincubated at room temperature for 10 minutes.  
1734 In a 90 μL reaction, 9 μg (2.7 μM) of 5-TAMRA-peptide/tetra-ubiquitin (K63- or K48-

1735 linked) was mixed with 9  $\mu\text{L}$  of diluted enzyme in 1 x PBS buffer (pH 7.5). Aliquots of 10  
1736  $\mu\text{L}$  of the reaction were mixed with 4  $\mu\text{L}$  2x SDS loading buffer at the time points  
1737 indicated to stop the reaction. Samples (14  $\mu\text{L}$ ) were subjected to SDS gel-  
1738 electrophoresis using precast BioRad Criterion TGX 10-20% gels (cat# 5671114).  
1739 Fluorescence was analyzed using the FluorChem imager from Protein Simple according  
1740 to the user manual. Densitometry values were analyzed using the software  
1741 AlphaViewSA, ProteinSimple.





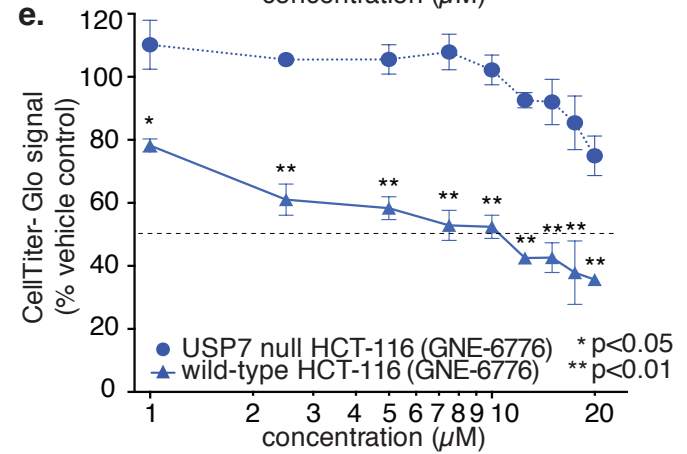
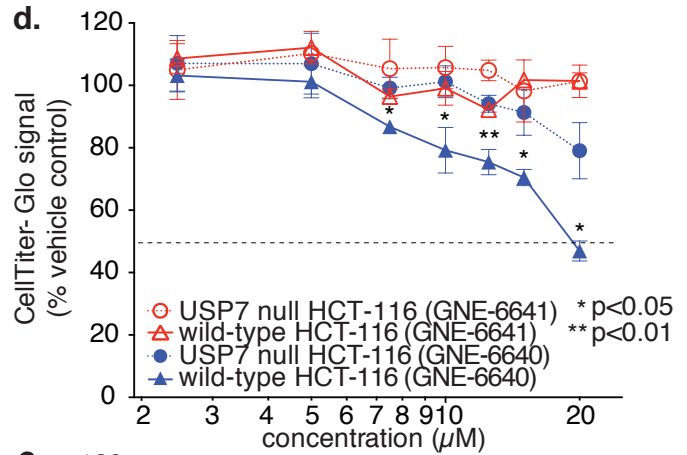
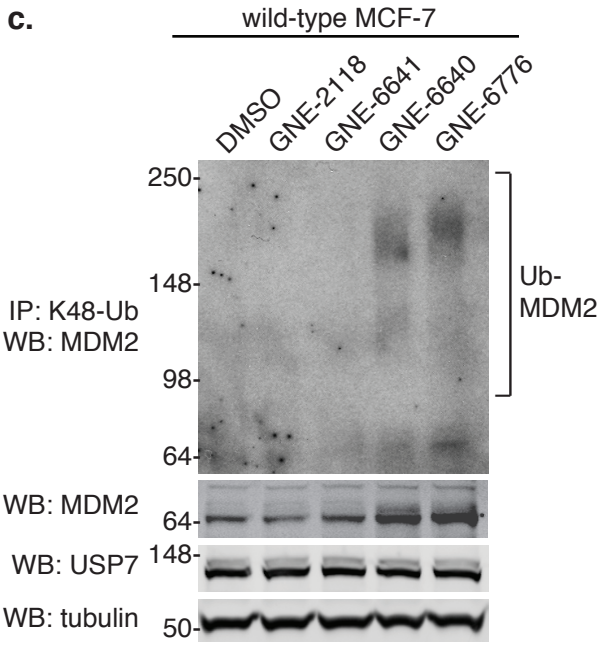
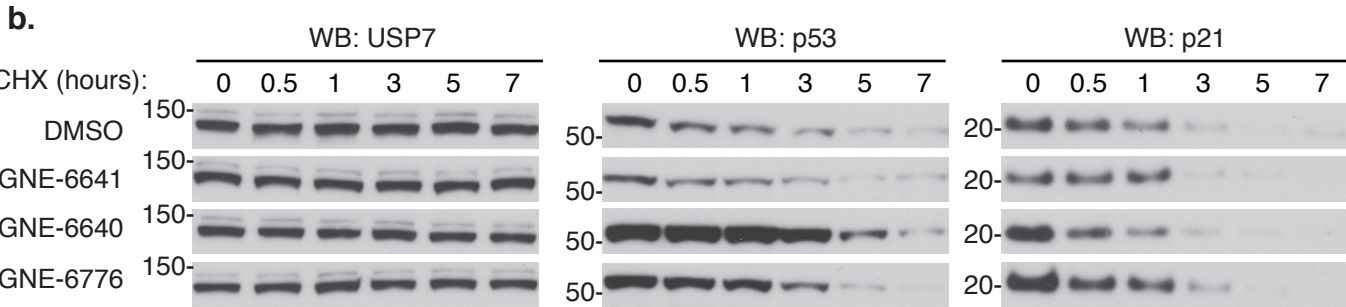
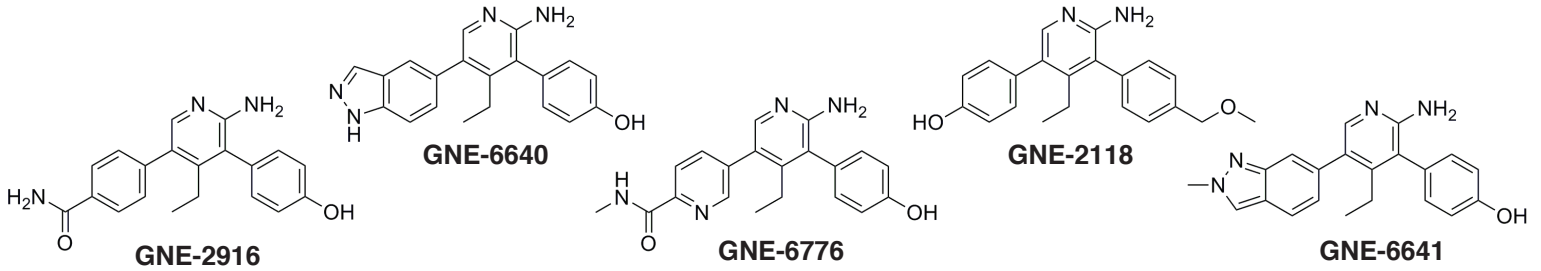


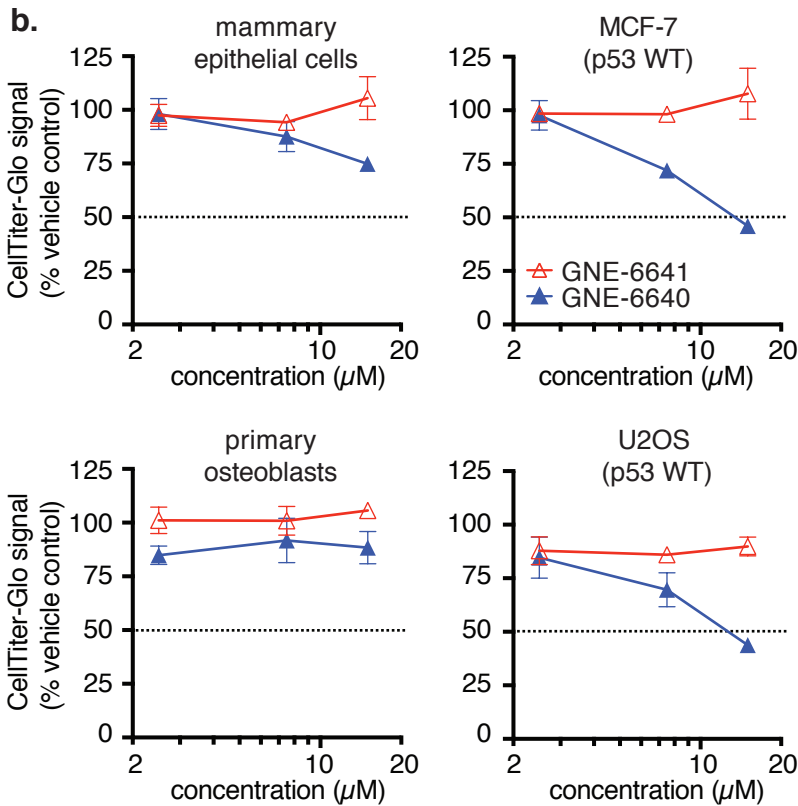
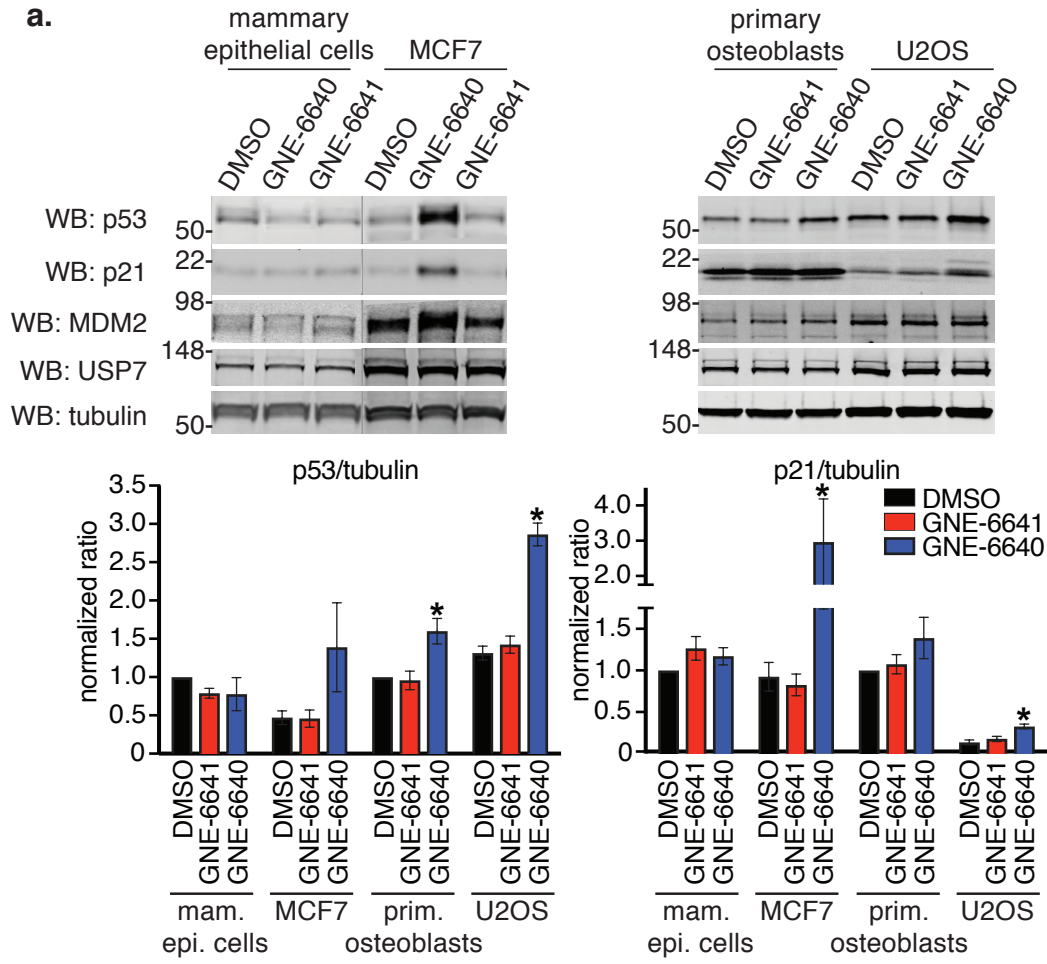


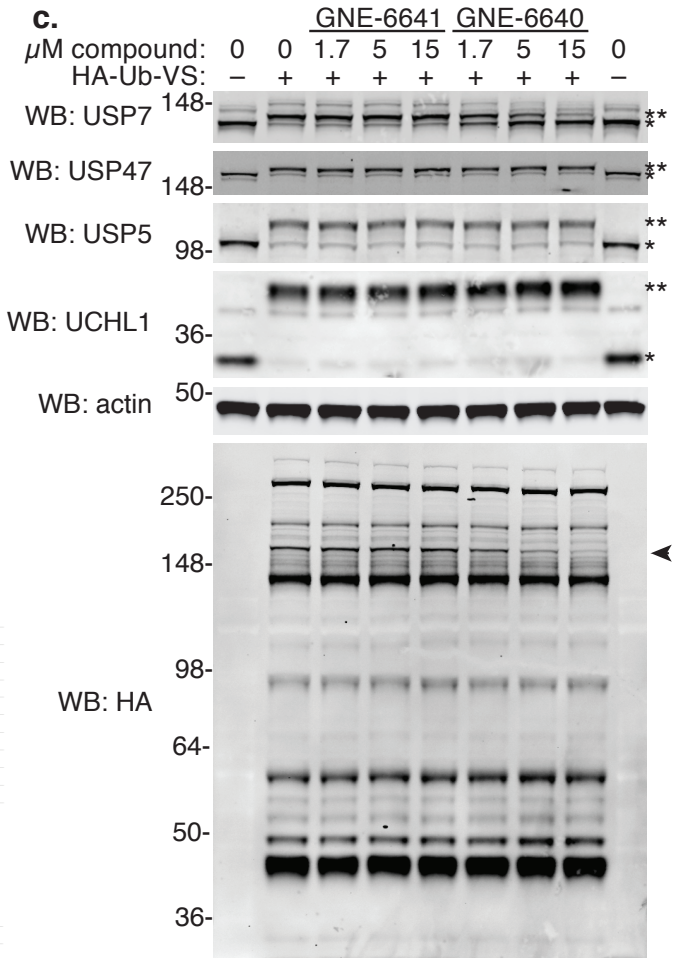
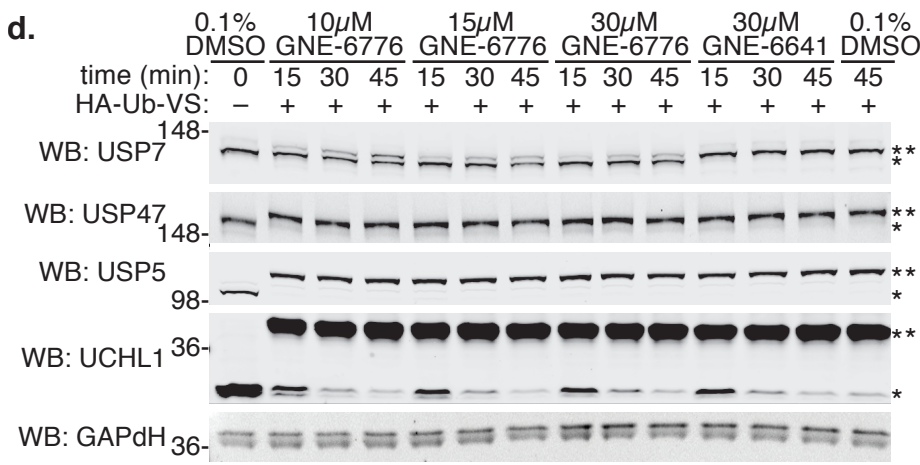
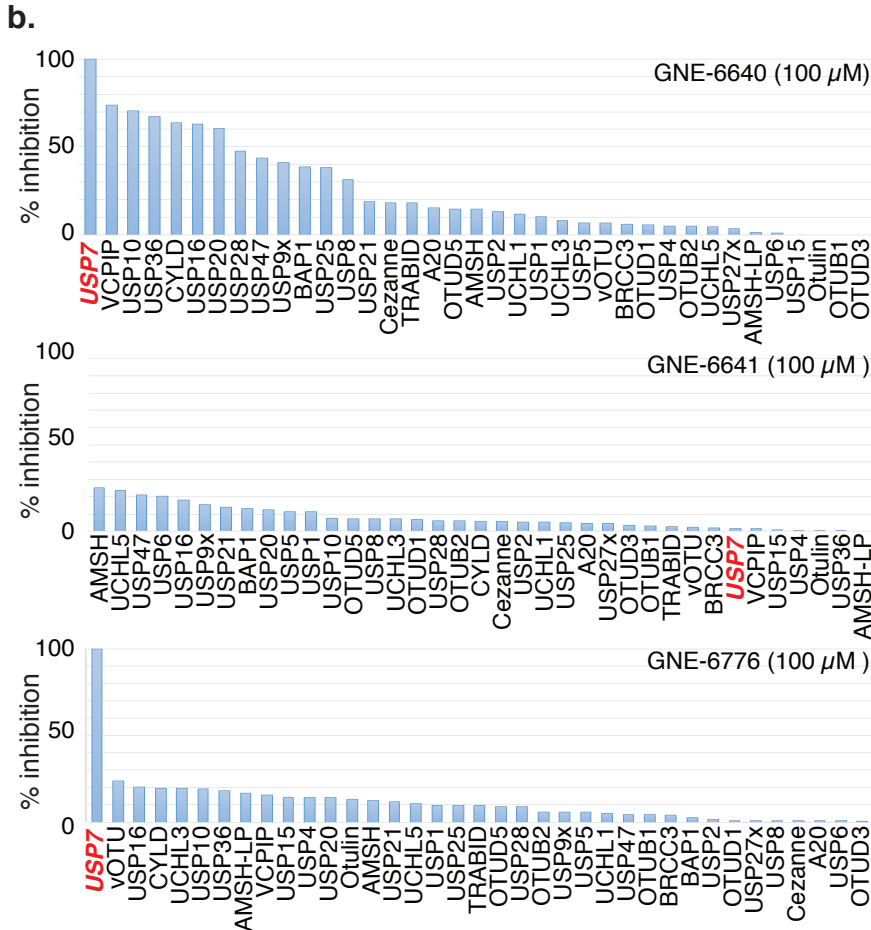
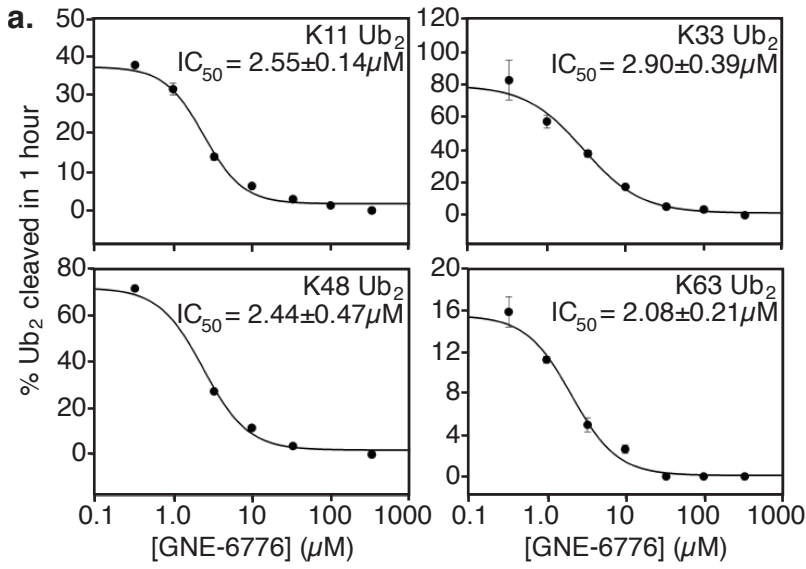


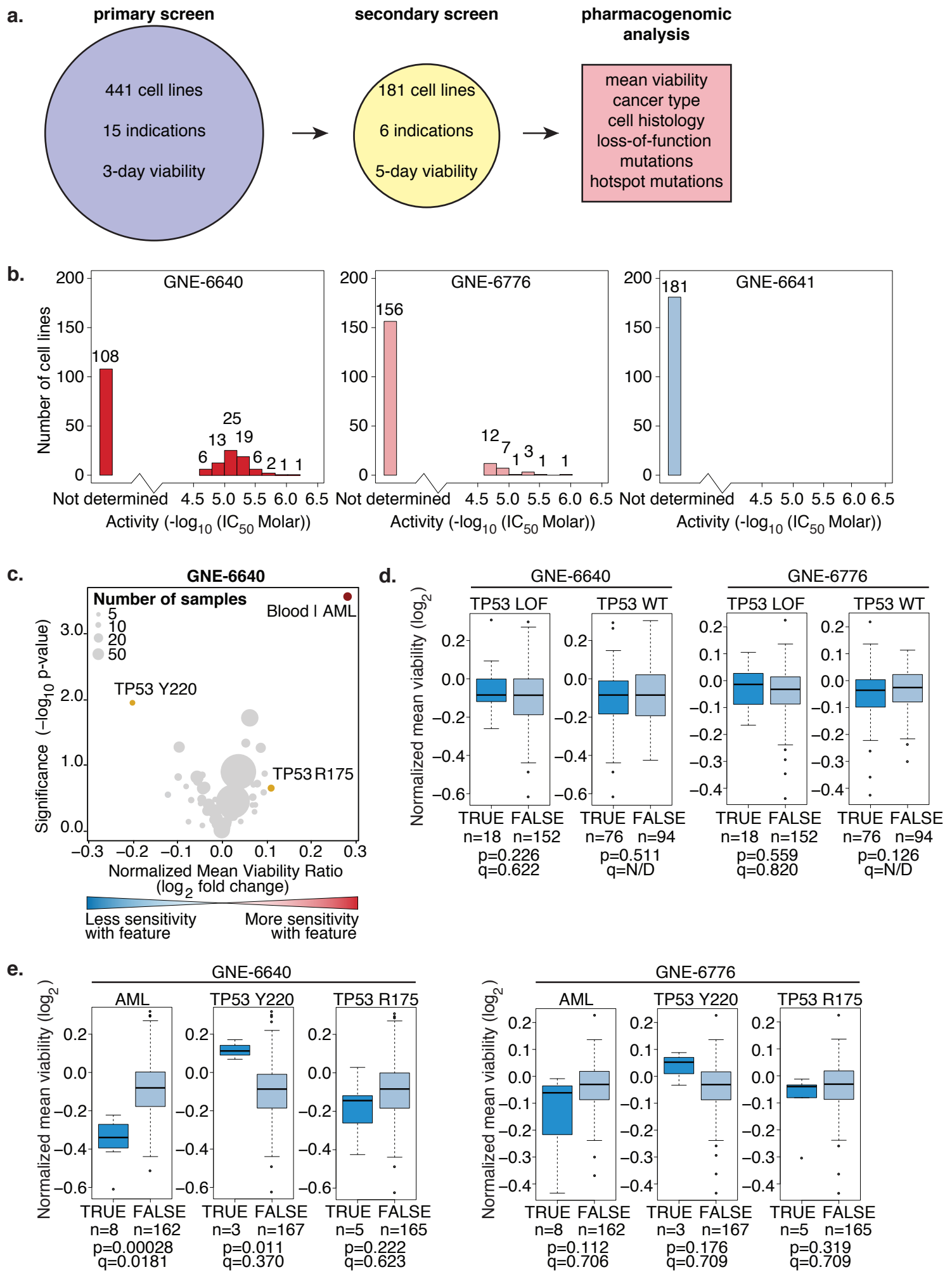
**a.** active compounds inactive control compounds

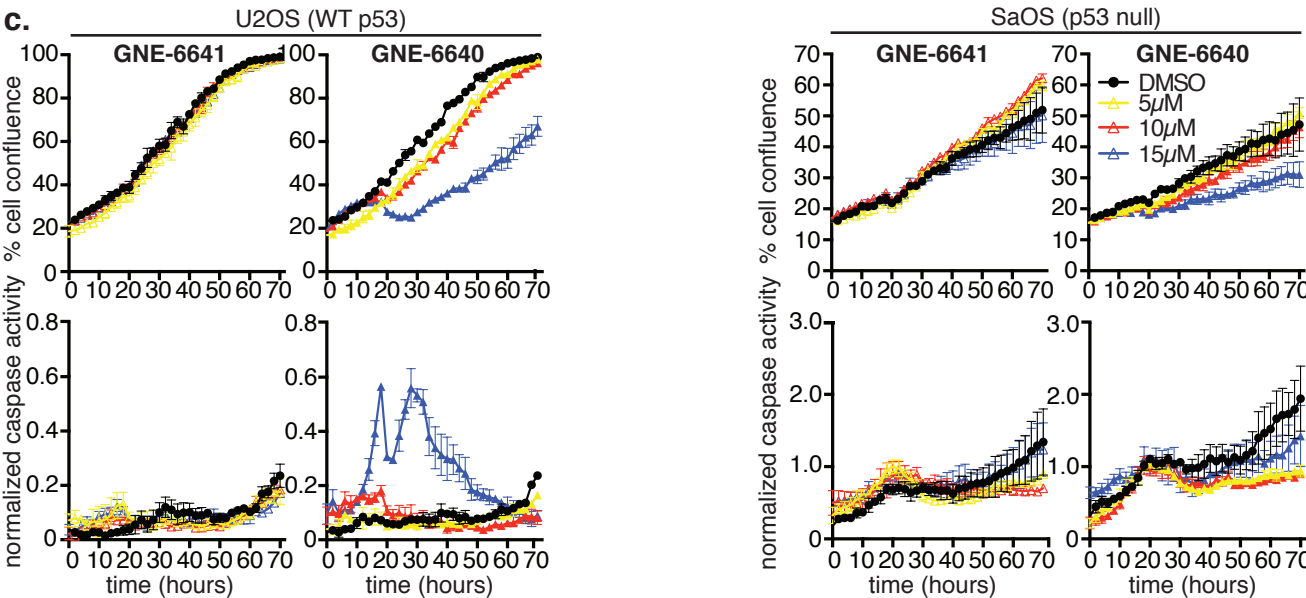
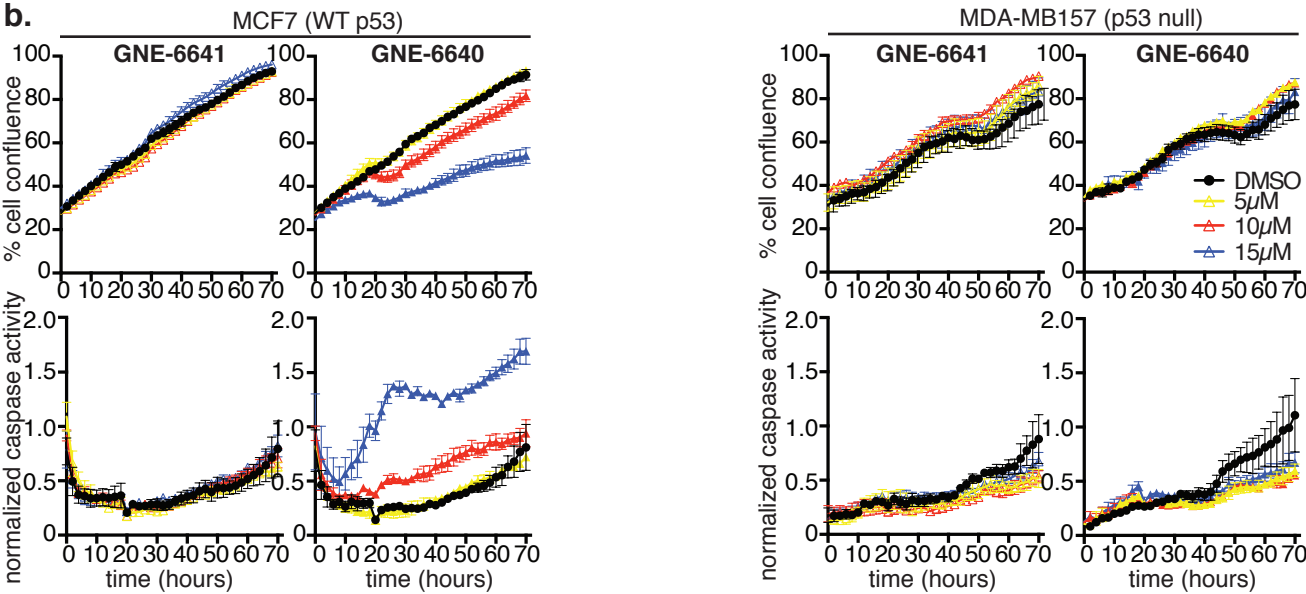
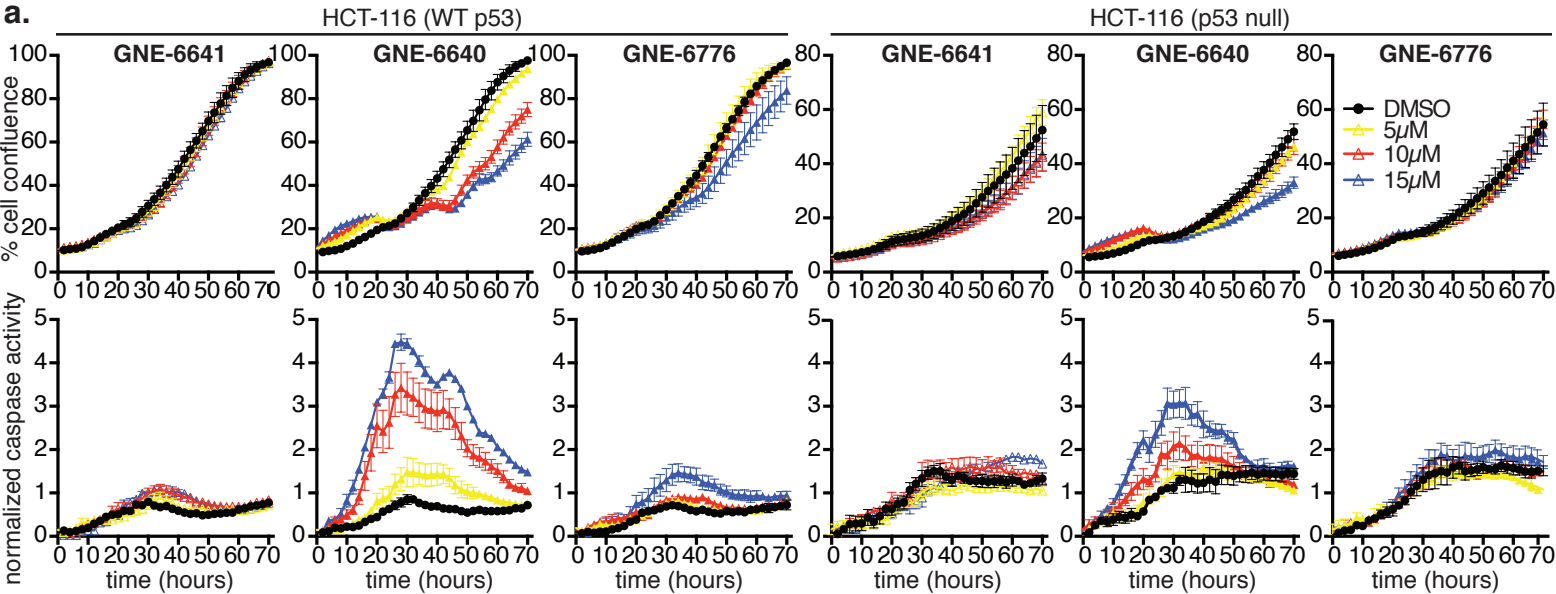
Compound	GENE-2916	GENE-6640	GENE-6776	GENE-2118	GENE-6641
Full Length USP7 IC <sub>50</sub> (μM)	2.63±0.43	0.75±0.37	1.34±0.24	>63.3	>63.3
USP7 Catalytic Domain IC <sub>50</sub> (μM)	1.40±0.14	0.43±0.07	0.61±0.15	>200	>63.3
Full Length USP47 IC <sub>50</sub> (μM)	>200	20.3±2.2	>200	>200	>200
Full Length USP5 IC <sub>50</sub> (μM)	>200	>200	>200	>200	>200
Ub-MDM2 MSD (μM)	7.60±0.57	0.89±0.73	1.5	>50	>50

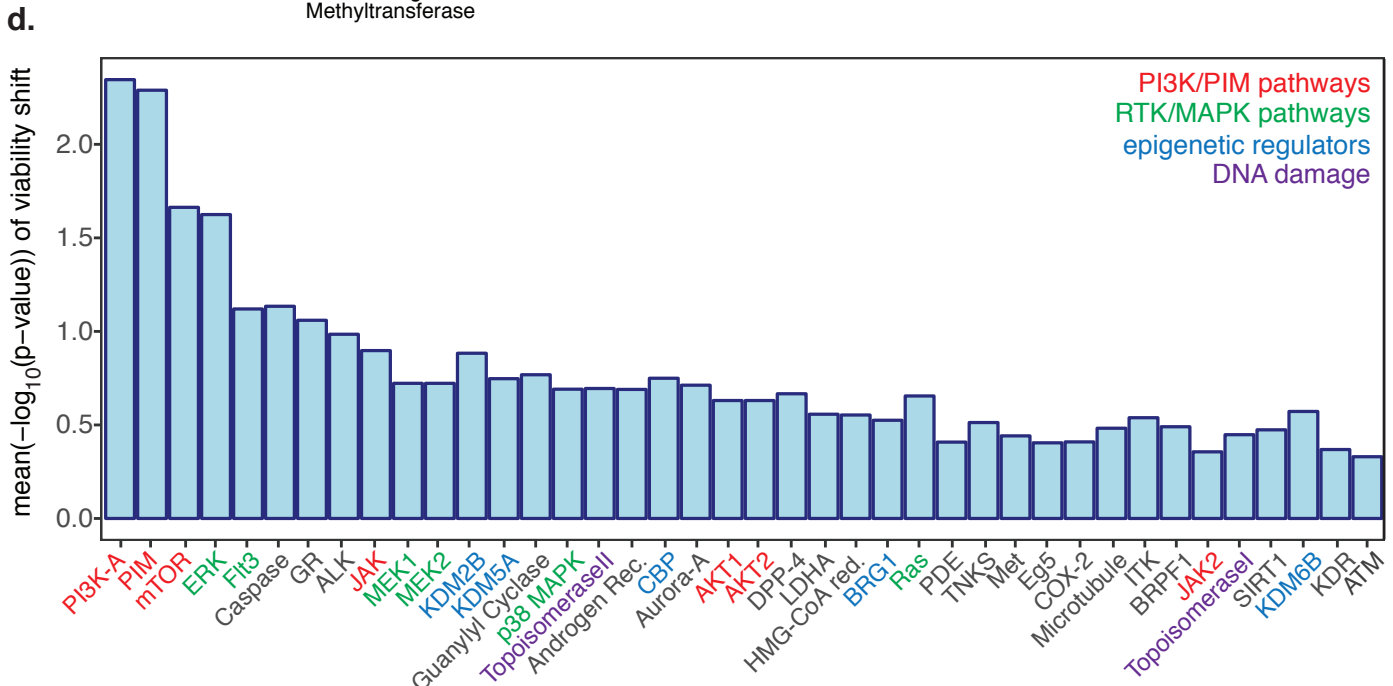
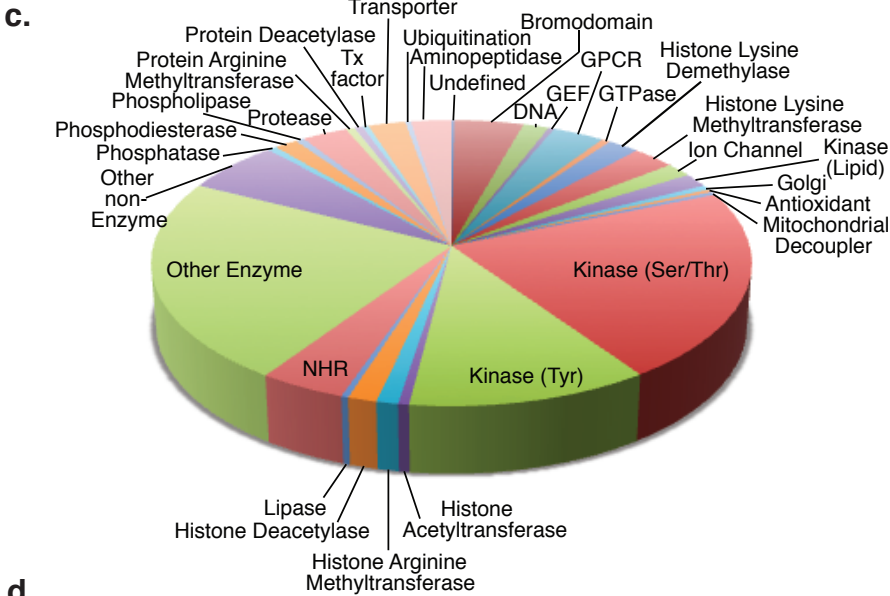
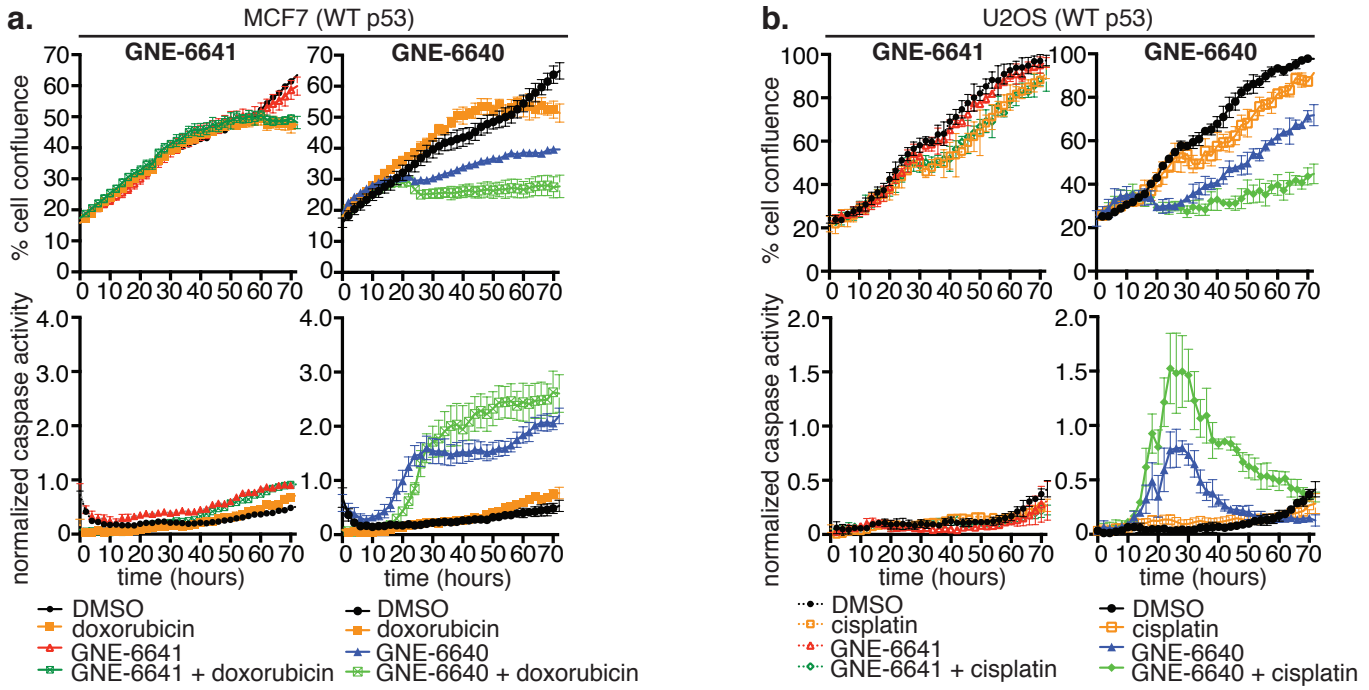




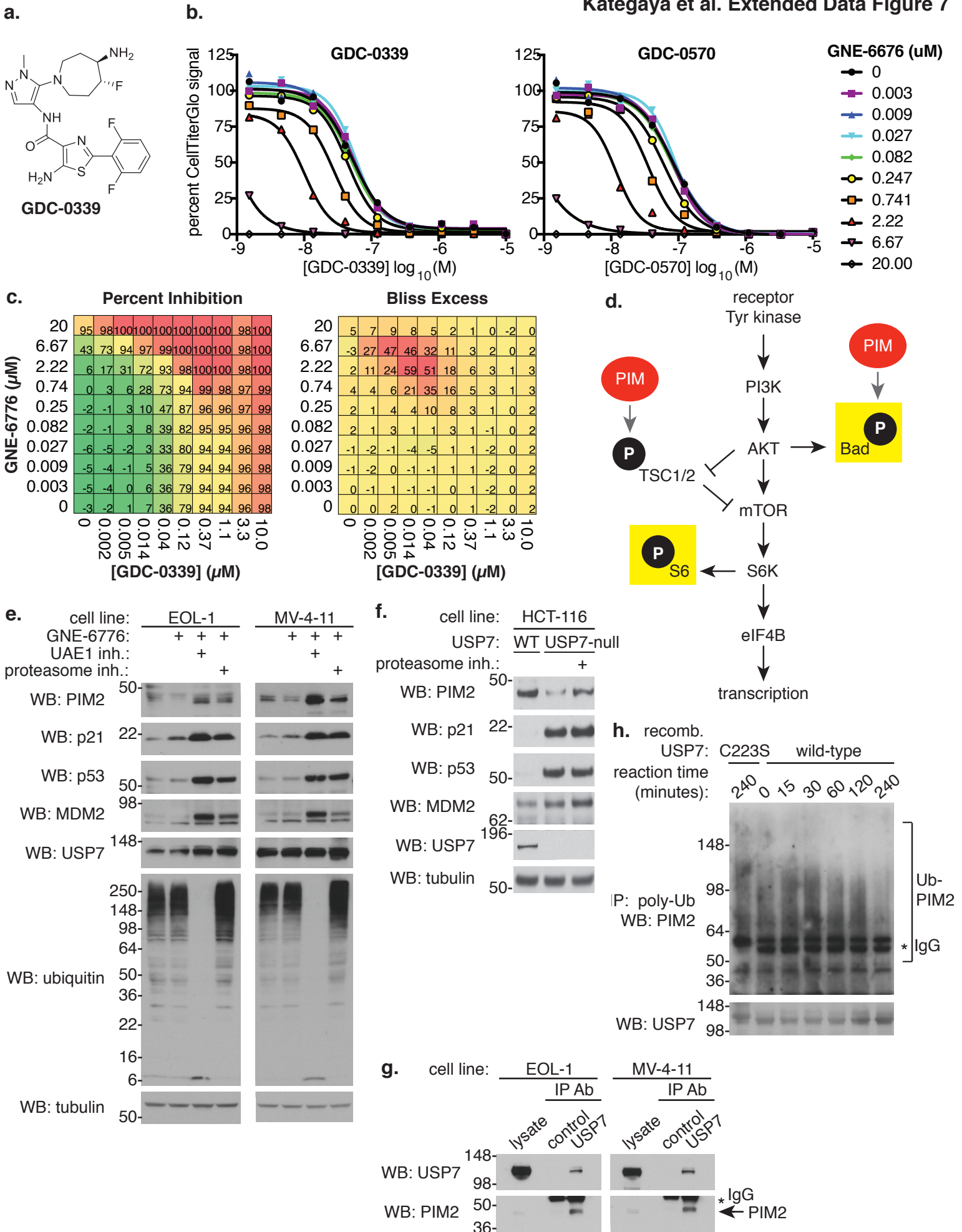










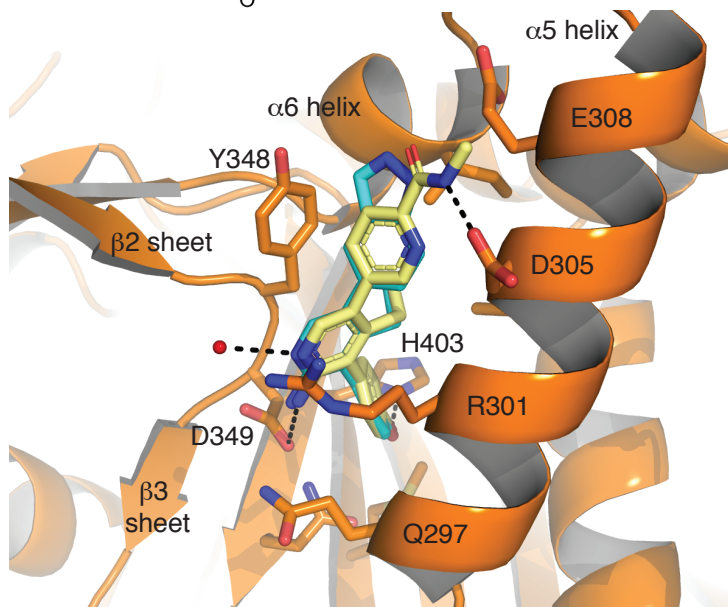
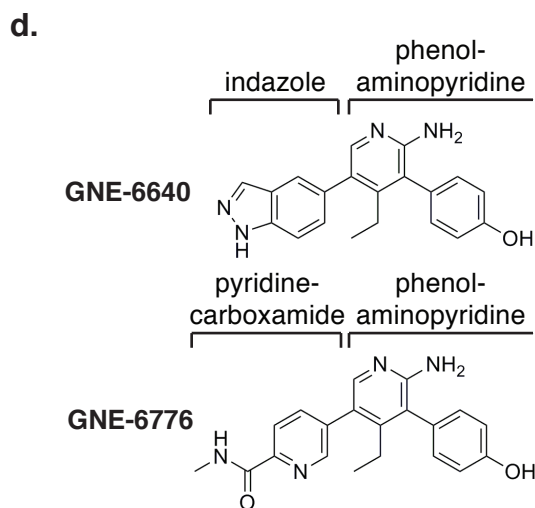
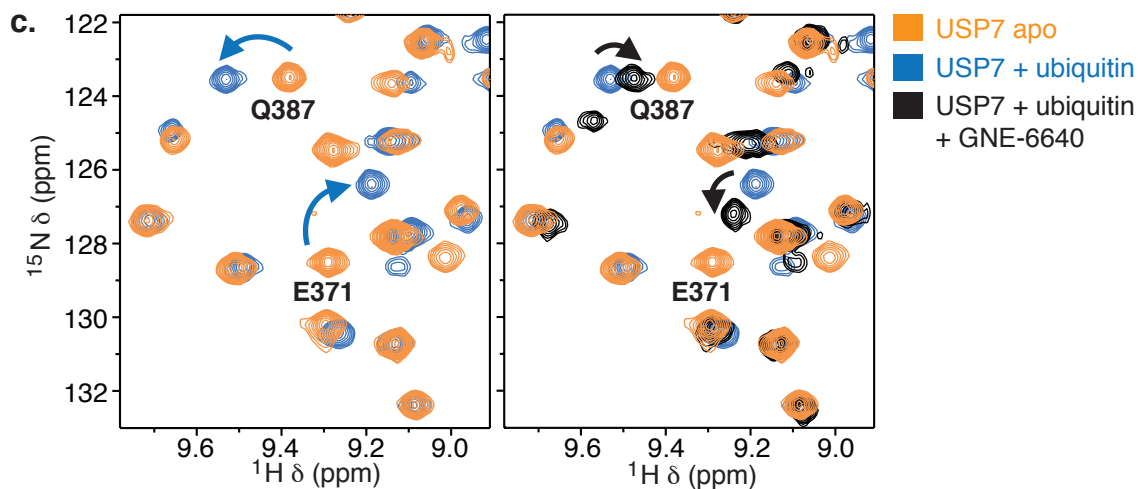


**a.**

USP7 inhibitor	$K_M$ ( $\mu\text{M}$ )	$K_{\text{cat}}$ ( $\text{s}^{-1}$ )	$K_{\text{cat}} / K_M$ ( $\text{M}^{-1} \text{s}^{-1}$ )
GNE-6640	$5.0 \pm 0.5$	$0.22 \pm 0.03$	$4.4 \pm 0.7 \times 10^4$
GNE-6776	$15.1 \pm 0.7$	$0.061 \pm 0.007$	$4.0 \pm 0.5 \times 10^3$
GNE-6641	$3.6 \pm 0.1$	$1.36 \pm 0.06$	$3.8 \pm 0.2 \times 10^5$
no inhibitor	$3.4 \pm 0.1$	$1.54 \pm 0.02$	$4.5 \pm 0.1 \times 10^5$

**b.**

USP7 inhibitor	USP7/ubiquitin $K_D$ ( $\mu\text{M}$ )
GNE-6640	$372.7 \pm 59.1$
GNE-6776	$246.0 \pm 20.3$
GNE-6641	$156.3 \pm 12.9$
no inhibitor	$133.4 \pm 7.1$



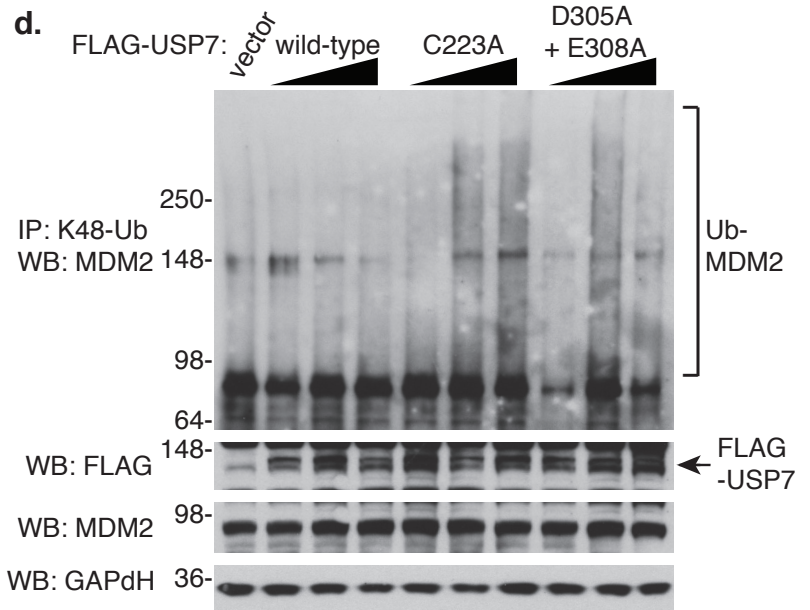
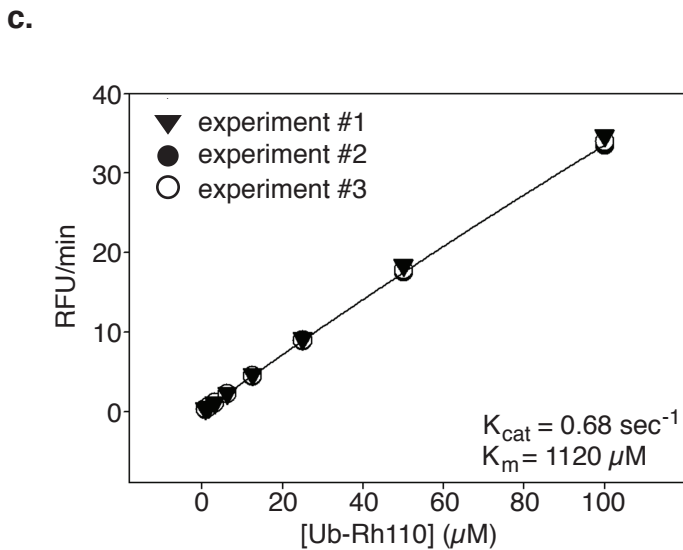
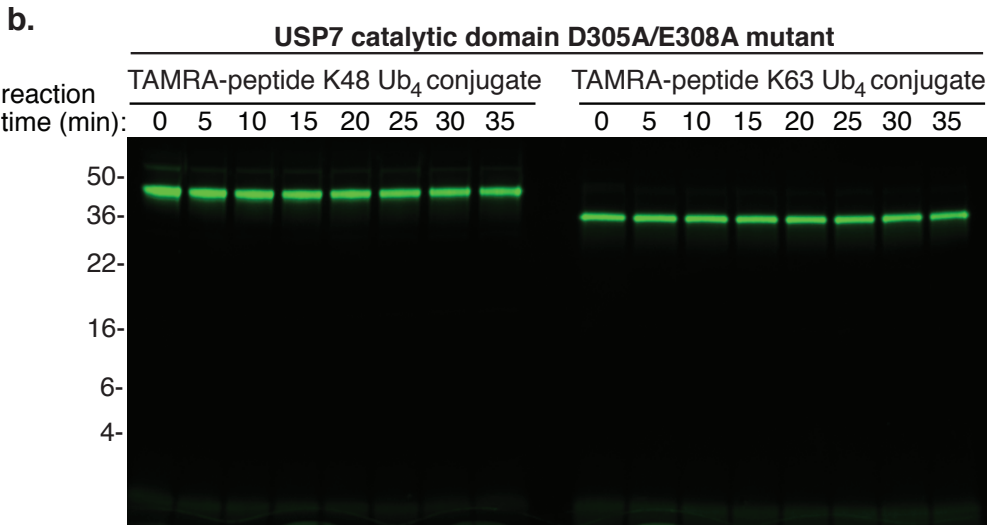
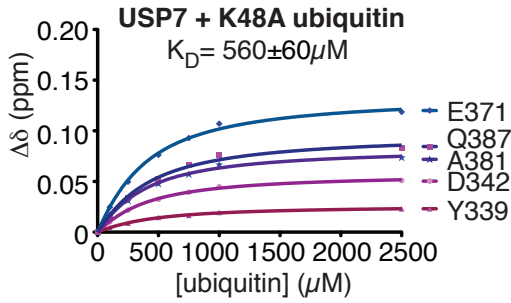
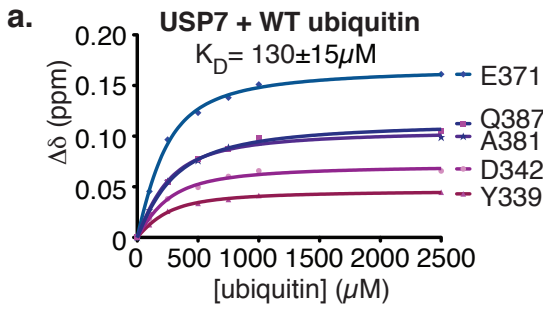
**e.**

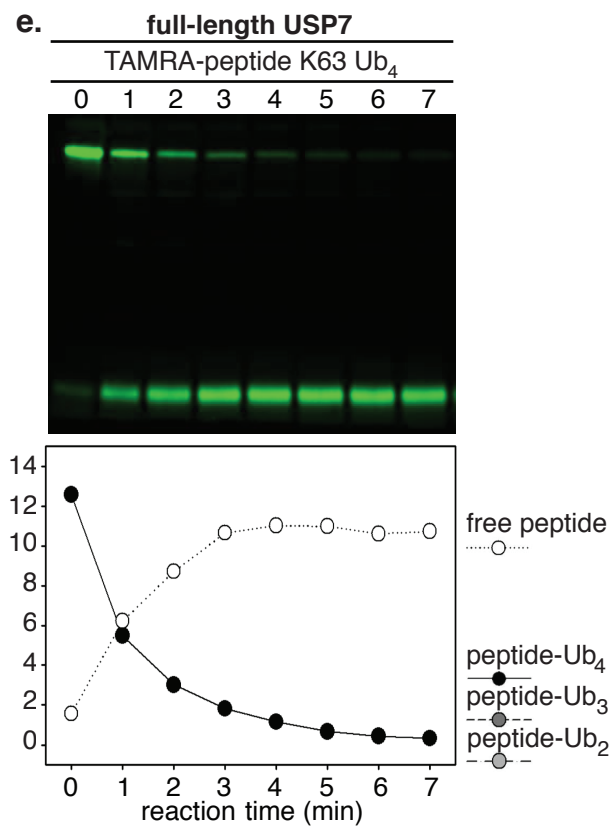
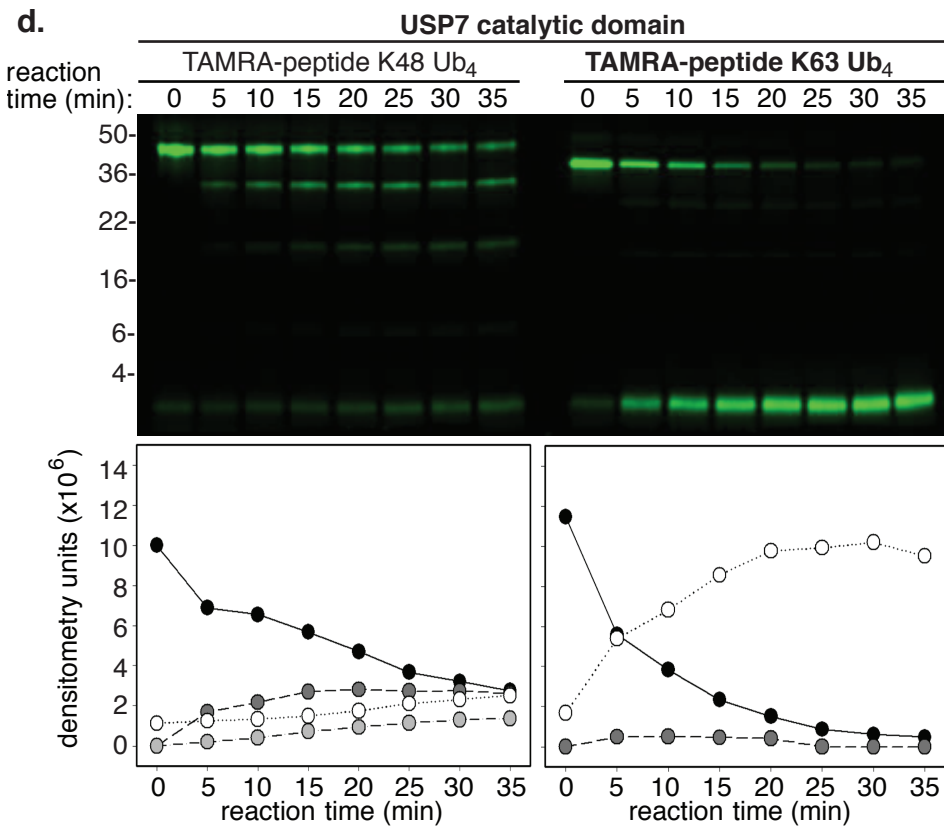
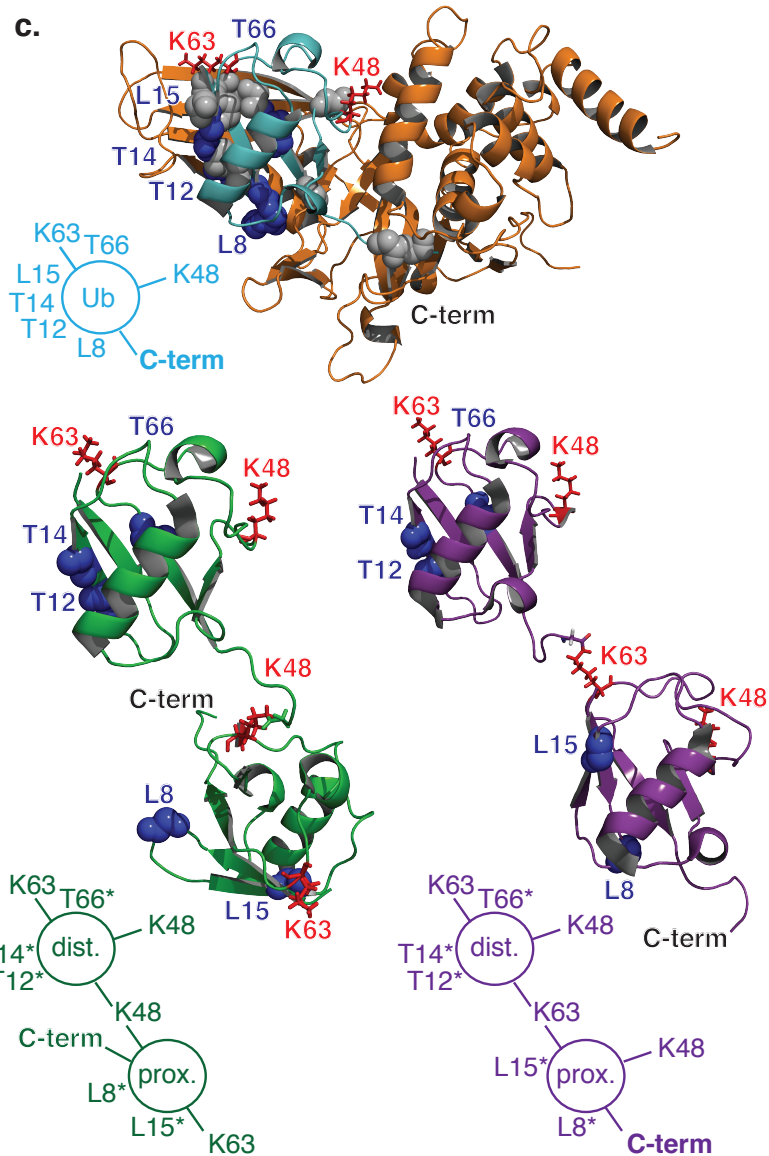
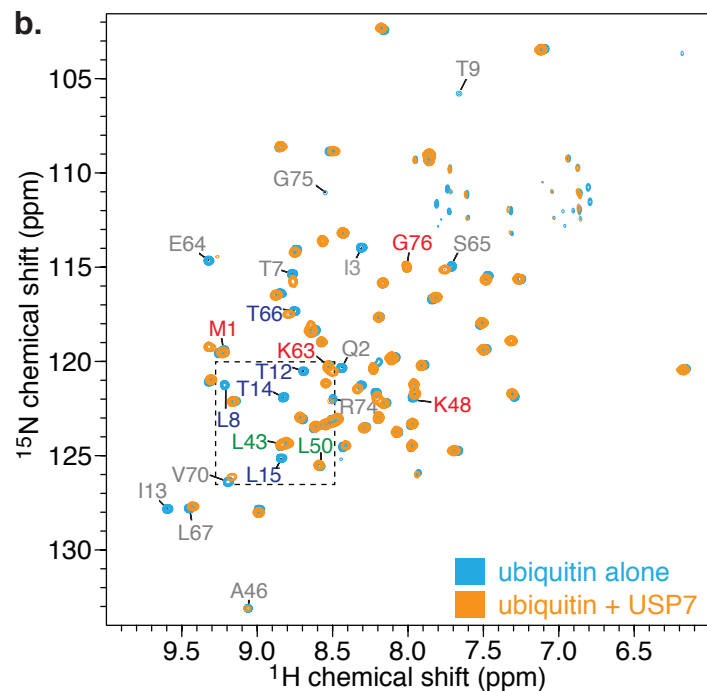
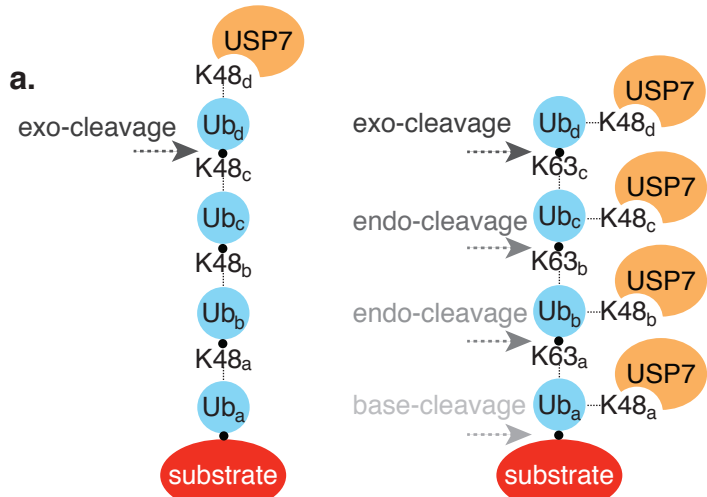
	GNE-6640 (PDB code 5UQV)	GNE-6776 (PDB code 5UQX)
<b>Data collection</b>		
Space group	P21	P21
Cell dimensions		
<i>a</i> , <i>b</i> , <i>c</i> ( $\text{\AA}$ )	75.79 68.44 76.74	76.36 67.53 76.86
$\alpha$ , $\beta$ , $\gamma$ ( $^\circ$ )	90 95.45 90	90 97 90
Resolution ( $\text{\AA}$ )	76.4-2.84 (2.85-2.84) <sup>a</sup>	67.8 - 2.23 (2.24 - 2.23)
Rmerge	0.052 (0.491)	0.18 (0.94)
<i>I</i> / $\sigma$ ( <i>I</i> )	15.7 (2.9)	9.1 (3.8)
CC1/2	0.999 (0.87)	0.6 (0.016)
Completeness (%)	96.3 (98.5)	96.8 (96.0)
Redundancy	3.6 (3.8)	3.8 (4.0)
<b>Refinement</b>		
Resolution ( $\text{\AA}$ )	43.5-2.84	38.2-2.23
No. reflections	17844	37714
<i>R</i> <sub>work</sub> / <i>R</i> <sub>free</sub>	0.221/0.278	0.19/0.223
No. atoms		
Protein	5384	5535
Ligand/ion	52	52
Water	2	221
<i>B</i> factors		
Protein	74	54
Ligand/ion	66	41
Water		48
R.m.s. deviations		
Bond lengths ( $\text{\AA}$ )	0.001	0.009
Bond angles ( $^\circ$ )	0.5	1.0

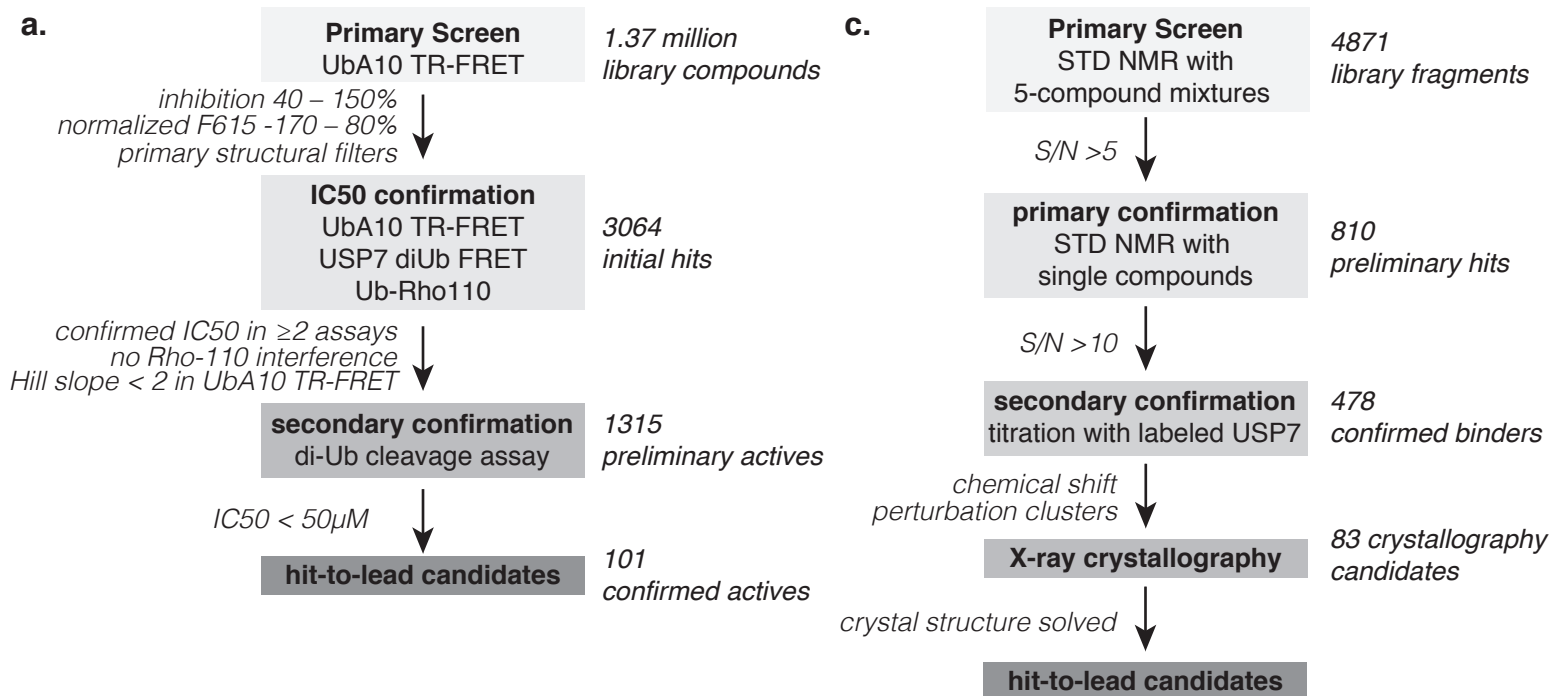
<sup>a</sup>Values in parentheses are for highest resolution shell

Molprobrity score for GNE-6640 = 2.53

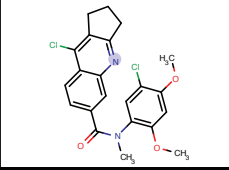
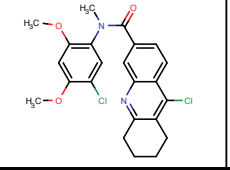
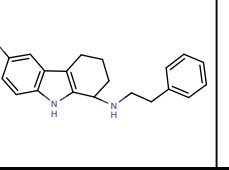
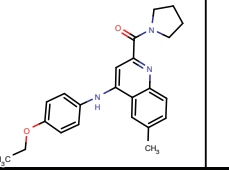
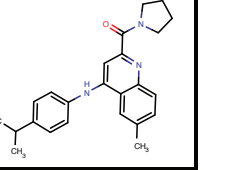
Molprobrity score for GNE-6776 = 2.42







**b.**

					
Cluster	1	1	2	3	3
% Inhibition Primary Screen	76.8	76.3	66.4	53.3	50.1
UbA10 IC <sub>50</sub> ( $\mu$ M)	1.17	1.37	> 49.5	2.58	2.79
diUb IC <sub>50</sub> ( $\mu$ M)	0.36	0.49	6.42	2.49	1.53
Ub-Rho110 IC <sub>50</sub> ( $\mu$ M)	0.29	0.31	2.16	2.65	N/D
MS Activity IC <sub>50</sub> ( $\mu$ M)	0.13	0.15	14.87	0.5	0.61
MS Activity Hill Slope	0.83	1.06	1.02	0.87	1.12

N/D = not determined

Indole tricyclic
Peptidomimetic
Tetrahydroacridine
Fragment

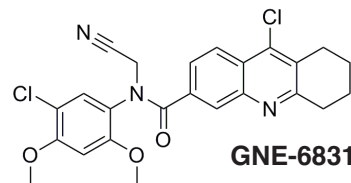
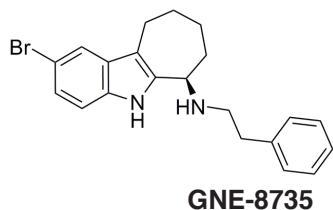
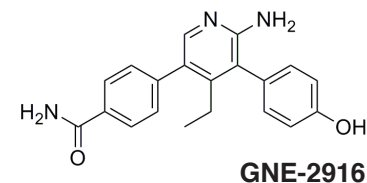
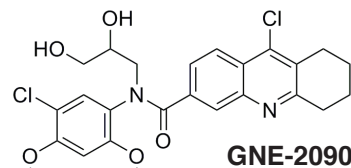
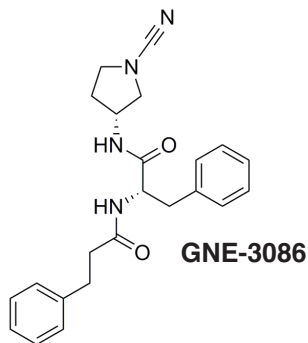
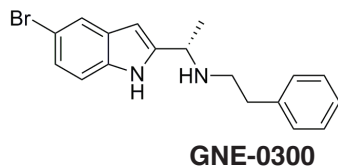
Compound	GNE-0300	GNE-8735	GNE-3086	GNE-2090	GNE-6831	GNE-2916
Full Length USP7 IC <sub>50</sub> (μM)	1.03	0.47±0.39	8.80±5.20	4.64±1.38	0.75±1.30	2.63±0.43
USP7 Catalytic Domain IC <sub>50</sub> (μM)	1.40	0.50±0.31	13.80	41.7±30.6	>200	1.40±0.18
Full Length USP5 IC <sub>50</sub> (μM)	160	>200	>100	>200	N/D	>200
Full Length USP47 IC <sub>50</sub> (μM)	140	>200	7.0	63.3	>200	>200
Total MDM2 increase (IF)	none >20μM	increase 2.9μM	none >20μM	none >20μM	none >20μM	none >20μM
Ub-MDM2 MSD (μM)	not done	>50.00	9.65±3.18	3.55±1.91	3.20±2.69	7.60±0.57
Cathepsin-B Inhibition (μM)	> 40.00	6.12	not done	not done	> 40.00	not done
Caspase-3 Inhibition	apparent precipitator	apparent precipitator	not done	not done	not done	not done
Dynamic Light Scattering	pass	pass	pass	pass	pass	not done
Covalent Modification	not done	not done	yes	not done	yes	not done

USP7 inhibition and selectivity

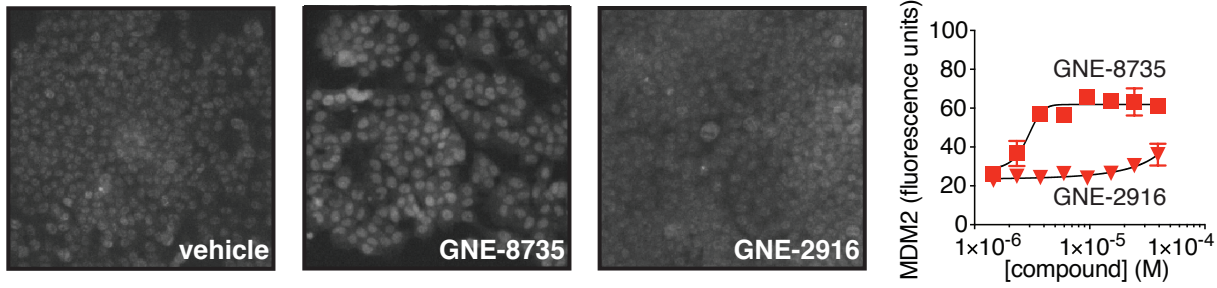
cellular MDM2 assays

protease selectivity

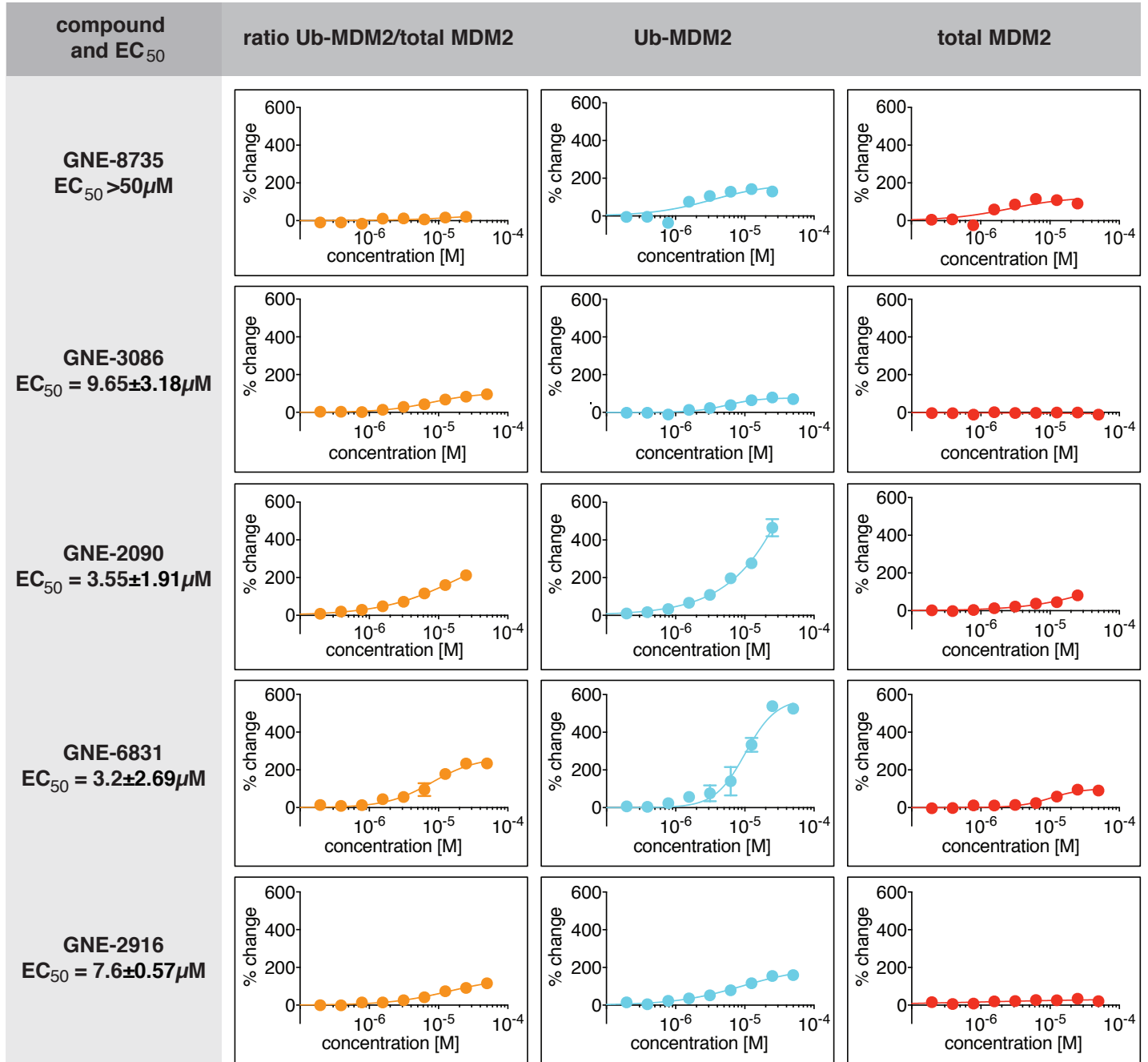
biophysical analysis

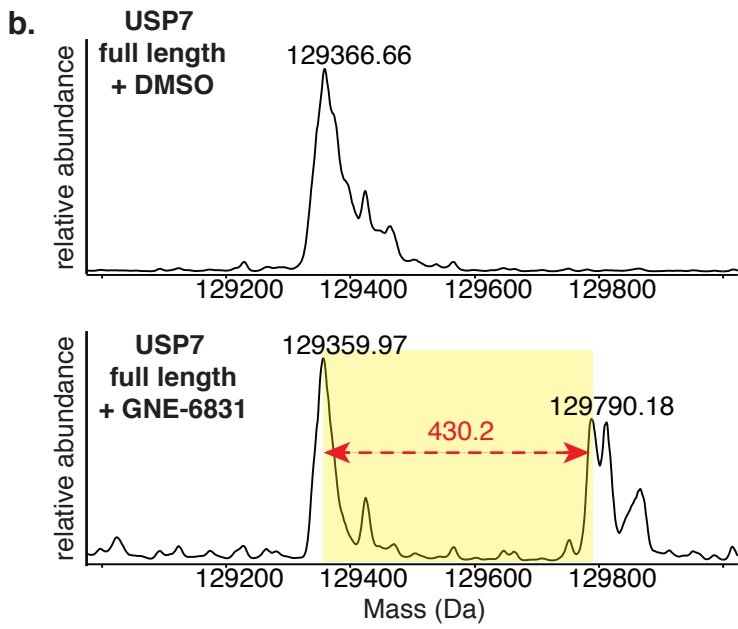
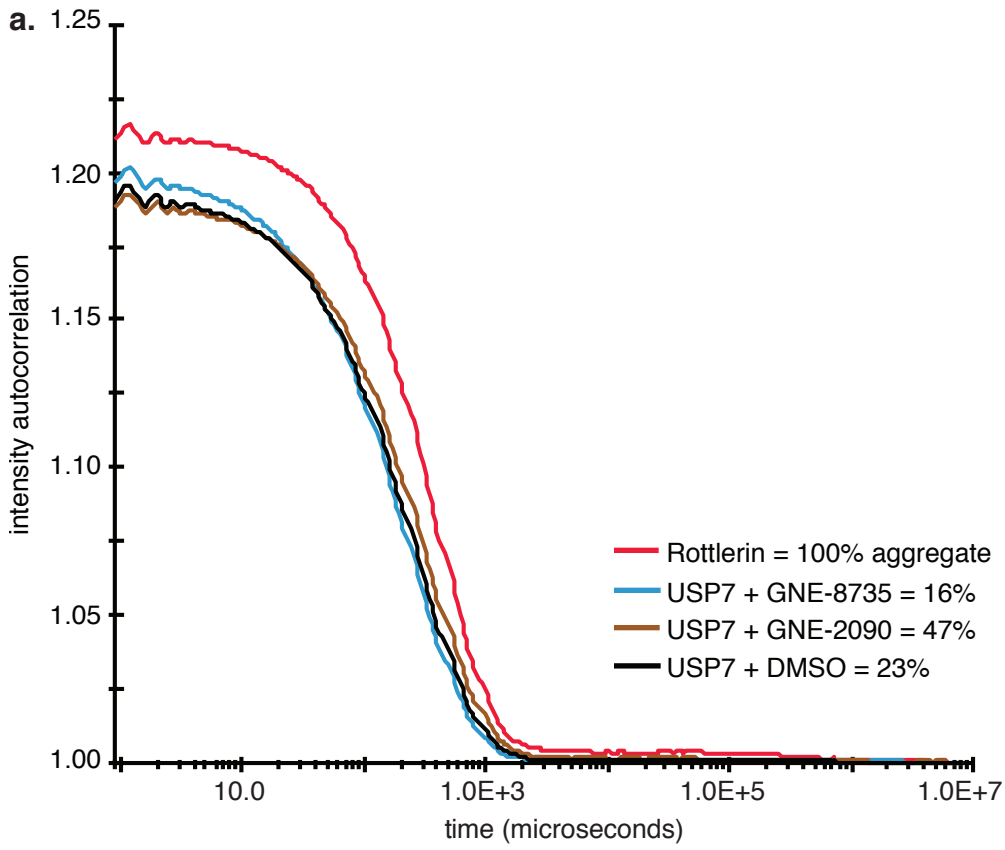


a.



b.

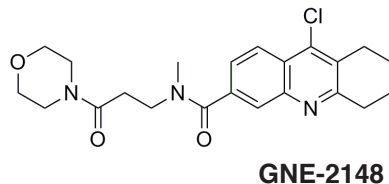
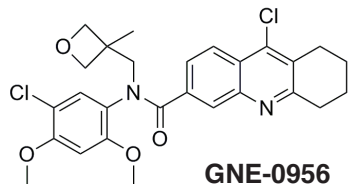
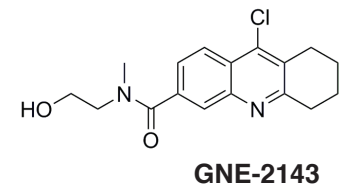
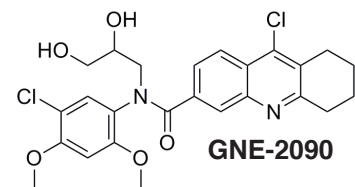
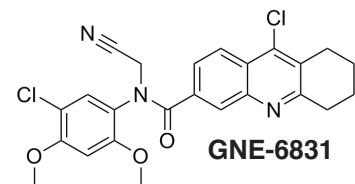






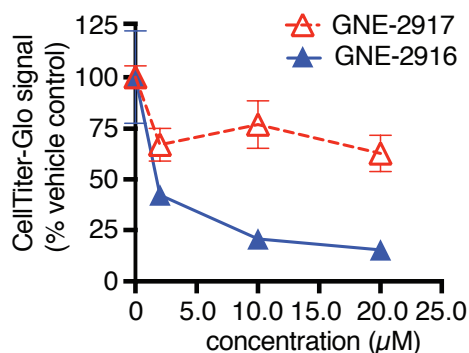
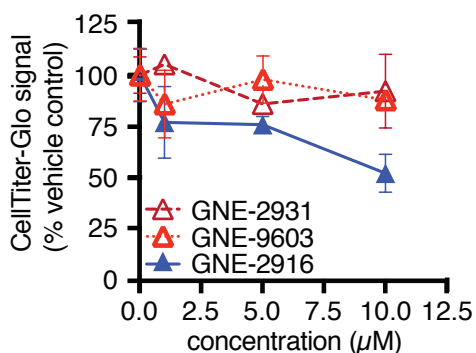
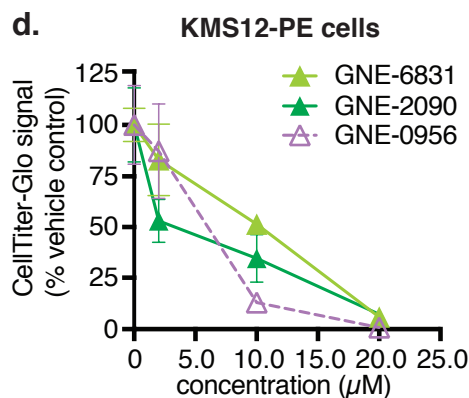
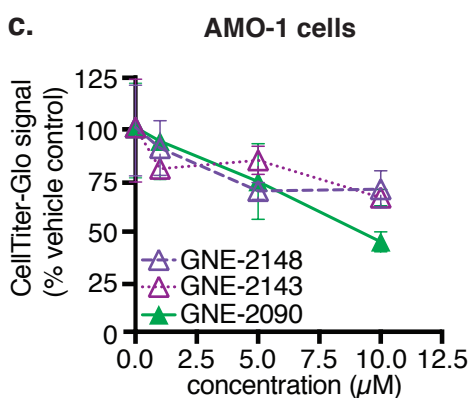
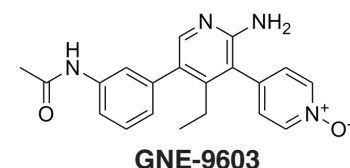
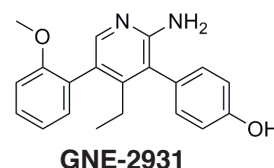
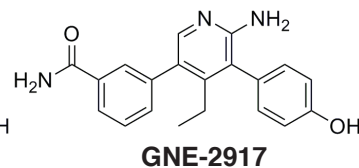
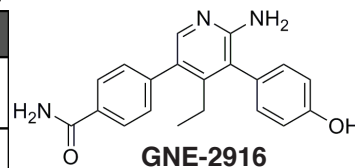
**a.**

Compound	active compounds		inactive control compounds		
	GENE-6831	GENE-2090	GENE-2148	GENE-2143	GENE-0956
Full Length USP7 IC <sub>50</sub> (μM)	0.75±0.13	4.64±1.38	>200	196	>20
USP7 Catalytic Domain IC <sub>50</sub> (μM)	>100	41.7±30.6	>200	>200	>63
Full Length USP47 IC <sub>50</sub> (μM)	>200	>200	>200	N/D	>200
Full Length USP5 IC <sub>50</sub> (μM)	N/D	>200	>20	>20	>63
Ub-MDM2 MSD (μM)	30.8±11.1*	24.2±12.3*	N/D	N/D	N/D



**b.**

Compound	active compound	inactive control compounds		
	GENE-2916	GENE-2931	GENE-9603	GENE-2917
Full Length USP7 IC <sub>50</sub> (μM)	2.63±0.43	>200	>200	114
USP7 Catalytic Domain IC <sub>50</sub> (μM)	1.40±0.14	N/D	>200	66.8
Full Length USP47 IC <sub>50</sub> (μM)	>200	>63.3	109	>200
Full Length USP5 IC <sub>50</sub> (μM)	>200	N/D	>200	>20
Ub-MDM2 MSD (μM)	7.60±0.57	N/D	N/D	N/D



**a.**

	GENE-6640	GENE-6776
MW/LogD <sub>7.4</sub> /tPSA	330.38/4.40/87.0	348.40/3.30/3.4/101
LM CLhep (h/r/m/d/c)	14/46/75/24/33	4.1/15/37/14/12
Hep CLhep (h/r/m/d/c)	16/45/68/24/39	9.4/39/44/18/33
PPB % (h/r/m)	99.6/98.7/99.0	97.3/93.4/93.4
MDCK P <sub>app</sub> ratio (B to A, A to B)	0.83 (12.17, 14.7)	0.75 (12.06, 16.10)

